Identification of Adsorption Mechanisms of Sulfur Heterocycles via Surface Analysis of Selected Metal-Doped Adsorbent Materials for Logistics Fuels Desulfurization

by

John M. Heinzel

A dissertation submitted to the Graduate Faculty of
Auburn University
in partial fulfillment of the
requirements for the Degree of
Doctor of Philosophy

Auburn, Alabama
December 14, 2013

Keywords: X-Ray Absorption Spectroscopy, Desulfurization, Adsorption, Fuel Processing, Surface Science, Heterocyclic Sulfur

Approved by

Bruce Tatarchuk, Chair, Charles E. Gavin III Professor, Chemical Engineering
Robert Ashurst, Associate Professor, Chemical Engineering
Bart Prorok, Professor, Materials Engineering
Allan David, John W. Brown Assistant Professor, Chemical Engineering

Michael Bozack (Outside Reader), Professor, Physics

Abstract

The removal of sulfur from distillate fuels is a difficult operation, which carries a cost associated with the capital equipment and production of hydrogen or other reagents necessary to drive the process. While specifications and environmental regulations have driven the allowable limits of sulfur content to lower levels, the content of sulfur present in military distillate and jet fuels in particular is too high to support utilization in high efficiency power generation systems such as fuel cells. Thus additional processes are necessary to provide suitable clean and usable fuel to ensure long life and continued high efficiency operation. Adsorption has been studied for a variety of materials and conditions, as an alternate to more severe or complex processes. The work described herein focuses upon unique approaches to study adsorption from the standpoint of all key atomic species to facilitate a better understanding of the material as well as the mechanisms for which they operate. Given the complexity of liquid fuels, this work attempts to utilize techniques which can provide insight based upon local atomic structure, and materials changes associated with the desulfurization process under selective adsorption.

The system of silver dispersed on anatase TiO_2 was studied because of its relevance as a practical, scalable adsorbent material that exhibited high capacity. Studies utilizing X-Ray Photoelectron Spectroscopy (XPS), and X-Ray Absorption Spectroscopy (XAS) were performed to better understand surface and overall structural characteristics, and were applied such that silver, sulfur and titanium could be studied, both in an unused form to understand basic structure, as well as *in situ* under calcination/activation and an adsorbed state to understand the basis of

materials structure changes for both the adsorbent surfaces and the adsorbed species. XPS was utilized to first probe the surface structure and better understand the differences in surface and lattice oxygen and other ratios to better understand stoichiometry and changes caused due to the loading of silver on the TiO_2 surface. XAS was utilized to study the structure of the dispersed silver and then also explore changes when it underwent adsorption. Application of XAS found a unique 2.32Å Ag-O bond structure which is consistent with a fully hydrated Ag^+ ion in fourfold coordination with oxygen, and with a highly ionic character as compared to solid references. The loading of silver did not change the surface structure of TiO_2, further validating that the silver is existing as a highly dispersed phase on a wet surface. High loading of silver causes a metallic phase to form, which is not interacting with the TiO_2 surface.

Upon adsorption of sulfur, XAS analysis indicates minor observable changes to the titanium and silver species, showing that they both appear to take part in desulfurization. Studies of the structure of sulfur via an *in situ* method has provided distillate fuel analysis by XAS, and clearly shows changes in the fuel from a benzothiophene type structure to both oxidized sulfate and reduced sulfide under adsorption. The behavior of conversion of the sulfur changed with different silver loading levels, helping to identify the effect of loading and dispersion of silver, as well as the support's own interaction. These results help to bring forth a notional adsorption mechanism.

Formation is also studied to determine the changes to the silver upon calcination, and means by which the sorbent might be damaged. These *in situ* studies indicate a complete decomposition from nitrate to metal, with subsequent dispersion to the new oxide form. When performed within the standard temperature range specified, the oxide appears stable, however higher temperature conditions induces metal agglomeration, even at low loading.

Acknowledgements

This work was supported by the Carderock Division of the Naval Surface Warfare Center, In-House Laboratory Independent Research program administered under the Office of Naval Research Program Element 0601152N. Support has also been provided by the Naval Surface Warfare Center Extended Term Training program. I appreciate the efforts of Drs. Golda, Mastro, Barkyoumb and Price, and Mrs. Audrey Bauer for their help in obtaining support through these programs, and Mr. Anthony Nickens and Don Hoffman for fuel cell programmatic support from the Office of Naval Research. I would like to thank Dr. Tatarchuk and the committee members for their time to support, evaluate and advise on this work. I would also like to thank Dr. Hongyun Yang and Dr. Sachin Nair for the collaborative work and exchange of knowledge since my first efforts in the Auburn University laboratories in 2006. I would also like to especially thank Dr. Azzam Mansour of the Naval Surface Warfare Center for his mentorship and teaching during extremely long hours on the BNL beamlines, and during the subsequent data analysis. Use of the National Synchrotron Light Source, Brookhaven National Laboratory, was supported by the U.S. Department of Energy, Office of Science, Office of Basic Energy Sciences, under Contract No. DE-AC02-98CH10886.

Table of Contents

List of Tables

Table of Figures

List of Abbreviations

F-76	Marine Distillate Fuel
JP-5	Marine Jet Fuel
BT	Benzothiophene
DBT	Dibenzothiophene
HDS	Hydrodesulfurization
PEM	Polymer Electrolyte Membrane
SOFC	Solid Oxide Fuel Cell
ATR	Autothermal Reformation
WGS	Water-Gas Shift
PrOX	Preferential Oxidation
XRD	X-ray Diffraction
XPS	X-ray Photoelectron Spectroscopy
XAS	X-ray Absorption Spectroscopy
(E)XAFS	(Extended) X-ray Absorption Fine Structure
XANES	X-ray Absorption Near-Edge Structure
S	Sulfur
Ag	Silver
Ti	Titanium
eV	electron Volt

1. Introduction and Background

Fuel cells have the potential to serve as highly efficient sources of power, superior to current processes for both generation and mobility[1]. While gas turbine and diesel technologies utilized currently by the U.S. Navy have the capability to operate at full rating utilizing F-76 and JP-5 logistics fuels with high sulfur content[2] [3], fuel cell systems have significant sensitivity to the sulfur content due to the materials utilized for unit operations' catalysis, piping, and within the fuel cell itself.[1,4,5,6] The sensitivity to sulfur makes the ability to remove sulfur from high flashpoint Navy-specific logistics fuels the most critical step in the fuel cell process from the standpoint of development and implementation of Naval fuel cell systems. The difficulty of the objective desulfurization process is the desire to desulfurize in liquid phase at ambient temperature and pressure, with high regeneration capability over high numbers of cycles.[7] However, given that the entire set of processing operations and electrochemical reactions require clean, low/no sulfur gas, it is a process that must be made viable and functional for long-term use.

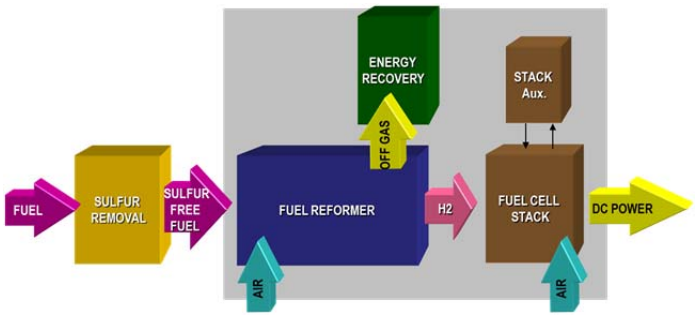

Figure 1-1 Navy Fuel Cell System (without water source and recovery)

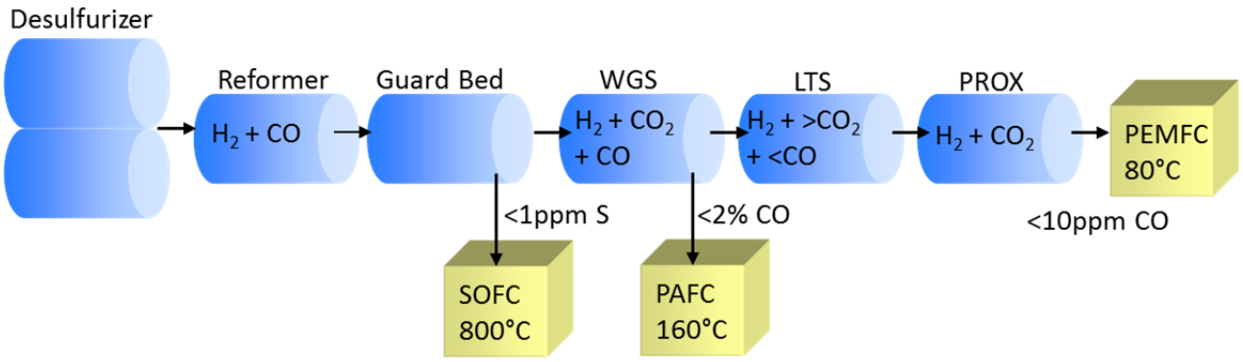

Figure 1-2 Fuel Processing Flow Diagram - Various Feed and Fuel Cell Options[1,8]

In the production of hydrogen for fuel cell applications, the overall reactions for reformation of fuels to hydrogen generally include autothermal reformation (ATR), water gas shift (WGS) and preferential oxidation (PrOX) of carbon monoxide. Autothermal reformation has typically been selected for Navy systems due to the balanced heat load and higher tolerance to low levels of sulfur present in fuel[8], and has been identified as an optimal balanced approach for many other instances of on-board reformation.[9] The reactions of interest are as follows[1]:

Autothermal reforming:

$$C_mH_n + (1/2)mH_2O + (1/4)mO_2 = mCO + ((1/2)m + (1/2)n)H_2 \quad (1)$$

Water gas shift:

$$CO + H_2O = CO_2 + H_2 \quad (2)$$

CO oxidation:

$$CO + O_2 = CO_2 \quad (3)$$

While some level of sulfur may be tolerated during a high temperature, optimized application of autothermal reformation, its effects upon gas composition and reforming efficiency are known to be detrimental.[10] In practice, the efficiency effect on reformation due to sulfur can be high, and

the remnant sulfur, which remains present at a quantity of roughly 1/10th the fuel concentration (i.e. 1000ppmw S in fuel yields ~100ppmv S in the reformate, as H_2S and trace COS) must still be dealt with.[8,11] This is still substantially excessive for protection of downstream processes and the fuel cells themselves, which have little to no sulfur tolerance[4]. Zinc oxide beds have utility to provide polishing of gasses, however the wet environment associated with an ATR operation affects the equilibrium for removal, and the nature of a zinc oxide polishing bed requires either design for substantial hours of continuous use, or its own multi-bed regeneration scheme that allows online bed changes under conditions with high pressure, high temperature reformate. Therefore, for service and reliability over long periods of operation (e.g. Mean Time Before Overhaul >3000 hours), the beds would either need to be impractically large, or there would need to be a constant regeneration scheme occurring, which drives systems to be overly large and complex.[8] The importance of a gas-phase adsorbent in the process (post-liquid fuel vaporization and reaction in the reformer) cannot be overemphasized, given the sensitivity to trace H_2S in a reformate stream,[12] but its application must be constrained to the application where it is most sensible. This drives the need for a preliminary stage to preferentially treat the sulfur content in logistics fuels, and to develop processes that can do so with a more compact footprint, reduced reactor inventory and high selectivity and performance to the specific compounds of interest, versus gas phase operations.

The removal of fuel-borne sulfur compounds is a challenge due to the refractory nature of the molecules themselves due to steric hindrance effects under refining reaction conditions, as well as their high concentrations. Typical refining processes have limitations in terms of the selectivity and specificity of the compounds removed, and the combination of blend stocks and processing utilized to create the product.[13] The presence of sulfur compounds found in fuels is

related to the inability of current processes to adequately react with these compounds.[14,15,16] Work performed elsewhere has characterized the remnant sulfur compounds into groups associated with the presence and placement of aromatic and hindering alkyl groups about the sulfur atom within the hydrocarbon.[13,14,17] Analytical work performed by the Navy and others have identified the sulfur content in fuels of interest to be consistent with the compounds identified in the above references, molecular examples of which can be seen in figure 1-3a. The sulfur presence is consistent with sterically hindered, aromatic-bound sulfur compounds in the benzothiophene and dibenzothiophene ranges with methyl group substitution.[18] Examples of the compound ranges can also be seen in figure 1-3b, for JP-5. F-76, which has a broader distribution of hydrocarbons and an equivalent flashpoint, tends to have sulfur constituents at even higher retention times, indicating more compounds with a dibenzothiphene type nature.

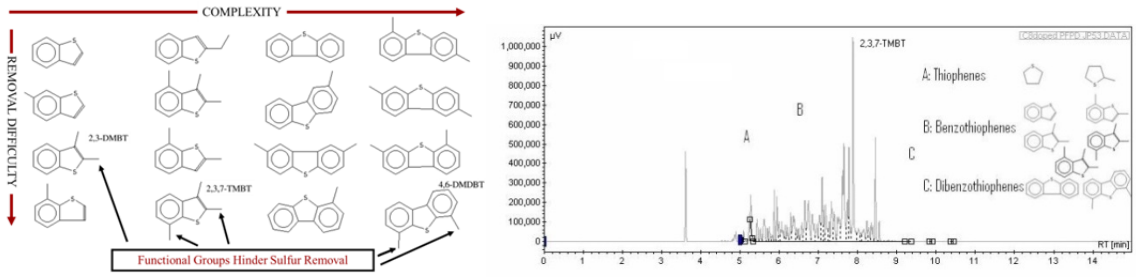

Figure 1-3 Structure of various compounds present in F-76 and JP-5 logistic fuels (a, left); and Pulsed Flame Photometric Detector chromatogram indicating sulfur compound distributions from 1172ppmw JP-5 fuel (b, right)

To facilitate system integration, maintain competitive power density, ensure safety, provide ability to be qualified for shipboard use, and offer long term efficiency and economy of operation, a robust approach to desulfurization is necessary. The key attributes for a sulfur treatment system for is the ability to provide the following characteristics:

a. Highest sulfur removal per reactor volume. Fuel cell systems must offer comparable power density to gas turbine generators currently employed, on the basis of fuel in to power and exhaust out. This drives the performance of all systems to as high a level as possible. Thus there is an interest in the figure of merit for adsorbent systems to maximize mg S / g sorbent (which relates to fuel throughput per volume and mass of reactor), and similar metrics for other processes. Maximized capacity ensures that there is both minimal reactor volume and longer runtime for a given reactor volume. Due to thermal integration and other aspects of system design and control, it also offers more flexibility for processes that require regeneration, bed changes, etc.

b. Stability of the process. For comparable performance, systems should be able to operate for the duration of at least one, and optimally multiple deployments without requiring major service, refurbishment or replacement of components, catalyst, etc. Thus an inherent stability and capability to be regenerated, refreshed or otherwise maintained at an "as installed" state is necessary.

c. Process economics. Cost is considered for system acquisition and adaptation, at a level that is equal to the technical basis of the system operation and application. Any system acquired must be able to compete at an economic level in terms of acquisition and life cycle cost/total ownership cost.

d. Serviceability of the process. Highly complex and integrated systems drive cost and effect maintainability. Thus systems must not only offer the performance and long-term performance, but also be easily refurbished as the need arises.

e. Process safety. In general, processes that require an inventory of hot, high pressure and/or flammable vapor negatively affect system integration, due to the necessity of

vessels and containment suitable to overcome safety events. It is desirable to minimize quantities of reagents at any state besides ambient temperature and pressure, and processes should minimize holdup and quantities locally present. Optimally, what is flowing through or reacted is directly used, with no accumulation or volume.

To date, the optimal approach to achieve best performance and optimize the elements previously discussed has been found to be regenerable liquid-phase adsorbent materials.[19] As it is critical that sorbent materials are able to perform with high capacity over multiple regeneration cycles, due to the necessary performance requirements of any notional fielded fuel cell system, developmental analysis has been performed upon various sorbent materials to determine their oxidative regeneration performance.[19] While it is critical that a proper regeneration profile be implemented, in the interest of maintaining sorbent capacity, fundamental understanding of the nature of the adsorbent structure, active site chemistry, and nature of the materials in general is required to allow improvement and optimization of materials to enable the utmost in capacity and stability. High capacity minimizes system size and quantity of adsorbent maintained. Optimized stability helps maintain the pore structure of the sorbent materials, particularly while undergoing oxidative regeneration, providing good long-term performance. **Thus this effort focuses specifically upon adsorbent materials and the fundamental characteristics which influence why and how they operate. The application of X-Ray Absorption Spectroscopy allows for the probing of specific key atoms (e.g. Ag, Ti, S) to identify their local coordination environment and oxidation state, and observe changes associated with the interaction of heterocyclic sulfur.**

2. Literature Review

2.1. Hydrodesulfurization

Hydrodesulfurization (HDS) uses hydrogen to chemically convert the sulfur in organosulfur compounds to H_2S and hydrocarbons. The process is carried out under high temperature and hydrogen partial pressure. This usually involves catalysts such as sulfided $CoMo/Al_2O_3$ and $NiMo/Al_2O_3$.[20] Deeper desulfurization can be achieved through increasing the severity of process conditions. Though this is successful, it also results in undesired side reactions, including the saturation of olefins, which causes a decrease in octane number for gasoline fuels. Also, coke formation is increased which results in deactivation of catalysts. Therefore it is of interest to develop improved catalysts that would result in deep desulfurization without extreme operating conditions. These catalysts should also improve octane/cetane number or aromatic content, both of which are important for quality of fuel and meeting environmental standards. HDS reactor design could also be improved by having multiple bed systems within one reactor or new internal design of the catalytic reactor. Advances in HDS are usually best made by improving both catalyst activity/selectivity and reactor design.[20]

The major challenge with HDS is that it is not particularly sensitive to the highly refractory, sterically hindered compounds found in logistics fuels[21,22,23], and particularly so for deep desulfurization, which may be desired to be lower than a US EPA mandated 15 ppm, due to its lower efficacy.[24] While advances are being made in deep-desulfurization processes and catalysis[25], both regulated fuel sulfur levels and commercial process equipment size are not amenable to mobile large-scale fuel cell power generation.[8]

Improving catalyst performance requires considering all steps in catalyst preparation: choosing the precursor of the active species, selecting the support, synthesizing the catalysts, and

post-treating the catalysts. CoMo and NiMo catalysts have been found to reduce sulfur levels to 2-5 ppm while also reducing polyaromatic content and improving cetane number and density of diesel. CoMo catalysts work for feeds with sulfur levels of 100-500 ppm and low pressure whereas NiMo catalysts are good for feeds with sulfur levels less than 100 ppm and high pressure. These catalysts have shown sustained performance over 400 days on stream. Employing CoMo catalysts in a conventional HDS units results in feed rates 30% higher having sulfur reduction to 10-20 ppm.[20]

Catalysts prepared through a new preparation process called NEBULA (NEw BULk Activity) are different in nature from typical HDS catalysts and remain active in sulfided form. These are suitable for HDS of diesel at medium severity and at high pressure. They had been installed in two commercial units as of 2003. CENTINEL catalysts by Criterion Catalysts and Technologies were also the result of modification of preparation. These come as CoMo or NiMo catalysts, with CoMo CENTINEL catalysts being best for lower hydrogen pressure and higher sulfur content and NiMo CENTINEL catalysts being best for higher hydrogen pressure and lower sulfur content.[20]

Supports for active catalysts have also been improved. For example, the application of ASA (amorphous silica-alumina) as the catalyst support results in extremely high desulfurization. In the desulfurization of gas oil, ASA-supported Pt and PtPd catalysts can reduce the sulfur content to 6 ppm and also reduce aromatics by 75%. PtPd/ASA catalysts were found to be good for low to medium sulfur content feeds with low levels of aromatics. With higher levels of aromatics, Pt/ASA catalysts were better. However, at high sulfur levels, these catalysts are poisoned and NiW/ASA catalysts are preferable.[20]

A new catalyst design to increase the sulfur resistance of ASA-supported noble metal based HDS catalysts is a bifunctional catalyst where the supports are combined with bimodal pore size distribution and two types of sulfur resistant active sites. The first type of active sites are placed in large pores. These are accessible for organosulfur compounds and are sensitive to sulfur inhibition. The second type of active sites is located in small pores, not accessible to organosulfur compounds, and is stable against sulfur poisoning. They are accessible to hydrogen, however, and so hydrogen is adsorbed dissociatively and transported between pore systems to regenerate the first type of active sites that have been poisoned by sulfur. It must be noted that this is simply a concept and has not been shown successful through experimentation as of 2003.[20]

Another method for improving the performance of HDS is to alter the process system. Conventionally, reactors are fixed beds with co-current supply of oil and hydrogen. This causes an unfavorable distribution of H_2 and H_2S including a high concentration of H_2S at the reactor outlet, preventing the removal of the last ppm of sulfur. Countercurrent supply can be a beneficial alternative. In this process, oil is fed through the top of the reactor and hydrogen is bubbled through the bottom, where it is most wanted. H_2S is then removed from the top, preventing olefins from possible recombination at the outlet. An example of a commercially applied system employing this process can be observed in Figure 2-1.

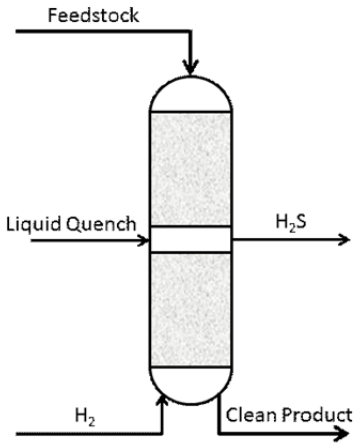

Figure 2-1 Co-current/countercurrent Syn Technology process diagram, adopted from (20)

This process works by initially feeding hydrogen and oil co-current to remove most of the organosulfur compounds. H_2S is then removed from the center of the reactor, above which, the countercurrent second stage begins. This enables more desirable profiles of H_2 and H_2S in the reactor for deeper desulfurization. Through this process, sulfur-sensitive catalysts that are very active, such as the ASA-supported noble metal based catalysts described previously, can be used. The process illustrated in Figure 2-1 utilizes noble metal catalysts and can reduce the sulfur content to 1 ppm and the aromatics content to 4 vol%.[20]

Another alternative HDS reactor process is the ebullated bed reactor. These work by having the catalysts fluidized into the stream by the feed. Since it is well mixed, bed plugging and channeling are avoided. The process is nearly isothermal with a low pressure drop. Added utility is obtained since the catalyst is fluidized, as this makes it possible to control catalyst activity by adding or removing catalyst. However, the catalyst selected must be mechanically stable and resistive to attrition. This process also has good heat transfer, so there is less overheating and formation of coke. It is used for desulfurization of heavy feeds such as deep cut

heavy vacuum gas oils, coker gas oils, and some residues. Application of this process has resulted in diesel with less than 50 ppm sulfur and FCC with 1000-1500 ppm, for a FCC gasoline sulfur content of 30-50 ppm.[20]

A process specially designed for desulfurization of FCC gasoline specifically, the ISAL process, includes a post-treatment of the products after HDS. It is composed of one fixed-bed reactor with a multiple bed configuration. Usually the catalysts employed are $CoMoP/Al_2O_3$ and GaCr/H-ZSM-5. The flow is co-current and similar to conventional HDS systems. Therefore, it is not difficult to upgrade and existing conventional HDS system to an ISAL one. This process can reduce the sulfur content in a naphtha feed from 1450 ppm to 10 ppm with insignificant effect on octane number.[20]

To achieve even deeper desulfurization of FCC gasoline stream without sacrificing octane number, a process called catalytic distillation hydrodesulfurization (CDHDS) was developed. In this process, the stream is fractionated by distillation before undergoing desulfurization at the appropriate severity for that fractionated stream. This works well in preserving octane number since olefins are mostly present in light naphtha whereas organosulfur compounds are mostly present in heavy naphtha. An issue is that this requires multiple HDS systems, one for each fraction.[20] CDTech Company has successfully simplified this process to desulfurize and separate the stream in one step. This can be observed in Figure 2-2. It works by controlling severity through boiling temperature. HDS catalysts are packed in stages of the distillation column. The lighter fractions with less sulfur and more olefins undergo desulfurization at a lower temperature. This causes higher desulfurization selectivity and less hydrocracking and/or saturation of olefins. The heavier fractions with more sulfur and less olefins undergo desulfurization at a higher

temperature. There is no overheating, since the heat released by the exothermic reaction is used as a heat source for the distillation column, so there is a very favorable integration of heat.

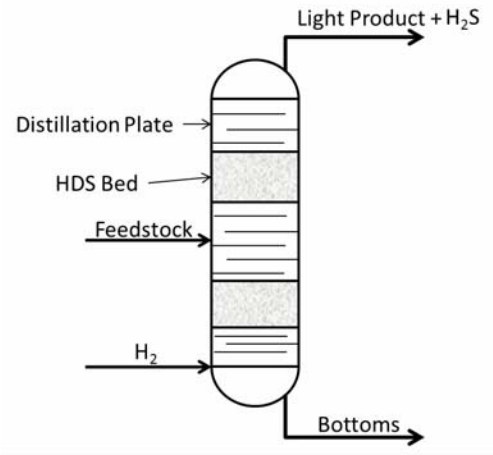

Figure 2-2 Simplified CDHDS process, adopted from (20)

In commercial application, CDHDS has reached a stable desulfurization level of 90% for the first four months of operation and resulted in an average octane number drop of less than one. It is also attractive from an economic standpoint, as it is roughly 25% less expensive than conventional HDS processes.[20]

2.2. Extraction

Extractive desulfurization is a liquid-liquid process in which an extractant, which is separable from the feed, is mixed with the feed and removes some of the sulfur from the solution. Then the raffinate and extractant are separated. The raffinate has a decreased sulfur level to an amount depending on the solubility of sulfur in the extractant.[20] A depiction of this process can be observed in Figure 2-3. This process has potential to be very effective, and offers positive benefit as it operates under ambient temperature and pressure [26]; however, it is primarily

being researched as a complementary process to another desulfurization process, such as HDS, since it removes certain sulfur compounds that HDS does not remove.[27]

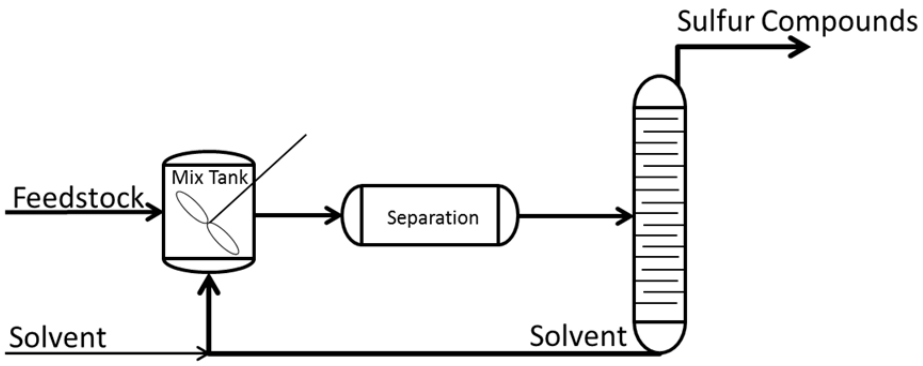

Figure 2-3 Extractive desulfurization process, adopted from (20)

Ionic liquids (ILs) are the state of the art as extractants and are currently being researched.[26,27,28] For example, pyridium-based ILs are insoluble in diesel and are therefore promising extractants for the purpose of sulfur removal in diesel fuel. Gao et al. found these ILs to be satisfactory is sulfur extraction from diesel.[27] In fact, Gao et al. found in a later study that the pyridium-based IL [BMIM][$FeCl_4$] can remove almost 50 wt % of the sulfur in diesel fuel within 10 minutes and can be recycled three times without a significant decrease in performance.[28]

2.3. Oxidative Desulfurization

In the process of oxidative desulfurization (ODS), organosulfur compounds are oxidized to produce polar compounds and then separated easily via extraction, adsorption, or distillation.[29] An example is illustrated in Figure 2-4 where a dibenzothiophene (DBT), which is regularly difficult to desulfurize, is oxidized and converted into a sulfone which can then be separated.[30]

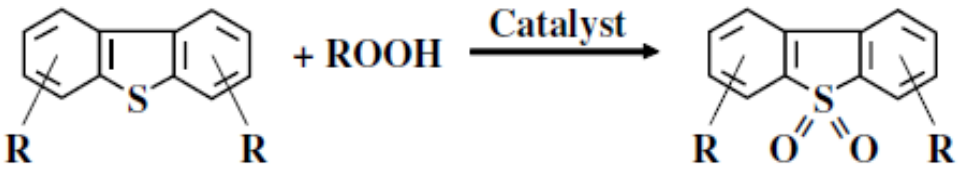

Figure 2-4 Oxidation of dibenzothiophene (30)

Oxidative desulfurization is best as a complementary process, since some sulfur containing compounds such as disulfides oxidize very slowly. This is attractive for application as a secondary process following HDS to produce ultra-low sulfur diesel (ULSD).[30]

There are different types of systems using this process: H_2O_2/organic acid, H_2O_2/heteropolyacid, H_2O_2/MoO_x, H_2O_2/Ti-zeolite, non-hydrogen peroxide, and emulsion catalysis.[29] In the H_2O_2/organic acid system, hydrogen peroxide and an organic acid, usually acetic acid or formic acid, are mixed with the feed and oxidation takes place at atmospheric pressure and under 100°C. Then the product is sent through a liquid-liquid extraction to remove the polar sulfones and sulfoxides. The high-sulfur extract undergoes further processing to remove the sulfur.[29] This process is illustrated in Figure 2- 5.

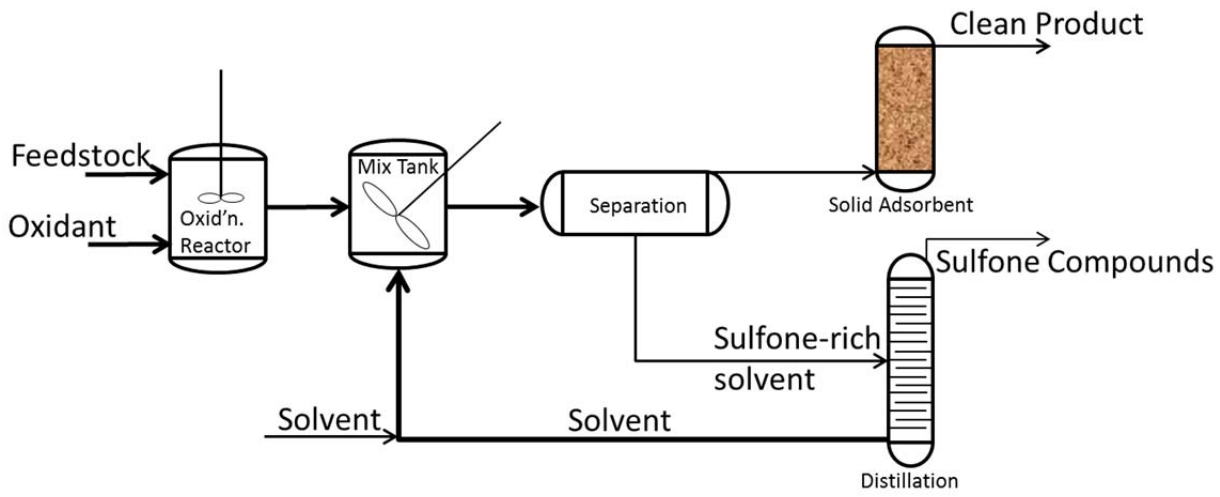

Figure 2- 5 ODS process diagram, adopted from (29)

The H_2O_2/heteropolyacid system is an alternative to the H_2O_2/organic acid system that does not use organic acids. Instead, a heteropolyacid serves as the catalyst. This system is used in an integrated HDS/ODS process[29], outlined in Figure 2-6.

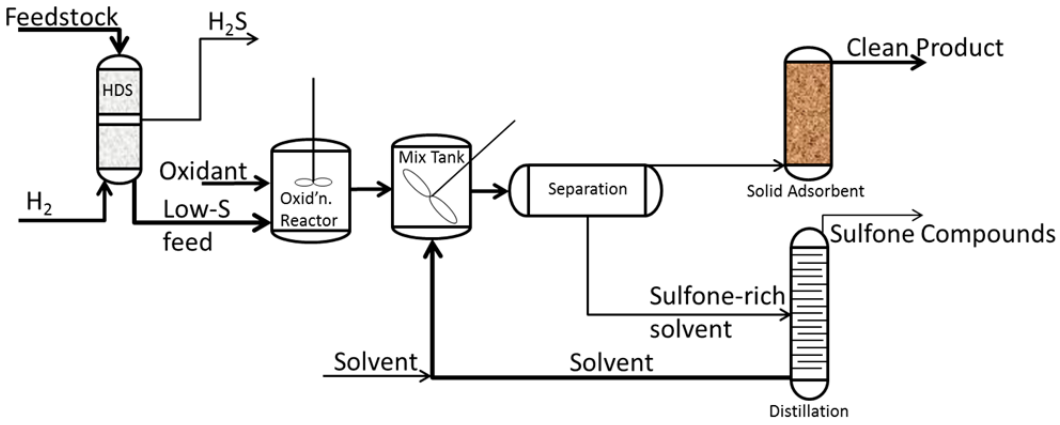

Figure 2-6 Integrated HDS/ODS process diagram, adopted from (29)

The H_2O_2/MoO_x and H_2O_2/Ti-zeolite systems use molybdenum oxide and titanium-containing zeolites as catalysts respectively, rather than an acid. Hydrogen peroxide is attractive

as an oxidant since it is inexpensive compared to other oxidants and "green," producing only water as a liquid degradation product. However, in the desulfurization of diesel fuel, the use of hydrogen peroxide as an oxidant results in an aqueous/organic biphase catalytic system. The sulfur compounds to be oxidized are in the organic phase whereas the oxidant and catalysts are in the aqueous phase. Because of this, oxidation rates are low. Fuel soluble oxidants such as *tert*-butyl hydroperoxide (TBHP) are also undesirable since it is more expensive and therefore unsuitable for industrial scale. Despite being cheap compared to other oxidants, even hydrogen peroxide as an oxidant is considered expensive in terms of process economics, and because of its low efficiency, it is also unsuitable for industrial scale. In order to solve these problems, emulsion catalysis was developed for ODS. This system works based upon the dispersion of one liquid in another liquid via surfactants. Sulfur-containing compounds, hydrogen peroxide, and catalysts interact in a narrow region surrounding each emulsion, called the interfacial membrane (See Figure 2-7). This is very important in ODS. For these reactions, colloidal particles form with surfactant molecules which provide a high interfacial surface area and thus improve the reaction by reducing mass transport limitations.[29]

Non-hydrogen peroxide systems exist, an example being the use of TBHP as an alternative oxidant. In this system, fuel and TBHP are fed over a fixed-bed catalyst under mild temperatures and pressures. The reaction takes place within ten minutes. *t*-Butyl alcohol is a co-product and is easily removable from the stream. Using TBHP as an oxidant reduces the sulfur content to less than 10 μg/g.[29]

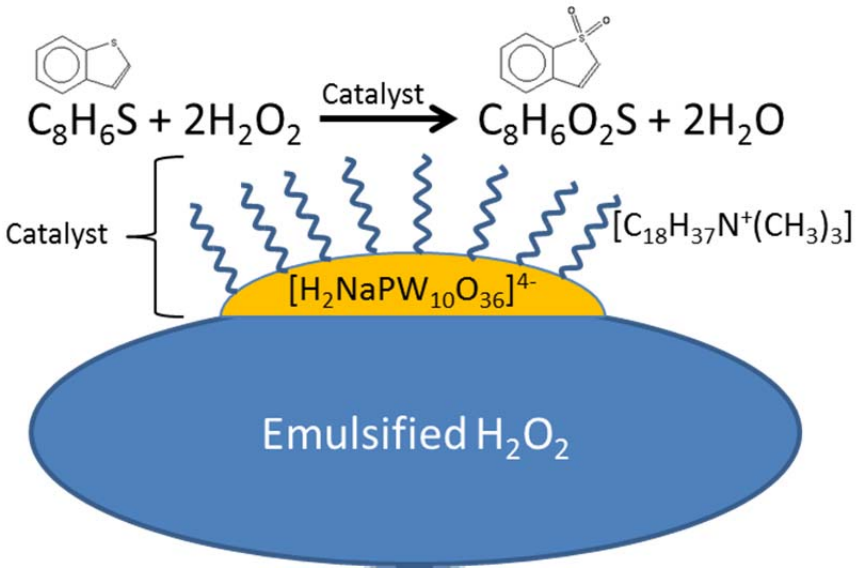

Figure 2-7 Oxidation of benzothiophene in biphase system, adopted from (29)

2.4. Alkylation

Alkylation as a desulfurization process operates by increasing the boiling point of organosulfur compounds through addition of an alkene. An example of this is seen in Figure 2-8.[20]

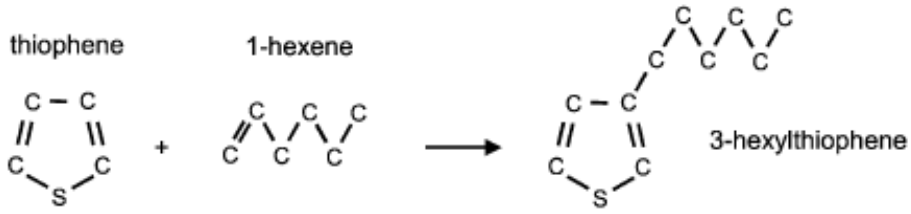

Figure 2-8 Alkylation of thiophene via addition of hexane (20)

This reaction is done with catalysts such as BF_3, $AlCl_3$, $ZnCl_2$, or $SbCl_5$ on silica and/or alumina. The heavier organosulfur compounds are then separated from light fractions by distillation and are concentrated in the heavy boiling part of refinery streams. This can then

undergo other desulfurization processes such as HDS since octane number is not important for diesel fuel. For the reaction in Figure 2-8, 99.5% of the sulfur is removed from the gasoline (light fraction) stream simply through olefinic alkylation of thiophenic sulfur (OATS). The efficiency is limited by competing reactions including alkylation of aromatic hydrocarbons and olefin polymerization. The OATS process is outlined in Figure 2-9.[20]

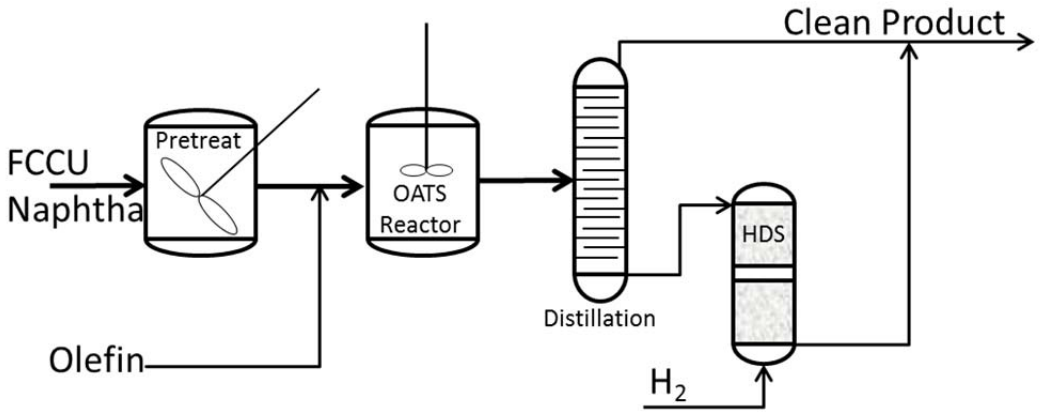

Figure 2-9 OATS process diagram, adopted from (20)

Research has been done into improved catalysts for this process. For example, Arias et al. found silica-supported heteropolyacids to be superior catalysts for OATS.[31] However, Guo et al. repeated their experiments and also tested the proposed catalysts under more realistic conditions and found that more research was necessary to optimize them.[32] In further work by Guo et al. it was predicted that an OATS system with Amberlyst 35 resin as the catalyst, operating at 443K, and applying reactive distillation could result in gasoline with a sulfur content less than 1 ppmw.[33]

2.5. Precipitation

Alkylation can also be used to cause precipitation rather than raising the boiling point of organosulfur compounds. In precipitation, organosulfur compounds are methylated using alkylating agents CHI_3 and $AgBF_3$ to produce *S*-methylsulfonium salts which are then removed as a precipitate. This process can successfully reduce the sulfur content of a vacuum gas oil (VGO) feed stream to 0.1% of the initial concentration.[34] However, this was performed under ideal conditions in the laboratory and in reality, precipitation as a desulfurization process results in a sulfur reduction of about 20% in one batch treatment.[20] Application of alkylation as a means of raising the boiling point is a newer, more state of the art desulfurization process and is superior to precipitation.

2.6. Pervaporation Membrane and Fractionation Separation Processes

Pervaporation membrane separation involves partially vaporizing a liquid through a selectively permeable membrane under a gradient of chemical potential with the downstream side usually being held under vacuum. Membrane materials used include polysiloxane, poly(ethylene glycol), polyimide, polyurethane, and organic-inorganic hybrid membranes.[35,36]

Pervaporation systems consist of a pervaporation cell with temperature control, a membrane housed in the cell, a vacuum system, condensation system, and recovery systems for the permeate and retentate. This is illustrated in Figure 2-10. For desulfurization of gasoline, the pervaporation membrane is usually a non-porous polymeric membrane through which sulfur compounds pass and then evaporate on the downstream side.[36]

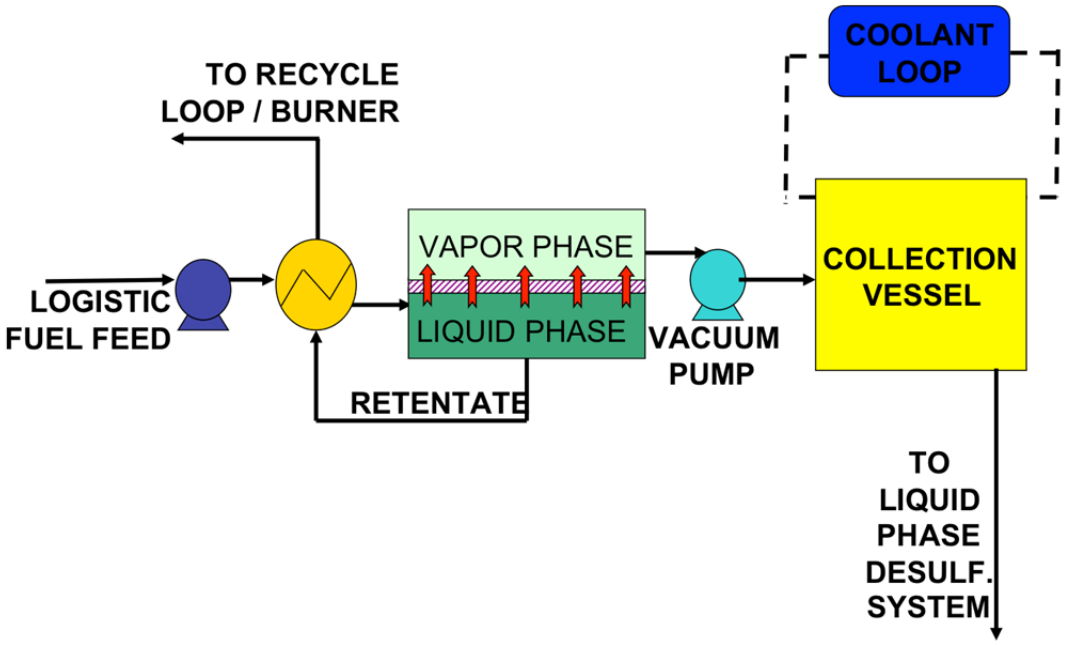

Figure 2-10 Pervaporation process diagram[35]

Pervaporation has many benefits, including[36]:

- Little reduction in octane number
- Low energy requirements
- Environmental benefits
- Simple operation with no eluents, sorbents, additives, catalysts, high flexibility regarding feed, and no feed pretreatment
- Easy scale-up
- Low cost
- High efficacy (reducing sulfur to about 10 ppm)
- Sturdiness of membranes (lasting a minimum of 5 years)
- No chemical transformations

Because of these benefits, pervaporation has already been implemented in pollution control, gasoline desulfurization, separation of azeotropic ethanol-water mixtures, fruit juice processing,

and esterification reactions. However, membrane material choice critically depends on the specific organosulfur compounds to be separated and efficiency depends on the combined effect of flux and sulfur enrichment factor. Research in membrane modification is being done to optimize desulfurization. Optimization of operation parameters is also being researched.[36]

Examples of the split of JP-5 fuel undergoing pervaporation within a Grace S-Brane based process can be seen in terms of the split of sulfur compounds in the pulsed flame photometric detector results seen in Figures 2-11 and 2-12, performed within a Navy laboratory. From PFPD analysis of both of these compounds, it is clear that most of the more complex sulfur compounds are present in the heavy cut (note y-axis intensity values), whereas most of the benzothiophene and simpler compounds are present in the light fraction.

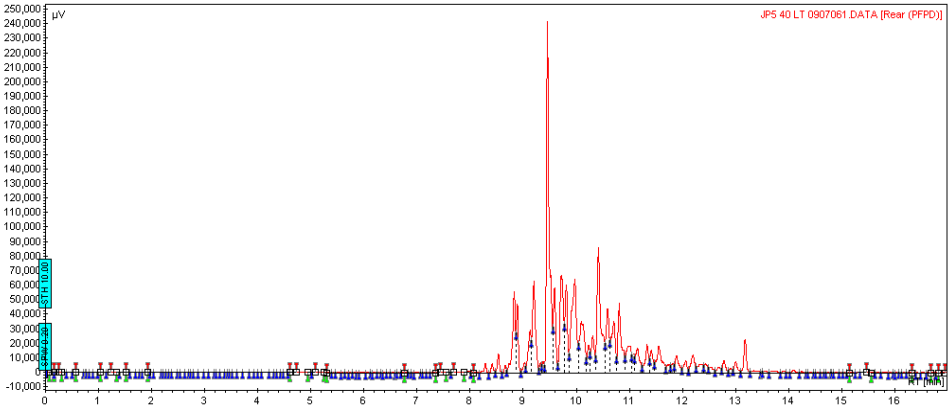

Figure 2-11 40% Light Cut JP-5

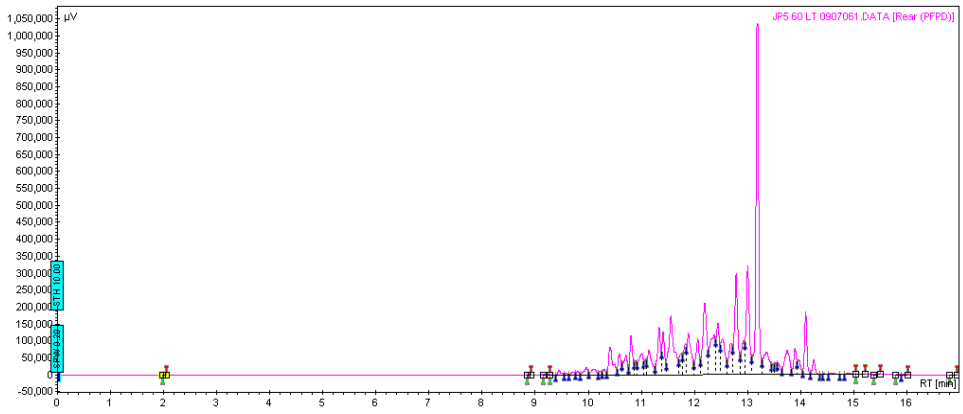

Figure 2-12 60% Heavy Cut JP-5

From observation of the relative levels of detector response, one can determine that more sulfur was contained in the heavy fraction of the fuel, as compared to the light fraction.[18,35,37]

2.7. Adsorption

Though HDS is effective in removing thiols and sulfides, it is not effective in removing thiophenes and thiophene derivatives, which is why one is typically most concerned with these compounds in logistic and diesel fuels. In order to comply with new standards of sulfur content in fuel, adsorptive desulfurization has received attention as a possible new desulfurization method to augment or even replace HDS. This requires finding highly selective sorbents since commercial sorbents are not desirable for this process due to low capacity.[19] Major advances in petroleum refining can be made through this research since adsorptive desulfurization occurs under ambient conditions.[7,38,39]

Adsorptive desulfurization operates by attracting organosulfur compounds to a sorbent, thus removing them from the liquid fuel. Previously explored approaches include adsorptive processes utilizing doped zeolite,[39,40,41,42,43] mixed metal oxides[12,44] and supported adsorbent

materials,[45,46,47,48,49,50] as well as membrane processes[51] and combinations of these with HDS and other adsorptive approaches.[52]

Cu(I)-Y zeolites have been studied by Yang et al.[39,53,54,55, 56,57] Previous studies indicated that the desulfurization capacities follow the order Cu(I)-Y > Ag-Y > H-Y > Na-Y[55] and other similar studies have explored the efficacy of Cu(I), Ni(II) and Zn(II) on X and Y type zeolites prepared under various conditions.[57] On a performance basis, aqueous phase copper(II)-exchanged Y-zeolites, when autoreduced to Cu(I)-Y, are capable of removing substantial quantities of sulfur down to very low levels[55,56]. Issues involving regenerability in moist, high temperature environments and sterically hindered intraparticle diffusion are limitations of these materials.

Another desulfurization approach utilizes supported adsorbent materials. Sorbents supported on templated mesoporous materials have been found to effectively remove sulfur from liquid fuels. Mesoporous materials used include MCM-41 and SBA-15, utilizing metal-based components including nickel,[58] Cu_2O,[18] CuCl, and $PdCl_2$ have been investigated.[59] Thermal hydrostability and loss of surface area and capacity may occur over regeneration and reuse.

Wang et al.[60] tested three desulfurization sorbents: activated carbon (AC), $AgNO_3$/MCM-41, and Cu(I)-Y zeolite. For all thiophenic sulfur compounds in both binary and ternary solutions, the sorbent adsorption capacities followed the order: Cu(I)–Y>$AgNO_3$/MCM-41>AC.[60] Chen et al. studied $AgNO_3$ supported on mesoporous silica SBA-15 and MCM-41 compared to Cu(I)-Y.[42] Molecular orbital calculations showed that Cu^+ (as that in Cu(I)-Y zeolite) formed stronger π-complexation bonding with the thiophenic compounds than Ag^+ (in $AgNO_3$), as evidenced by experimental heats of adsorption. However, pore diffusion limitation

of the large sulfur molecules (alkylated benzothiophenes) became an important factor for desulfurization of high molecular weight jet fuels such that the $AgNO_3$-supported mesoporous sorbents yielded substantially better results than Cu(I)-Y, although Cu(I)-Y was better for a model fuel that contained only small sulfur molecules. Among all sorbents that were investigated, the $AgNO_3$/MCM-41 sorbent showed the best desulfurization performance for high sulfur jet fuels.[42]

The desulfurization properties of titania (anatase) have been studied. It was suggested that the oxygen-rich surface areas where oxygen is dissociatively or associatively absorbed as an "activated O_2" species on the surface may play an important role in adsorption desulfurization.[61] Molecular modeling studies have indicated that these oxygen rich areas are favorable as compared to less oxygen-rich TiO_2 surfaces, and that increased concentration of O_2 on the surface may result in improvement of the adsorption capacity of the adsorbents.[61] The supported adsorbent which is the topic of this paper is silver impregnated onto titania. In a study by Nair and Tatarchuk, Ag (4 wt%)/TiO_2 demonstrated a saturation sulfur capacity of 6.3 mgS/g for JP-5 fuel containing 1172 ppmw sulfur, which is higher than the baseline capacity of titania.[45] Nair and Tatarchuk identified Ag/TiO_2 as a highly performing adsorbent material, and identified the adsorptive capacity characteristics of various loadings of Ag under studies utilizing high molecular weight JP-5 jet fuel.[45] Desired application targets require adsorbents that are low cost and readily manufacturable, utilize commonly available support materials that are well understood and can be obtained in bulk, and are easy to regenerate. The system of Ag/TiO_2 is of particular interest because of its cyclic performance under simple oxidative regeneration conditions in air, high capacity at low Ag metal loading, and no substantial consideration for wastewater or specialty processing equipment.

This Dissertation discusses evaluation of Ag/TiO_2 utilizing various analytical approaches to better understand the nature of the absorbent, the effect of Ag on the support, and the overall influence of Ag on adsorptive capacity.

2.7.1. **Studies of Sulfur Adsorption Interaction**

TiO_2 has been well characterized as an adsorbent and as a catalyst under photochemical processes. The system has been especially studied with SO_2 gas under wet and dry conditions, to better discern the function of surface hydroxyl groups in the interaction and reaction[62], and has shown the presence of hydroxyl groups with FTIR signals consistent with those reported for the Ag/TiO_2 system[63] and other TiO_2 studies.[64] For the SO_2 experiments, oxidation to SO_3 and SO_4 surface species has been indicated and also shown elsewhere under photocatalytic conditions.[65] However, other experiments with direct elemental sulfur interface on TiO_2 appears to avoid oxidation to SO_x, with chains of sulfur atoms arranging to orientations with different surface oxygen structures differing by temperature.[66] Studies of nitroaromatics interfacing with Au/TiO_2 have demonstrated the capability of surface hydroxyls and Ti^{3+} sites to take part in the cleavage and rearrangement of molecular structure, without interfering with the aromatic constituent.[67] Other work has demonstrated that TiO_2 anatase offers mobility of H to move to the subsurface readily as needed under reaction conditions, to serve as a potential source or a reservoir.[68]

One area of limited insight is the interface and interaction of sulfur-bound aromatics with TiO_2 and particularly metals supported on TiO_2. Studies under photo oxidation conditions have shown the oxygen-rich sites in TiO_2 react with sulfur in aromatic molecules and utilize a deprotonation reaction to create the sulfoxide compounds found. This study emphasizes the importance of the surface oxygen in this pathway, and more importantly, indicates multiple cracking reactions occurring including a C-S cleavage, with different pathways occurring

depending upon the different molecules present[69]. Studies of thiophene on TiO_2 also reiterate an importance of oxygen-rich areas on the ability for interaction. Density functional theory calculations on anatase indicate that for the oxygen-rich sites, sulfur in thiophene is bonded with one bridging oxygen and two other free surface oxygen atoms present. It also indicates a weakening of the C-S bond in this condition. Under oxygen-poor site interactions, interaction between a positive charge on surface Ti with a negative charge on the sulfur creates a coordination similar to if the sulfur were an oxygen atom[70]. Overall the preferential adsorption path is the interface with oxygen-rich surface areas, with these results possibly explained on a basis of hydroxyl group formation[71], which would support the presence of a sulfone-like compound, and the observed result that treatment in H_2 decreases capacity as compared to treatment in O_2.[44] These results are consistent with the operation of our Ag/TiO_2 sorbent, which is activated and regenerated in air, and adsorption performed under ambient conditions.

3. Overview of Research Efforts

3.1. Complementary Efforts

Desired application targets require adsorbents based upon scalable, practical and commonly available support materials that are well understood industrially and can be obtained in bulk and at low cost, as this is key to having a practical, functional system that does not have excessive acquisition costs associated with it. The system of Ag/TiO_2 is of particular interest because of its cyclic performance under simple oxidative regeneration conditions in air, high capacity at low Ag metal loading, and no substantial consideration for wastewater, or specialty processing equipment.

Recent efforts have explored the characteristics of the Ag/TiO_2 utilizing techniques such as electron spin resonance (ESR)[47,48], high-vacuum temperature-programmed desorption (HV-TPD)[48], high-vacuum temperature-programmed reaction spectroscopy (HV-TPRS)[48] and X-ray photoelectron spectroscopy (XPS).[46, 47,48 ,49] The sorbent was characterized and found to contain Ag, Ti, O and adventitious C on its surface, as seen by XPS. Analysis of the XPS Auger parameter (AP) and complementary electron spin resonance (ESR) spectroscopy confirmed the silver to be an oxide with the majority present in the Ag^{1+} form, with an extremely minor concentration present as Ag^{2+} in samples of 2, 4 and 8 wt%. The findings by XPS and ESR were supported by X-ray Diffraction (XRD), UV⁺Vis spectroscopy and thermodynamic considerations. Supported Ag was found to be highly dispersed on the surface of the titania support. O_2 chemisorption was used to determine particle size in the range of ~30⁺60 Å depending on the Ag content (4-17 wt%), with an Ag specific surface area of ~7⁺14 m^2/g, vs.

the total surface area of $\sim 114^{+}58$ m^2/g.[49] Difficulties associated with O_2 chemisorption arise because of the baseline assumption that the silver is in the zero valent metallic state.

One area of limited insight is the interface and interaction of sulfur-bound aromatics with TiO_2 and particularly metals supported on TiO_2. Studies under photo oxidation conditions have shown the oxygen-rich sites in TiO_2 react with sulfur in aromatic molecules and utilize a deprotonation reaction to create the sulfoxide compounds found. That study emphasized the importance of the surface oxygen in this pathway, and more importantly, indicates multiple cracking reactions occurring including a C-S cleavage, with different pathways occurring depending upon the different molecules present[78]. Studies of thiophene on TiO_2 also reiterate an importance of oxygen-rich areas on the ability for interaction. Density functional theory calculations on anatase indicate that for the oxygen-rich sites, sulfur in thiophene is bonded with one bridging oxygen and two other free surface oxygen atoms.[70] These DFT studies also indicate a weakening of the C-S bond in this condition. Under oxygen-poor site interactions, interaction between a positive charge on surface Ti with a negative charge on the sulfur creates a coordination similar to if the sulfur were an oxygen atom[79]. Overall the preferential adsorption path is the interface with oxygen-rich surface areas, with these results possibly explained on a basis of hydroxyl group formation[80], which would support the presence of a sulfone-like compound, and the observed result that treatment in a reducing H_2 environment decreases capacity as compared to treatment in O_2[44]. These results are consistent with the operation of our Ag/TiO_2 sorbent, which is activated and regenerated in air, and adsorption performed under ambient conditions.

3.2. Basis of Work Performed

The application of a technique that allows for an *in situ* analysis of specific atoms in their natural environment is beneficial for the study of adsorbed sulfur within a sorbent material, and validation of the structural changes postulated on the basis of simulation and XPS. Application of The X-ray Absorption Near-Edge Structure (XANES) and Extended X-ray Absorption Fine Structure (EXAFS) supports atom-specific structural analysis in an *in situ* application of a realistic material, system and conditions. Thus it is an ideal technique to study the structure and potential changes to the atomic structure around the atoms of interest under adsorption conditions. A body of work does exist to show the basis for K and/or L-edge EXAFS for model compounds. Even complex multicomponent mixtures have been analyzed, primarily for use as an approach to understand the constituents present in bitumen, asphaltines and other heavy crude products[81,82,83,84]. The approach has been found to be useful due to the strong dependence of the XANES on the oxidation state and local coordination geometry of the environment[84,85,86]. In this work, the nature of the adsorbent materials and their changes under adsorption of sulfur for real distillate fuels (Navy F-76 distillate and JP-5 jet fuel) as well as benzothiophene (as a single component) are reported. The basic understanding of the surface, coupled with operational insight helps to identify unique changes to the overall molecular structure that may occur upon adsorption, and may facilitate the creation of superior adsorbents, methods for treatment, or other improvements in the body of knowledge associated with adsorption, dispersed metal adsorbents and catalysts, and the application of X-ray spectroscopy techniques to develop materials.

3.3. Overview of Studies Performed

This work utilizes multiple techniques to better identify the surface structure and interactive character of sulfur heterocycle adsorption. The approaches include X-Ray Dispersion (XRD) and X-Ray Photoelectron (XPS) analysis, as well as a major emphasis on Extended X-

Ray Absorption Fine Structure (EXAFS), via Silver K-edge (22514 eV), Silver L-edges (3806, 3524, 3351 eV), Sulfur K-edge (2472 eV), and Titanium K-edge (4966 eV) studies and analysis. The intent is to better understand the basis of the dispersed silver phase's role in enhanced adsorptive performance based upon information discerned from the EXAFS-based materials structure[87,88,89], coupled with the other techniques. Application of these techniques helps to elucidate the dispersed nature of silver oxides on TiO_2 and SiO_2 supports, and supports the identification of the structures and characteristics of the silver phase. To support this analysis framework, it is beneficial to have reference materials analyzed that exhibit known structure and metal-oxygen bonding characteristics, so that characteristics can be compared to support the theoretical analysis which identifies the local coordination structure.[90] In order to create the background for analysis of the Ag/TiO_2 system, characterization of references including Ag, AgO, Ag_2O, $AgNO_3$, TiO, TiO_2, Ti_2O_3, S, BT, DBT, methyl-substituted DBT, Mg and Zn sulfates, the Ag/TiO_2 system at various metals loading points, and Ag/SiO_2 at 2wt% metal loading were performed. As applicable, materials were investigated under XPS, XRD and XAS. The utilization of the techniques and approaches provide a unique perspective to the mechanisms and interaction effects associated with the adsorption performance identified previously.

3.4. EXAFS Technique Discussion

The use of X-ray Absorption Spectroscopy as a tool to discern the fundamental characteristics of the Ag/TiO_2 system is central to the resolution of hypothesized characteristics proposed previously and discussed within this document. Specifically, utilization and analysis of the X-Ray Absorption Near Edge Structure (XANES) and Extended X-Ray Absorption Fine Structure (EXAFS) regions of the X-ray spectra obtained when measuring the absorption coefficient for a sample of a material under evaluation at a high

intensity X-ray source. The typical source of such X-rays is a synchrotron, and for this work, specifically the National Synchrotron Light Source (NSLS) at Brookhaven National Laboratory. At the highest level, EXAFS provides an indication of the distance between a central atom and its nearest neighbors[91], the nature and type of which may be determined by comparative or theoretical evaluations.

The collection of X-ray absorption spectra can be performed by multiple techniques which will be covered within this document. In terms of general technique, spectra are collected by measurement of the absorption coefficient, μ, which is defined as a function of the intensity of an X-ray source transmitting through a material in the form:

$$I = I_0 e^{-\mu t}$$

Equation 1 – Absorption coefficient as based upon Beer's Law

Where the value I_0 is the measured intensity of the x-ray beam aimed to the material, and I (typically defined with a subscript related to the detector in a multi-stage beamline) being the intensity transmitted through or given off by the material sample of thickness t.[97] The technique is performed by comparing incident X-ray intensity to the value measured through or off of a sample, with the most basic measurement performed as a count of photoionization within a sealed chamber filled with a noble gas.[89] The value of the absorption coefficient is related to the X-ray source energy, as well as the density of the material, and the atomic mass and number of the material of interest.[97] The absorption coefficient is then defined as:

$$\mu(E) = \log(I_0/I)$$

Equation 2 – Measurement of energy dependence of the absorption coefficient

which can be monitored for its characteristic change about the binding energy at which an inner-shell electron can be excited.[97]

X-rays are directed from a synchrotron light source via a beamline, which provides the isolation of specific energy light. An unfocused beam is taken from the synchrotron ring, through entrance slits to a double crystal monochromator, which isolates specific energy X-rays. This monochromatic light can be tuned stepwise through an energy range as is required for the material of interest. The beam passed out of the monochromator is further restricted by slits to decrease the beam to a useful and manageable size, and to prevent detector saturation. This beam passes through a first ionization chamber to provide a measurement of the incident X-rays, providing the valuation for I_0.[88,89] For the example of a transmission experiment, the beam then passes through a sample, into another ionization chamber which measures the transmitted beam, then through a reference material (generally a metal foil of the element being studied) and through another ionization chamber, to measure the remnant beam. An example of such an experiment can be seen in Figure 3-1.

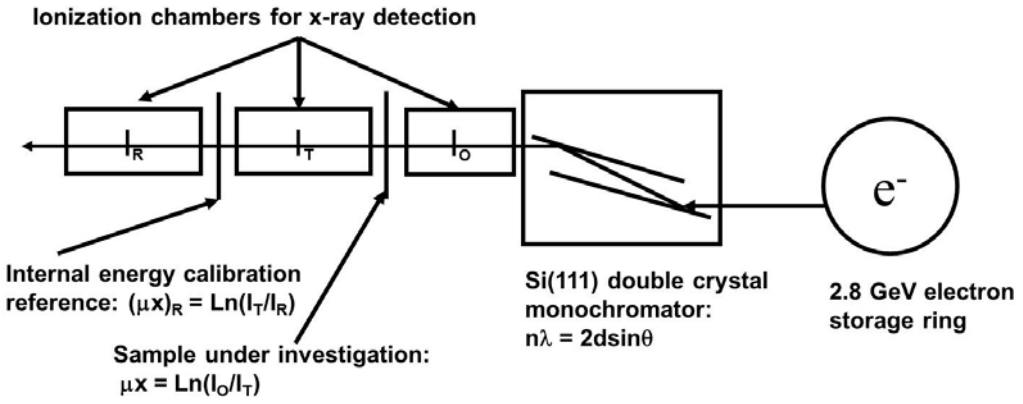

Figure 3- 1 Schematic of a transmission EXAFS experiment with reference

X-rays focused upon a sample are gradually changed through an energy range suitable to perturb inner shell electrons. The energy range is well established for pure materials, and the technique can generally be considered element specific, given the tunability of the X-ray range within the experiment. During an experiment, the intensity of μ is measured as a function of the energy range about the binding energy for the electron ring of the material of interest. As the X-ray energy approaches that of the binding energy of the core-level electron, the absorption increases greatly, causing a substantial rise, or "edge", which provides substantial information pertaining to the material being studied. The energy of the X-ray utilized may be tuned to both the material, as well as the electron shell of interest. For example, in Figure 3-2, the analysis is on EXAFS for the K-edge, which is specific to the 1s electrons. The application of the silver L-edge is also of interest because of its ability to probe multiple final states, specifically those associated with the transitions originating from the 2s (L_I), 2p1/2 (L_{II}), and 2p3/2 (L_{III}) orbitals. Specific edges are probed either due to the energy level required (for example, for actinides, the energy of the K-edge is sufficiently high that a beam to experimentally probe these states cannot be accessed while the L-edges can be readily studied, i.e. ~100keV versus ~18keV), or because of differences in the information that may be accessed from edge to edge.[92]

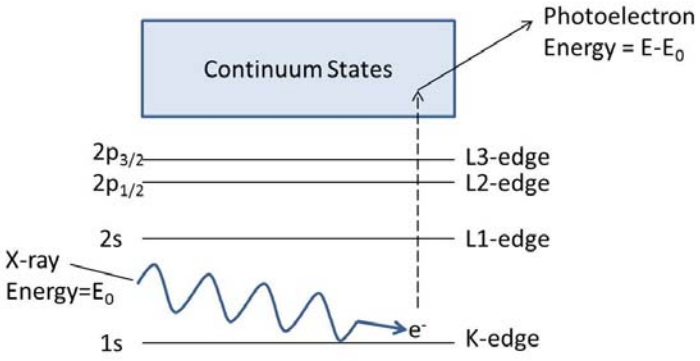

Figure 3- 2 Example of K-edge EXAFS experiment, which excites 1s electron[92,97]

The techniques that may be utilized to collect EXAFS spectra include transmission, fluorescence, and electron yield measurement. The transmission measurement is the most basic, with ionization chambers present to measure absorption through a sample of optimal thickness to provide an absorption edge jump of an optimal value. Transmission experimentation probes the bulk of the material, the depth of the analyzed region being determined by the foil thickness or powder particle size mass, parameters optimized during the EXAFS measurement preparation. As indicated in Figure 3-1, a monochromatic beam is passed through a series of detectors filled with a noble gas. The first chamber measures a quantity related to the incident intensity while the second chamber (behind the sample) measures a quantity related to the transmitted intensity. The same effect is measured around a reference sample. Figure 3-3 shows a picture of the beamline X11A at Brookhaven National Laboratory[93] as set up for performing experiments on the Ag/TiO_2 system in both transmission and fluorescence mode.

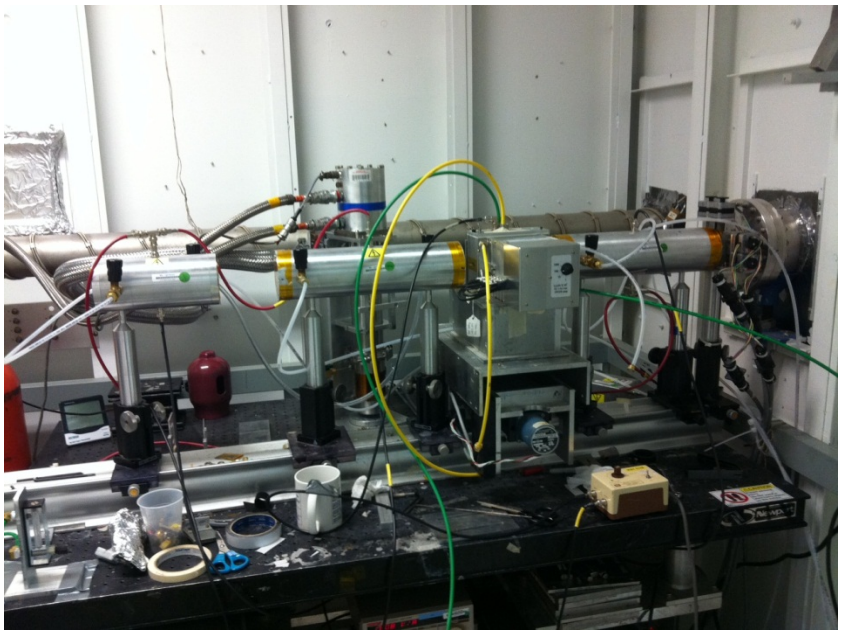

Figure 3- 3 Transmission and fluorescence detector setup on X11A, BNL NSLS

The transmission within the sample is a function of the photoionization cross section and is energy dependent accounting for final state effects as the photoelectron is scattered by neighboring atoms. The oscillations are created due to the interference of the outgoing photoelectron wave with the backscattered wave from neighboring atoms, as depicted in Figure 3-4. The interference process depends mostly on the energy of the outgoing photoelectron, the distance between the atoms, and the phase shifts of the central and backscattering atoms.[94]

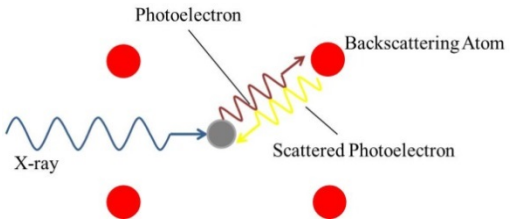

Figure 3- 4 Example of X-ray excitation with photoelectron emission and backscattering

The fluorescence yield and electron yields are the product of X-ray absorption, related to the decay of an excited atom. The decay process yields a fluorescent photon, an Auger electron and other secondary electrons. Their yield is proportional to the energy-dependent photoionization cross section, similar to Equation 3, where,

$$\mu(E) \propto I_f / I_0 \propto |\langle i|H|f\rangle|^2$$

Equation 3 – EXAFS fluorescence proportionality and Fermi's "Golden Rule"

with *i* indicating the initial state and *f* the final state, with *H* being the interaction term, which represents the change of energy and momentum.[97] Thus the signal obtained is similar to what is observed in transmission EXAFS. The intensity of the fluorescence signal is measured by an

ionization chamber with multiple collection grids, while the electron yield signal is measured with an aluminized Mylar window current collector biased positively with respect to the sample. The variations in the number of fluorescent photons or electron current as a function of incident photon energy is measured as a quantity related to the absolute intensity.[94] Fluorescence detection is useful because of the added range that is provided by the technique. Depending upon sensor type, more than two orders of magnitude of additional sensitivity can be obtained, allowing extension to substantially dilute samples.[91] Electron yield detection offers substantially increased sensitivity at very shallow probing depths[95], thus making it a quite surface-selective approach, since electrons can only escape from a near-surface region of the sample.[96]

Figure 3-5 Electron Yield Detector

In general, the X-ray Absorption Spectroscopy technique is commonly called X-ray Absorption Fine Structure (XAFS), and includes a full spectra of the oscillations and position and slope of the edge and nearby areas. The slope and character of the absorption edge is specifically called X-ray Absorption Near Edge Structure (XANES); and the oscillations overall, including at higher energies, which is called Extended X-ray Absorption Fine Structure (EXAFS). The term EXAFS is generally used to define the whole experiment, which is typically run from some energy slightly before the edge, to an energy much higher than the edge.[88] Figure 3-5 depicts the areas per these definitions, for a silver system.

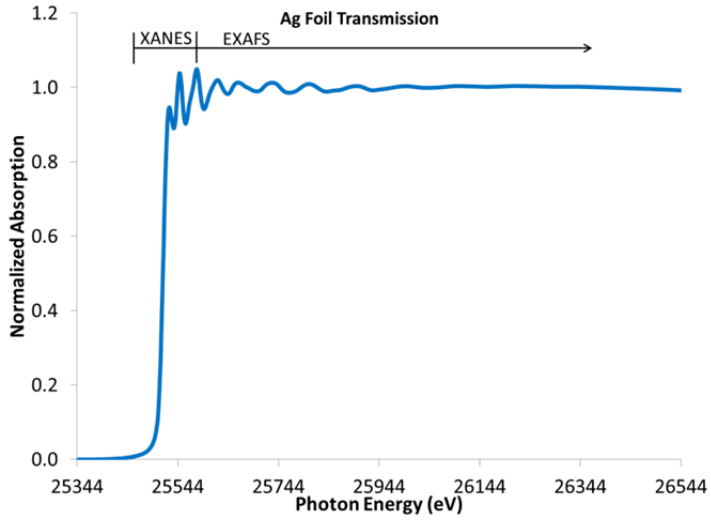

Figure 3-6 Transmission spectra showing range of XANES and EXAFS

Data reduction is performed via mathematics coded within software packages, and the derivations of the fundamental equations can be found elsewhere.[88,97, 98] The reduction of the spectra as shown in Figure 3-6 and 7 can be performed via a function that considers all scattering paths for the emitted photoelectrons. Through identification of edge features and extension of pre and post-edge lines, a background subtraction can be performed via a spline function that models only the low frequency components of the absorption coefficient, assumed to be the value of $\mu_0(E)$, which is indicative of a theoretical absorption parameter for an atom with no nearest neighbors.[99,100,101] An example of the drawing of the pre and post edge lines and creation of the background spline can be seen in Figure 3-7. The remaining information is a valuation of the oscillations associated with the backscattering amplitude of nearest neighbor atoms, which can be mathematically described as the equation:

$$\chi(E) = \frac{\mu(E) - \mu_0(E)}{\Delta\mu_0(E_0)}$$

Equation 4 – EXAFS fine structure formula

where the denominator term is the valuation of the edge step, which is the difference of the pre and post edge lines. The value χ(E) is converted to a wavenumber value by the equation:

$$k = \sqrt{\frac{2m(E - E_{0)}}{\hbar^2}}$$

Equation 5 – Conversion of EXAFS in terms of wavenumber

(where m is the mass of an electron) yielding the value χ(k). To provide emphasis to higher values of k, where the oscillations tend to be weaker, often the χ(k) value is multiplied by an exponential value k^x, where x=1,2,3.[97,99] The oscillations seen will be unique in terms of backscattering, due to the unique electron configuration of the atom.[89,102]

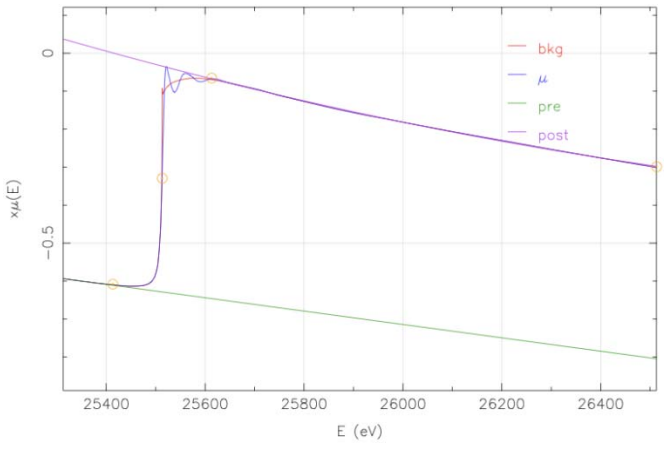

Figure 3-7 Example of a 4wt% Ag/TiO_2 spectra with pre and post edge valuations and a background spline fit

With the actual EXAFS data extracted, and converted into the wavenumber form of k-weighted χ(k), a Fourier transform may be performed over a selected range of k-values, which provides insight into the spacing of coordination shells[87,102]. These shells are phase shifted analogies to bond distances to other neighboring atoms.[97] Thus, by plotting the Fourier transform value χ(R), one can discern the nearest neighbor structure of the material studied in terms of distance from the absorbing atom, number of atoms, and interaction characteristics of the coordination shells.[87] Thus, from data obtained from an EXAFS experiment, one can obtain useful insight into the local structure and electronic nature around a specific atom, and potentially have sufficient satisfactory insight from this alone.

For materials where there are multiple variants of a specific coordinated atomic structure, further analysis will be required. This is the case for materials such as the oxides of silver, where AgO, Ag_2O and $AgNO_3$, amongst others, all have locally coordinated oxygen. Thus, modeling based upon theory associated with the crystallographic data must be performed, in order to attempt to capture behaviors and characteristics unique to the specific atomic structure character of a reference material. To perform such analysis, one must consider the EXAFS equation:

$$\chi(k) = \sum_j \frac{N_j S_0^2 f_j(k) e^{-2R_j/\lambda(k)} e^{-2k^2\sigma_j^2}}{kR_j^2} \sin\left[2kR_j + \delta_j(k)\right]$$

Equation 6 – The EXAFS Equation

where f(k) and δ(k) are known, atomic number-dependent scattering properties, and λ(k) the mean free path. Given insight to these parameters, the distance to neighbor j, R, the coordination

number of the neighboring atom, N, and the mean-square disorder of neighbor distance, σ^2 can be calculated based upon fits associated with the theory of paths for nearest backscattering atoms.[97] The fit of a data form (as opposed to experimental form) of $\chi(k)$ is obtained by evaluation of the above equation for one or more paths, and then performing summation of all paths. Within the equation is a multiplicative term, $N_j * S_0^2$ in the summation numerator. N is the coordination number and S_0^2 is a parameter associated with the overlap of the electronic states (relaxation of electrons) of the absorbing atom before and after the creation of the core-hole.[94,103] The coordination number is an important parameter to understand as it provides indication of number of nearest neighbors.[104] However, the two values cannot be measured independently[105], thus the value for S_0^2 must be assumed, evaluated or obtained by another means. Experimental evaluation, which is the method utilized within this work, is obtained through temperature-dependent evaluation of a pure foil. For example, experimentation on a silver foil within the range of 19-300K provided a value of S_0^2 of 0.94. Generally the value can be assumed to be near one[94,103], and it is generally chemically transferrable between compounds with the same central scatterer. With crystallographic insight to provide characteristics of scattering paths, along with the values mentioned, fits of one or more paths can be performed to evaluate the structure of a material studied within an EXAFS experiment. Fit of the $\chi(k)$ value can be performed with the valuation of bond length shift as compared to the crystal structure given as a path basis, with statistics provided to allow comparison in terms of goodness of fit. Through the comparison of fitting different and possibly multiple paths, one can determine the exact nature of the material studied.

3.5. Experimental

3.4.1. **Sample Preparation**

- Silver

Ag/TiO_2 and Ag/SiO_2 samples were prepared according to the techniques outlined by Nair and Tatarchuk,[45,50,106] which utilized $AgNO_3$ over support materials from St. Gobain (Norpro Grade ST61120 3.2 mm pellets) as well as Alfa 44429 (lot K14T024) TiO_2 pellets. Grade 21 SiO_2 was obtained from Grace Davison Co. $AgNO_3$ was sourced from Alfa as product 11414 and combined with deionized water from the laboratory. The $AgNO_3$ solution was produced based upon knowledge of pore volume required to reach incipient wetness and desired silver metal loading. Pellets of support material had the solution applied until incipient wetness and then were dried and calcined in air at 450°C. Previous work by Nair and Tatarchuk has confirmed the level of variability and performance using sorbent materials made by this approach.[45] After sorbent materials were produced, sample particles were ground in a mortar and pestle and then sifted, with the fine particles smaller than a No. 325 Tyler mesh retained for the tests.

Reference materials for the X-ray Absorption Spectroscopy (XAS) measurements were procured from different manufacturers. Ag_2O and Ag(I,III)O from Aldrich, $AgNO_3$ from Salt Lake Metals, and 10 micron thick Ag foil from Materials by Metron. One micron size particles of Boron Nitride (BN) from CERN was utilized as needed in producing self-supporting pellets for the reference materials to optimize the quality of the X-ray absorption measurements.

- Sulfur

Ag/TiO_2 sorbent material and a TiO_2 "blank" (impregnated with HNO_3 and calcined) were produced as reported previously[45]. The samples which were impregnated and calcined as

larger particles were crushed to a -325 mesh powder to ensure fast contacting and wicking of the liquid and sorbent in a consistent manner.

Fuel samples were taken from U.S. Navy sources and included an 8800ppm(w) F-76 distillate fuel and an 1172ppm(w) JP-5 jet fuel. These fuels are high-flashpoint cuts designated for shipboard use, and differ from common #2 diesel and Jet-A fuels. Standards were produced at 2000ppm(w) concentrations from benzothiophene (BT), dibenzothiophene (DBT) and 4,6-dimethyl dibenzothiophene (4,6 DMDBT), in octane, all from Sigma Aldrich, for use as comparison with the XANES spectra of the fuels. Benzothiophene was selected because of its variants' existence in both JP5 and F-76 fuels, per chromatography previously performed by the Navy for studies of our fuels.

The use of kapton tape for preparation of samples for S k-edge analysis is established in the prior literature[107] , and the materials were verified to be sulfur free. Reference thiophenic compounds and unadsorbed fuel samples were prepared by wicking into Millipore Type HA 0.45μm cellulose filter paper until the paper was fully and consistently wet. The samples of Ag/TiO_2 at different loadings, and TiO_2 powder were segregated into small masses and isolated, and each was impregnated with a liquid sample of fuel or benzothiophene solution until incipient wetness. The samples were impregnated in a darkened fume hood, and were mixed during the impregnation sufficiently to see that all particles were wetted by the liquid sample in a consistent manner. Visually it was observed that the samples that utilized octane as a solvent slowly dried out in the fume hood, while the samples of JP-5 and F-76 retained a liquid sheen of slight wetness. All samples were placed into vials, capped, and kept out of light until prepared for XAFS analysis. Additional reference standards of magnesium and zinc sulfate and sulfur

powder were also utilized in the course of studies and were produced by rubbing a consistent layer of material onto kapton tape and affixing the tape to the sample holder.

- Titanium

Ag/TiO_2 samples were prepared in the same procedure as above, which utilized $AgNO_3$ over support materials from St. Gobain (Norpro Grade ST61120 3.2 mm pellets) as well as Alfa 44429 (lot K14T024) TiO_2 pellets. Reference materials of TiO_2 (anatase and rutile), Ti_2O_3, and TiO were sourced from Alfa. One micron size particles of Boron Nitride (BN) from CERN was utilized as needed in producing self-supporting pellets for the reference materials to optimize the quality of the X-ray absorption measurements. Fuel samples used for adsorption were taken from U.S. Navy sources and included an 8800ppm(w) F-76 distillate fuel and an 1172ppm(w) JP-5 jet fuel. 2000ppm(w) benzothiophene (BT) reference solution (in octane, both from Sigma Aldrich) was also utilized as a reference material with known structure and characteristics.

Powder material for all samples was ground and sifted to -325 mesh. When samples were used for adsorption experiments, powders were impregnated in a darkened fume hood, and were mixed during the impregnation sufficiently to see that all particles were wetted by the liquid sample in a consistent manner. Visually it was observed that the samples that utilized octane as a solvent slowly dried out in the fume hood, while the samples of JP-5 and F-76 retained a liquid sheen of slight wetness. All samples were placed into vials, capped, and kept out of light until prepared for X-ray Absorption Fine Structure (XAFS) analysis. For the experiments, -325 mesh powder was spread on conductive carbon tape.

- In Situ Sample Preparation

Sorbent samples were prepared using standard processes for the production of Ag/TiO_2 material. $AgNO_3$ solution from Alfa (product 11414) was impregnated into TiO_2 pellets from St. Gobain (Norpro Grade ST61120 3.2 mm pellets) based upon manufacturer's stated pore volume, until incipient wetness was reached. The pellets were then crushed and pressed into a shape and form suitable for insertion into the in situ cell. A control sample of $AgNO_3$ in Boron Nitride (BN) from CERN was also made for comparison purposes. Boron Nitride was selected because of its favorable X-ray properties and use as a diluent in other silver EXAFS studies. The BN powder was sifted to -400 mesh and separated, then small drops of $AgNO_3$ solution were added slowly, into the powder until it had the appearance of near-wetness. This powder was then dried and pressed into a pellet form identical to the $AgNO_3/TiO_2$ mixture used. While the silver loading of the samples is not consistent due to the inconsistent pore structure and particle sizes between BN and TiO_2 in this preparation, it was not considered to be a major concern for the analysis of trends and comparative studies. Samples were pressed in a 5x11mm die at 500psi, which was sufficient to produce a self-supporting pellet that could be inserted into the cell. An image of the catalyst furnace installed on the beam line is shown in Figure 3-8.

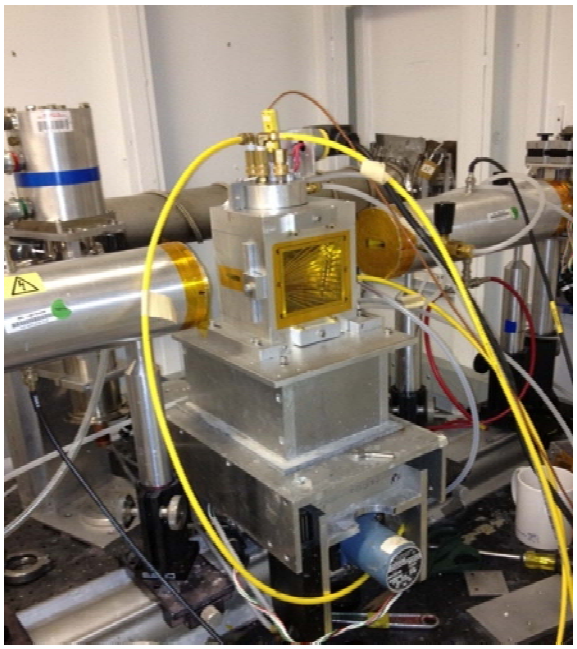

Figure 3-8 Catalyst furnace with air, inert gas and water cooling connections made Chamber shows "solar slits" behind yellow kapton sheet, to direct fluorescence into a 5-grid detector that would attach at that side

3.4.2.**Measurements**

3.4.2.1. **XRD measurements**

The phase composition of the Ag/TiO_2 catalysts and the standards were investigated by powder diffraction using the Bruker D8 Advance diffractometer with Cu K_α X-rays (λ = 1.5404 Å).

3.4.2.2. **XPS measurements**

The XPS spectra of the Ag/TiO_2 and the standards were measured using a Physical Electronics model 5400 X-ray photoelectron spectrometer. The powder material was pressed into a thin self-supporting pellet and mounted directly onto the sample holder with the aid of copper clips placed next to the pellet to restrict its movement. The pellet was then transferred to the introduction chamber, which was evacuated for 10-15 min before transferring the sample to

the analysis chamber. The data were collected at room temperature using nonmonochromatic Al Kα (1486.6 eV) X-ray source operating at 400 W (15 kV and 27 mA). Data collection proceeded when the pressure in the analysis chamber reached ≈2 x 10^{-8} Torr. Survey spectra (0 – 1200 eV) were collected at analyzer pass energy of 89.45 eV, which corresponds to analyzer resolution of 1.34 eV, 0.5 eV/step, integration interval of 50 ms/step and averaging over 10 cycles. Multiplex spectra (C 1s, O1s, Ag 3d, Ag MNN, and Ti 2p or Si 2p) were collected with analyzer pass energy of 22.35 eV which corresponds to analyzer resolution of 0.34 eV, 0.1 eV/step and an integration interval of 50 ms/step. The multiplicity of each region with each cycle was adjusted based on its intensity in the survey spectrum and averaging over 20 cycles. All spectra were collected at an electron takeoff angle of 45°. The binding energies for all samples were referenced to the binding energy of the C 1s line for adventitious carbon at 284.6 eV. Curve fit analysis of the photoemission lines was done using a combined Gaussian-Lorentzian line shape except in the case of the Ag 3d line where an asymmetric line-shape function was used. A Shirley-type function was used to account for the background intensity. The composition in atomic percent of the relevant elements was determined from survey and multiplex spectra using the integrated areas after subtracting the satellite contributions and a Shirley-type background and using the relative sensitivity factors provided by Physical Electronics for our spectrometer.

3.4.2.3. **XAFS Measurement and Analysis Process**

- Silver K-edge

The X-ray absorption fine structure (XAFS) experiments were conducted on the bending magnet station X-11A of the National Synchrotron Light Source with the electron storage ring operating at electron energy of 2.8 GeV, 25 bunch and a stored current in the range of 200 to 300 mA.[108] The XAFS spectra at the Ag K-edge (25514 eV) were collected in transmission mode

using a variable exit double-crystal monochromator with two flat Si(311) crystals detuned by 20% to minimize the harmonic-content of the beam. The incident and transmitted beam intensities were monitored using 30 cm long ionization chambers with flowing argon. A third 15 cm long ionization chamber with argon was used to monitor the transmitted intensity of the Ag foil reference to insure accurate calibration of the energy scale for the Ag K-edge spectra. The XAFS spectra were collected at temperatures in the range of 19-300 K. Temperature control was achieved with a closed cycle Displex helium refrigerator (Air Products).

Powder material for all samples was ground and sifted to -325 mesh. For the Ag_2O, AgO, and $AgNO_3$ standards, an appropriate quantity of the sifted powder for each specimen was thoroughly mixed with boron nitride. Approximately 100 mg of the mixture was placed in a die and pressed into self-supporting pellet with dimensions of 5 mm x 12 mm. The weight fraction of the material in the mixture was adjusted to yield an absorption edge jump near 1.0. For the Ag/TiO_2 adsorbent materials, an appropriate quantity of the sifted Ag/TiO_2 powder (without mixing with BN) was pressed into self-supporting pellet. In this case, the loading/unit area was adjusted such that the absorption edge jump remains near 1.0 while the total absorption above the edge does not exceed 2.6. For all samples, the X-ray absorption edge jump in transmission mode was kept below 1.5 in order to minimize the effects of pinholes[109] and particle size[110] on XAFS amplitudes. Two layers of a 10 micron thick Ag foil were used throughout the experiments to insure accurate calibration of the monochromator energy scale. A summary of the absorption edge jumps for all samples is given in Table 4-5.

The XAFS data analysis was carried out using the IFEFFIT suite of programs (Athena and Artemis).[98,99] The XAFS spectra were calibrated with respect to the Ag foil energy at half-height, which has been assigned to 25514 eV. The K-edge absorption was isolated by fitting the

pre-edge region (-300 to -100 eV for Ag) to a first order polynomial, extrapolating over the entire range of the spectrum, and then subtracting the background from the entire spectrum. Energy independent step normalization was applied by fitting the post-edge region (100 to 860 eV) to a cubic polynomial and extrapolating back to the edge energy. The extended X-ray absorption fine structure (EXAFS), $\chi(k)$, was extracted using multi-node cubic spline procedures, which minimized the amplitude of non-physical peaks in the 0-1.0 Å region of the Fourier transform. The k-range for the EXAFS spectra was limited to 2-10.2 $Å^{-1}$ in order to avoid significant distortions in the amplitudes of the EXAFS spectra above k=10.2 $Å^{-1}$ due to multi-electron effects as demonstrated earlier by Fulton et al.[111]

The XAFS data were fitted using theoretical standards calculated based on the curved-wave scattering formalism of the FEFF Code (version 8.2).[112,113] The FEFF calculations were performed using Ag crystallographic data for the Ag-Ag path[114] of a silver central atom with cluster size of 6.0 Å, containing 55 atoms, and $AgNO_3$ crystallographic data was utilized as a basis for the Ag-O path.[115] According to this report given by Wycoff, $AgNO_3$ has rhombohedral symmetry with a space group R-3c. However, no specific estimate was provided for the oxygen coordinates. A value of 0.25 for the U parameter was used based upon values given for other nitrates in the same report. The fits were performed in real space using Fourier transforms generated from k^3-weighted EXAFS spectra over the range of 3-10.0 $Å^{-1}$ and a Hanning window of 1.0 $Å^{-1}$. The value of the many body amplitude reduction factor (S_0^2) for Ag was estimated from multi-data sets of temperature dependent XAFS spectra of the Ag foil in order to reduce the correlation with the Debye Waller factor. These spectra are shown in Figure 3-9, where strong temperature dependence is clearly observed. Its value was determined to be 0.94 ± 0.02 and was used in the analysis of all other samples. The value was validated by performing additional

temperature-dependent measurements of an Ag_2O reference, which yielded the same value, within the bounds of error of the original analysis. For the Ag/TiO_2 adsorbents with Ag loading of 4 wt% or less, the first coordination sphere was satisfactorily analyzed using a single Ag-O path. For 8, 12 and 20 wt% loadings, the major contributions were analyzed as the sum of an Ag-O path from an oxide phase and an Ag-Ag path from metallic Ag. For each path, the coordination number (N) distance (R), disorder (σ^2), and inner potential (E_0) were used as adjustable parameters. The number of fitting parameters was kept below the maximum number of independent data points allowed by the Brillouin theorem.[116] The goodness of each model is given by the value of the R-factor, which is the sum of the square of residuals between measured and model data normalized to the magnitude of the measured data.

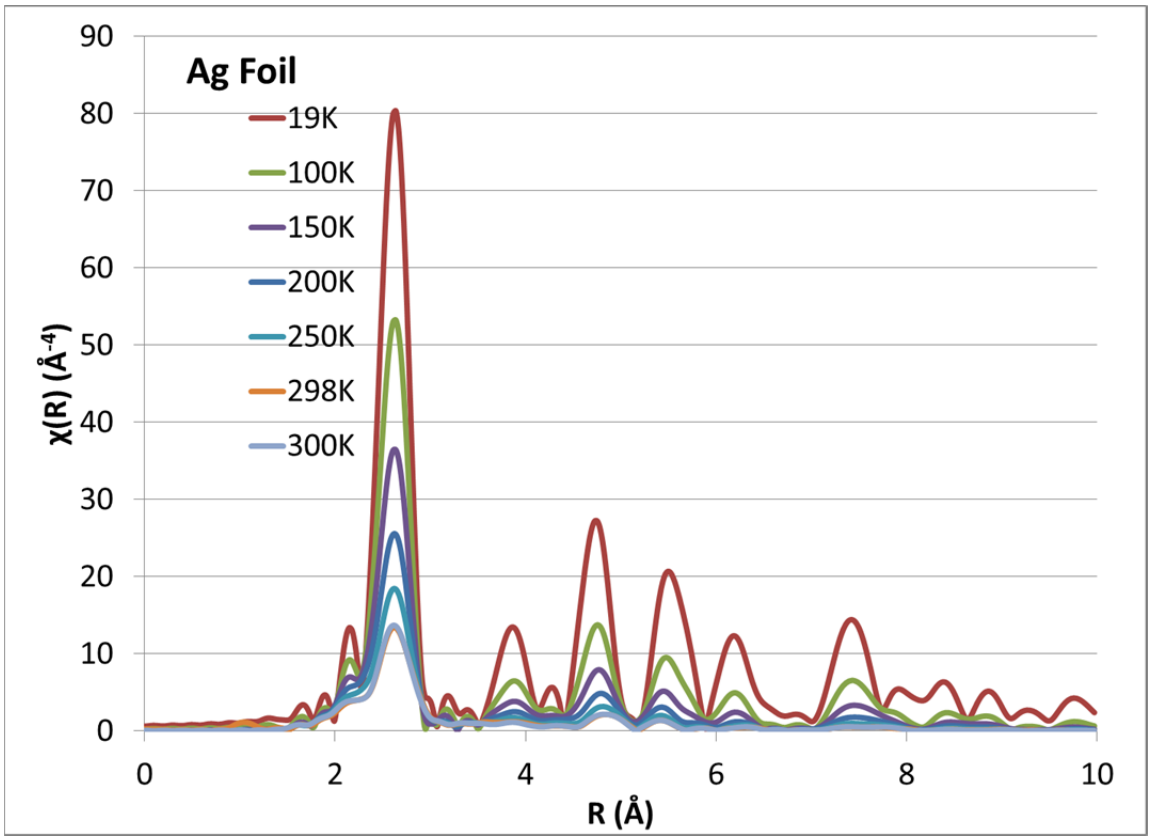

Figure 3-9 Temperature Dependence on Disorder of Reference Silver Foil

- Silver L-edge

The XAFS Ag L-edge experiments were conducted on the bending magnet station X-19A of the National Synchrotron Light Source with the electron storage ring operating at electron energy of 2.8 GeV, 25 bunch and a stored current in the range of 200 to 300 mA. [117] X19A is a focused beamline with Rh coated collimating and toroidal focusing mirrors. The silver L_{III}-edge (3351 eV) spectra were collected at room temperature using a He purged sample chamber arranged with aluminum holder oriented at 45 degrees with respect to the incident X-rays. A fluorescence detector (Canberra PIPS) was mounted inside the chamber. The beamline utilizes fixed exit Si(111) double-crystal monochromator with feedback on the second crystal for detuning to minimize the harmonic-content of the beam. In our experiments, the detuning was set to reduce the peak intensity by 70%. The energy resolution near the silver L_{III}-edge is 0.7 eV. The chamber and the safety hutch were both kept completely dark to prevent unwanted signal in the fluorescence measurements. The intensity of the incident X-rays was monitored using an ionization chamber with He flow. The XAFS data were collected in increments of 4, 0.25 and 1 eV over the energy ranges of 3251-3331, 3331-3401 and 3401-3521 eV, respectively. Integration interval was set to 1 second for all regions

For the L-edge experiments, approximately 75 mg of the adsorbent material was placed in a die and pressed into self-supporting pellet with dimensions of 5 mm x 12 mm. Due to the low silver content except in the case of the 20 wt%), these samples satisfied the thick-dilute limit for fluorescence data collection, which is required to avoid distortions in the XAFS amplitudes due to self-absorption phenomena. [118] Initial studies indicated that beam reduction occurred, and thus samples were placed into the sample chamber, gasses allowed to equilibrate, and then

spectra immediately collected without further beam alignment or other operations. This caused the spectra to be collected with zero prior exposure to the beam, ensuring that the damage was kept to a minimum.

For the Ag_2O, AgO and $AgNO_3$ references, the -325 mesh powders were thoroughly mixed with BN at weight percentages of 20.8, 21.8 and 27.9, respectively, and then 80 mg of the mixture for each sample was pressed into a self-supporting pellet.

The XAFS data analysis was carried out using the IFEFFIT suite of programs (Athena and Artemis).[98,99] The energy scale was calibrated by assigning the inflection edge energy of Ag foil to the well-established value for metallic Ag, namely 3351 eV. The Ag L_3-edge absorption was isolated by fitting the pre-edge region (-90 to - 30 eV for Ag) to a first order polynomial, extrapolating over the entire range of the spectrum, and then subtracting the background from the entire spectrum. Energy independent step normalization was applied by fitting the post-edge region (50 to 150 eV) to a cubic polynomial and extrapolating back to the edge energy. The extended X-ray absorption fine structure (EXAFS), $\chi(k)$, was extracted using multi-node cubic spline procedures, which minimized the amplitude of non-physical peaks in the 0-1.0 Å region of the Fourier transform. The L_3 edge k-range for the EXAFS spectra was limited to 6.5 $Å^{-1}$ due to the overlap with the L_2 edge.

- Sulfur K-edge

The X-ray absorption fine structure (XAFS) experiments were conducted on the bending magnet station X-19A of the National Synchrotron Light Source , as described previously. In our experiments, the detuning was set to reduce the peak intensity by 70%. The energy resolution near the sulfur K-edge is 0.7 eV. The chamber and the safety hutch were both kept completely

dark to prevent unwanted signal in the fluorescence measurements. The intensity of the incident X-rays was monitored using an ionization chamber with He flow. The XAFS data were collected in increments of 2, 0.25 and 1 eV over the energy ranges of 2402-2452, 2452-2501 and 2501-2641 eV, respectively. There was no indication that the beam induced significant radiation damage (beam reduction) under these conditions, which was verified by collecting and comparing multiple scans for each sample.

Samples were mounted within the He purged chamber over a rectangular window in an aluminum holder oriented at 45 degrees with respect to the incident X-rays direction and the surface of the PIPS detector. The organic model references and fuels on Millipore paper were taped in place to the window of the holder. However, the impregnated TiO_2 and Ag/TiO_2 adsorbents were pressed into self-supporting 75mg pellets of $5x12mm^2$, and mounted with the aid of scotch tape on the back-side edges, outside of the beam path. No noticeable reaction of the tape occurred with the remnant fuel vapors. Due to the low sulfur concentrations in the model compounds and the fuels, these samples satisfied the thick-dilute limit for fluorescence data collection, which is required to avoid distortions in the XAFS amplitudes due to self-absorption phenomena.[118] The Mg and Zn sulfate references do not appear to suffer from significant distortions due to self-absorption but the amplitude of the white line for the sulfur reference is significantly reduced due to self-absorption and apparent pinholes in the coverage of sulfur on the tape. However, these inorganic references were used only to establish the relationship between edge energy and oxidation state and results were found to be consistent with previously reported results as will be discussed later in the text.

The XAFS data was reduced using the IFEFFIT suite of programs (Athena).[98,99] Athena was utilized to subtract the pre-edge, post-edge normalization, and to merge multiple scans to

enhance the signal to noise ratio of the spectra. For the purpose of extracting the background and performing normalization, the edge energy was assigned to the inflection point energy of the main peak (most intense white line) for all of the reference samples. However, in the case of the JP-5, F76, and BT adsorbed on TiO_2, 4 wt% Ag/TiO_2 and 20 wt% $AgTiO_2$, the edge energy was assigned to the inflection point energy of line which corresponds to organic sulfur (near 2474 eV). The pre-edge background was determined by fitting a linear polynomial over the energy range of -40 to -15 eV relative to the edge energy, then extrapolating over the entire energy range and subtracting it from the entire spectrum. The post edge background was determined by fitting a second order polynomial over the energy range of 50-150 eV relative to the edge energy. The XANES data was normalized by dividing the background-subtracted absorption by the value of the post edge absorption calculated at the edge energy. The spectra were exported to Excel for plotting purposes. The curve fitting of the XANES was performed in the (D) Athena version (Demeter 0.9.18) using Ifeffit 1.2.11d.

- Titanium K-edge

The XAFS Ti K-edge experiments were conducted on the bending magnet station X-11A of the National Synchrotron Light Source as described previously. The XAFS spectra at the Ti K-edge (4966 eV) were collected in the electron yield mode using a variable exit double-crystal monochromator with two flat Si(111) crystals detuned by 50% to minimize the harmonic-content of the beam. The energy resolution at the Ti K-edge is ~1.4 eV. The incident and transmitted beam intensities were monitored using 30 cm long ionization chambers with flowing argon. The electron yield current was measured in a Lytle detector (The EXAFS company) using an aluminized Mylar foil biased at +48 V with respect to the sample. The sample compartment contained helium to increase the detector gain by generating secondary electrons. A third 15 cm

long ionization chamber with argon was used to monitor the transmitted intensity of the Ti foil reference to insure accurate calibration of the energy scale for the spectra. The Ti XAFS data were collected in increments of 5 and 0.4 eV and 0.05 $Å^{-1}$ over the energy ranges of 4666-4936, 4936-5016 and 5016-6070 eV, respectively. Integration intervals were set to 1 second for the first and second regions (pre-edge and XANES) and linearly proportional to the wave number in the third region in order in order to increase the signal to noise ratio in the EXAFS region.

The -325 mesh powders from the adsorbent material and TiO, Ti_2O_3 and TiO_2 references were spread onto electrically conductive carbon tape from TED PELLA, Inc., Redding, CA. In this way, the XAFS amplitudes are not expected to suffer from distortions related to the particle size or thickness effects.

The Ti K-edge absorption was isolated by fitting the pre-edge region (-100 to - 30 eV) to a first order polynomial, extrapolating over the entire range of the spectrum, and then subtracting the background from the entire spectrum. Energy independent step normalization was applied by fitting the post-edge region (50 to 650 eV) to a cubic polynomial and extrapolating back to the edge energy. The extended X-ray absorption fine structure (EXAFS), $\chi(k)$, was extracted using multi-node cubic spline procedures, which minimized the amplitude of non-physical peaks in the 0-1.0 Å region of the Fourier transform. The upper limit of the k-range for the EXAFS spectra of the oxide samples was limited to 2- 12.0 $Å^{-1}$ based on the signal to noise ratio for the oxide samples.

4. Results

4.1. Silver XRD

XRD was utilized to gain insight into the crystal structure and physical properties of the sorbent materials. The XRD patterns for the Ag/TiO_2 adsorbents at various Ag loading levels are shown in Figure 4-1. All of the Bragg diffraction lines are characteristic of anatase TiO_2 reference (ICDD # 01-071-1166) with no indicative metallic silver character (ICDD # 00-004-0783) or silver oxide character is seen except in the case of the 20 wt% sample where a small contribution from metallic silver is seen. Because of lack of sensitivity to the structure of the supported Ag at loadings below 20 wt%, XRD was determined to be inconclusive and so alternate techniques were utilized.

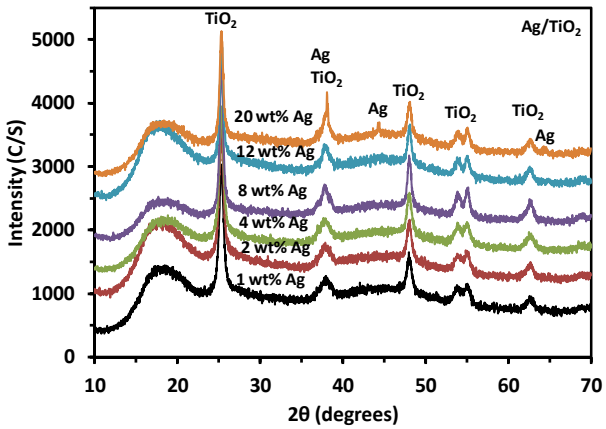

Figure 4-1 X-ray diffraction data of the Ag/TiO_2 adsorbent materials as a function of the Ag loading in wt%. The silver phase is detectable only at the highest Ag loading of 20 wt%.

4.2. XPS Results

XPS investigation was carried out in order to identify the composition and chemistry of the surface region and in particular the oxidation state of Ag in the sorbent material as a function of the Ag loading. The compositions of the surface regions for the sorbent materials as determined

from survey spectra and multiplex spectra are summarized in Tables 4-1 and 4-2. Clearly, the compositions for the Ag/TiO_2 are dominated by oxygen, titanium, moderate amount of carbon, some silver and a small amount of nitrogen. As one would expect, the surface silver intensity increases in the Ag loading. Typical spectra of the C 1s and O 1s regions are shown in Figure 4-2 and Table 4-4 while those of Ti 2p and Ag 3d regions are shown in Figure 4-3 and Figure 4-6. The C 1s and O 1s regions display multiple chemistries and therefore, deconvolution of these peaks into three and two contributions, respectively, is necessary to extract the binding energy (BE), full width-half-maximum (FWHM), and percent area for each component. Summary of the deconvolution results of various photoemission lines for the Ag/TiO_2 and Ag/SiO_2 sorbent materials is included in Table 4-3. In addition, we included the results for a sample of anatase TiO_2 impregnated with HNO_3 dried and calcined at 450 ^oC, Ag, Ag_2O, $AgNO_3$ and AgO reference materials. In Table 4-3, we list the BE, FWHM, and atomic percent for each component. In Table 4-4 we list the Auger parameter (α) defined as the sum of the binding energy of the Ag $3d_{5/2}$ photoelectron line and the kinetic energy of the X-ray induced Ag ($3d_{3/2}4d4d$) Auger line, the spin-orbit splitting for the Ti 2p doublets, the difference between the binding energy of the O 1s line for lattice oxygen and the Ti $2p_{3/2}$ line (ΔO_{1s}-$Ti2p_{3/2}$), the ratios of the atomic concentrations for lattice O to Ti (O_{lat}/Ti), surface oxygen to lattice oxygen in TiO_2 (O_{surf}/O_{lat}), total oxygen to Si (O/Si), and titanium to silver (Ti/Ag). Hereafter, the various photoemission lines will be discussed in detail.

Table 4-1 Summary of XPS results from Survey Spectra

Sample	**At% C**	**At% N**	**At% O**	**At% Ti or At% Si**	**At% Ag**
TiO_2 calcined in HNO_3 at 450C	7.1	2.10	64.4	26.4	N/A
0.24 wt% Ag/TiO_2	15.6	0.61	60.2	23.5	0.15
1 wt% Ag/TiO_2	13.1	0.81	61.3	24.5	0.31
2 wt% Ag/TiO_2	10.6	0.84	62.3	25.3	0.98

4 wt% Ag/TiO_2	13.3	0.58	60.0	23.7	2.42
8 wt% Ag/TiO_2	20.1	0.65	54.7	21.0	3.60
12 wt% Ag/TiO_2	16.6	0.57	56.2	21.5	5.23
20 wt% Ag/TiO_2	17.9	0.82	54.8	20.7	5.81
2 wt% Ag/SiO_2	2.20	0.0	70.8	26.6	0.38
Ag (sputtered)					100.0
Ag_2O	31.3	N/A	26.6	N/A	42.2
AgO	23.9	N/A	38.4	N/A	37.7
$AgNO_3$	22.5	13.1	45.9	N/A	18.5

Table 4-2 Summary of XPS results from multiplex spectra

Sample	**At% C**	**At% N**	**At% O**	**At% Ti or Si**	**At% Ag**
TiO_2 calcined in HNO_3 at 450C	6.60	2.04	64.44	26.92	N/A
0.24 wt% Ag/TiO_2	14.33	N/D	60.27	25.23	0.17
1 wt% Ag/TiO_2	12.12	N/D	61.47	26.11	0.29
2 wt% Ag/TiO_2	9.82	N/D	62.93	26.33	0.92
4 wt% Ag/TiO_2	12.84	N/D	59.38	25.27	2.50
8 wt% Ag/TiO_2	19.76	N/D	54.38	22.13	3.73
12 wt% Ag/TiO_2	15.45	N/D	56.19	23.05	5.31
20 wt% Ag/TiO_2	16.49	N/D	55.41	22.28	5.82
2 wt% Ag/SiO_2	1.80	N/D	71.13	26.73 (Si)	0.34
Ag (sputtered)	N/A	N/A	N/A	N/A	100
Ag_2O	26.72	N/A	28.24	N/A	45.04
AgO	21.51	N/A	40.47	N/A	38.01
$AgNO_3$	19.72	13.00	44.45	N/A	22.83

C 1s region

The C 1s regions for all samples are deconvoluted into three components except in the case of the Ag/SiO_2 sample where a single component is sufficient. As shown in Figure 4-2 and Table 4-3, all samples display a contribution from adventitious carbon and its biding energy is set to 284.6 eV and is used to calibrate the spectra of all samples in order to account for charging. The second component with binding energies in the range of 286.1-286.3 eV is normally attributed to carbon singly bound to oxygen or a hydroxyl group. However, this

scenario can be ruled out in this case since the oxygen region does not show a component with binding energy in the range of 532.6-533.6 eV, which corresponds to oxygen or the hydroxyl group singly bound to carbon. The third component with binding energies in the range of 288.5-288.7eV is normally attributed to a carboxylic or ester group (O-C=O).[111] Again, this scenario can be ruled out since the oxygen region does not show a contribution from oxygen, which is singly bound to carbon as in the carboxylic group.[119] Based on the binding energies for the second and third components, we believe that the second and third components can be assigned to the two carbon atoms in the C2N-C=O functional group. The reported binding energy for the carbon singly bound to N is near 286 eV, which is in close agreement to our measured binding energy of the second carbon component. Furthermore, the reported binding energy for the carbon bound to both the nitrogen and the oxygen atoms is 288.3 eV[120], which is in close agreement with our experimentally measured binding energy for the third carbon component. The reported binding energy for the doubly bound oxygen in the C2N-C=O functional group is 530.9 eV[120], which is in close agreement with our experimentally measured binding energy of the minor component in the oxygen region, as will be shown later in the text.

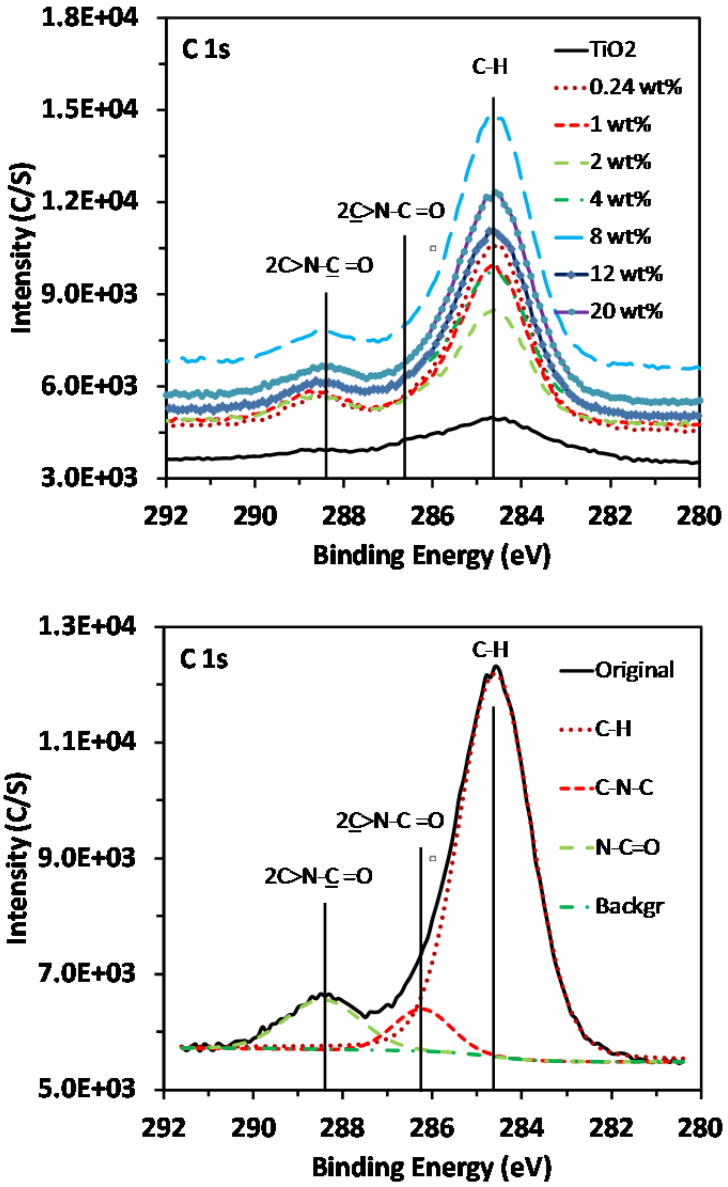

Figure 4-2 Carbon 1s photoemission region for the TiO_2 and Ag/TiO_2 adsorbent materials as a function of the Ag loading in wt%
The vertical lines indicate the presence of multiple chemistries. The spectra are calibrated with respect to hydrocarbon at 284.6 eV to correct for sample charging.

Ti 2p region

The binding energies for the Ti 2p3/2 line for all samples are in the range of 458.2-458.4 eV, which are consistent with those reported for TiO_2, namely, 458.3 eV[121] and 458.1 eV.[120] As

pointed out by Atuchin et al., the reported binding energies for Ti 2p3/2 in TiO_2 differ by as much as 1.55 eV due to energy referencing issues, especially based on adventitious carbon. Atuchin et al.[122] introduced the parameter Δ(O-Ti), which is calculated as the difference in the binding energy of the lattice oxygen 1s line and that of the Ti 2p3/2 line, as a sensitive measure for changes in the oxidation state and local structure of Ti since its value is independent of sample charging. As shown in Table 4-4, the values of Δ(O1s-Ti3/2) for the TiO_2 and Ag/TiO_2 samples are within a narrow range of 71.20-71.24 eV indicating no obvious change in the electronic structure of the TiO_2 support occurred upon incorporation of Ag into the support. These values are in close agreement with that reported by Atuchin et al. for anatase TiO_2 (71.4 eV)[122] but are significantly smaller than those reported for Ti_2O_3 (72.9 and 73.1 eV)[123] and TiO (75.0 and 76.7 eV)[123] indicating that the Ti4+ state is retained in the adsorbent material regardless of the Ag loading in the range 0-20 wt%. It is postulated that Ag may interact with the TiO_2 support, inducing electronic changes in the interfacial region between the silver phase particles and the TiO_2 support. However, depending on the size of the Ag particles, such changes may not be detectable due to the attenuation of photoelectrons from the bottom of the Ag agglomerate. It is to be noted that the FWHM for the Ti 2p3/2 line remained unchanged with Ag loading in the range of 0-4 wt% and increased only slightly from 1.35 to 1.47 eV upon increasing the Ag loading to 20 wt%. These results indicate that at 8, 12, and 20 wt% loadings, the structure of the TiO_2 support may become somewhat defective but the oxidation state of Ti remains as +4. The ratio of the surface atomic concentrations of Ti and Ag, Ti/Ag in Table 2, was calculated based upon the concentrations given in Table 4-1. The ratios indicate a trend of reduced surface Ti atoms as the Ag loading increases. A major change is observed at ca. 4 wt% Ag, where a rapidly decreasing ratio is followed by a fairly slowly decreasing ratio. Between

0.24 and 4% Ag loading (~17x change), the Ti/Ag ratio decreases by a factor of approximately 21 times. From 4 to 20 wt% Ag (5x change), the Ti/Ag ratio decreases by less than half. This indicates that the initial loading of silver disperses well in vacancies or at other locations on the TiO_2 surface, which rapidly masks the Ti signal. However, after these locations are depleted, the Ag phase grows in such a way that it does not substantially affect the exposure of the TiO_2 surface, i.e. through the formation of large crystals without substantial reduction in surface area. At 2wt%Ag, it is interesting to note that Ti/Ag ratio is significantly lower that of the Si/Ag ratio. For the same Ag loading on Ag/TiO_2 and Ag/SiO_2, the higher ratio in the case of the Ag/SiO_2 sorbent material indicates that Ag particles have a lower degree of dispersion on the SiO_2 support.

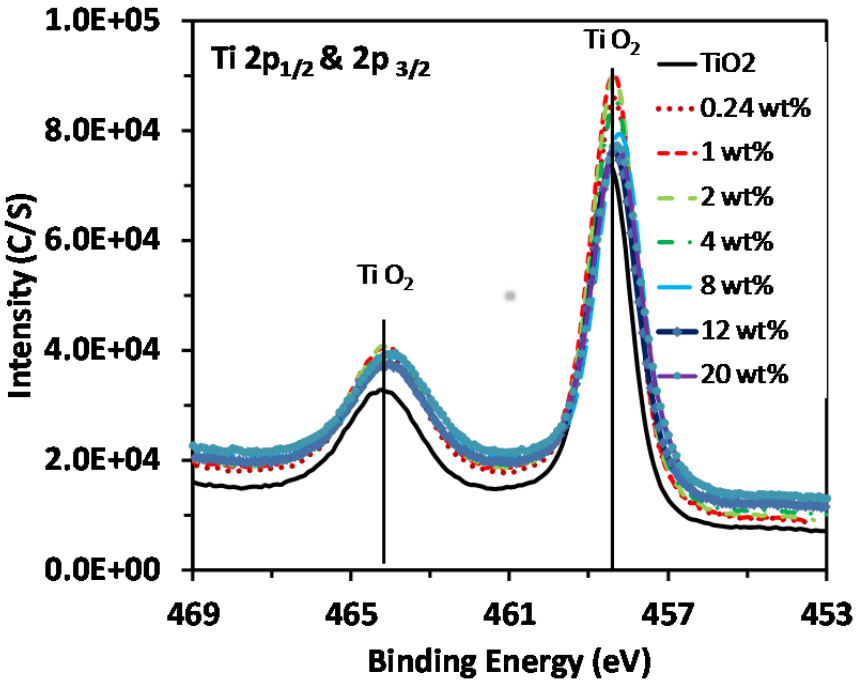

Figure 4-3 Ti 2p photoemission region for the Ag/TiO_2 adsorbent materials as a function of the Ag loading in wt%.
The vertical lines indicate the binding energies for the spin-orbit doublet for metallic silver.

O 1s region

As shown in Figure 4-4 and Table 4-3, the oxygen 1s region for the TiO_2 and the Ag/TiO_2 adsorbent material display a major component with binding energies in the range of 529.3-529.5 eV and a minor component with binding energies in the range of 531.1-531.2 eV. The double peak structure is prominent in many of the earlier XPS reports on TiO_2 prepared with different methods. [122,123,124,125] The low binding energy component has been attributed to lattice oxygen in TiO_2. This assignment is supported by the measured ratio of the atomic percentage for lattice oxygen and titanium (O_{lat}/Ti) for the calcined TiO_2 support, which was found to be 2.2, close to the nominal value of 2.0. This ratio remained within a narrow range (2.1-2.2) regardless of the silver loading suggesting that the oxidation state of Ti is unchanged upon silver incorporation, which is in agreement with conclusion based on the Ti 2p data. The FWHM remained unchanged for loadings in the range of 0-4 wt% Ag, but increased slightly from 1.44 to 1.53 eV upon 20 wt% of Ag; this trend is similar to that observed for the Ti $2p_{3/2}$ line. The high binding energy component has a contribution from O doubly bound to carbon as determined on the basis of the C 1s region and discussed above. However, based on the carbon concentration, only a moderate amount (~1.5 atomic %) can be attributed to this oxygen chemistry. Based on previous reports,[124,125] the majority of this signal can be related to the presence of hydroxyl groups on the surface. [124,125] This assignment is consistent with the fact that transition metal hydroxides (such as $Cu(OH)_2$, $Co(OH)_2$ and $Ni(OH)_2$) display a major component in their oxygen 1s spectra with binding energy ≈531 eV.[126]

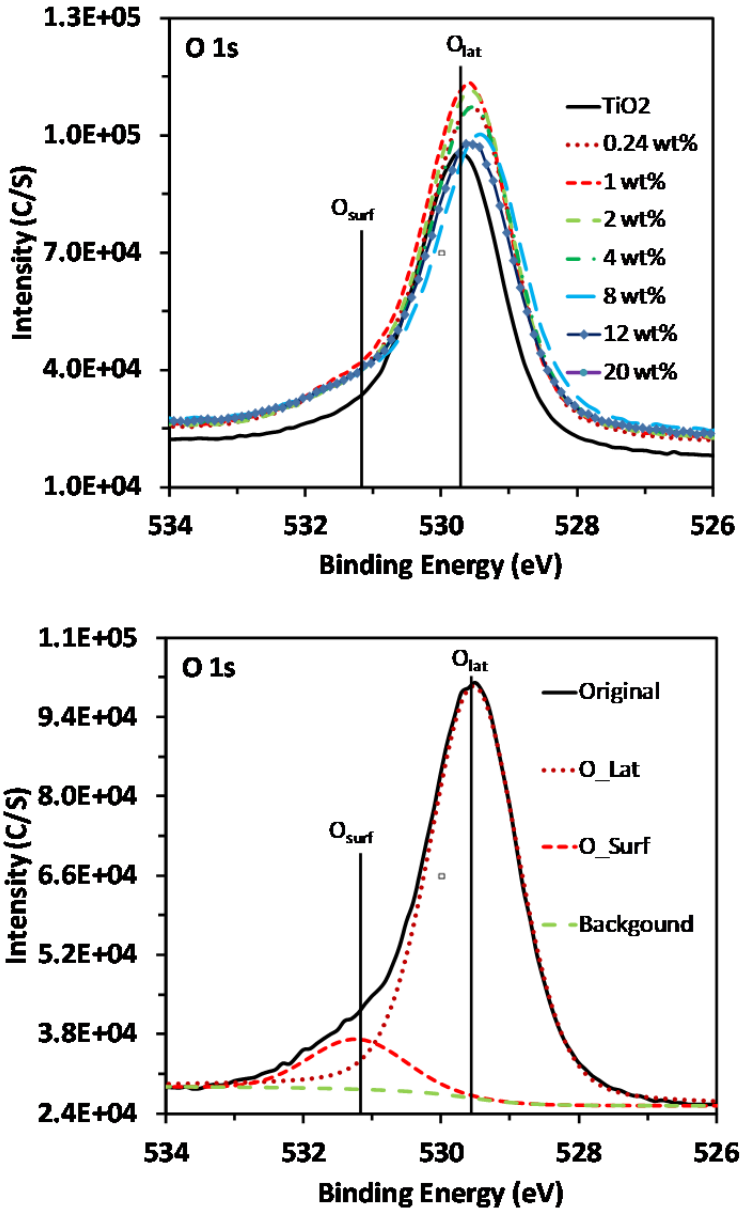

Figure 4-4 Oxygen 1s photoemission region for the TiO_2 and Ag/TiO_2 adsorbent materials as a function of the Ag loading in wt%
The vertical lines indicate the binding energies of the lattice oxygen and surface oxygen in TiO_2.

Since these surface hydroxyl groups play an important role in the desulfurization of benzothiophene and sulfur containing fuels, further discussion is warranted.[63] As shown in Table 4-4, calcination in the presence of $AgNO_3$ resulted in a significant increase in the ratio of

the number of surface oxygen to lattice oxygen (O_{surf}/O_{lat}) relative to calcination of a sample impregnated with HNO_3. The ratio increases from 0.076 (sample impregnated with HNO_3 and calcined without any silver content) to 0.155 and 0.134 for Ag loadings of 0.24 and 1 wt%, respectively. As the amounts of silver in these two samples are very small, the doubling in the O_{surf}/O_{lat} ratio is most likely not due to the physical presence of silver in the support but rather to heat-treatment of the TiO_2 support in the presence of $AgNO_3$ vs. HNO_3. For higher loadings (2-20 wt% Ag), the ratio decreases and remains within a narrow range of 0.11-0.12, which is still an increase from the TiO_2 without any silver content. As the Ag loading increases, the size of the Ag particles and/or the number of particles is expected to increase and subsequently, the accessible TiO_2 surface area may be reduced; thus an optimal capacity at ca. 4 wt% can likely be attributed to the formation of metal causing hindrance to diffusion and/or clogging of some pore mouths to large refractory molecules. If one assumes that the surface oxygen is associated with the TiO_2 support, the ratio of O_{surf}/O_{lat} is expected to decrease with increase in the Ag loading. The lack of a significant decrease in the O_{surf}/O_{lat} ratio as the Ag loading increased from 2 to 20 wt% suggests that the surface hydroxyl groups can be associated with the TiO_2 and the silver phase particles.

It is to be noted that the binding energy of the O 1s line for the Ag/SiO_2 sorbent material is consistent with values reported for different forms of SiO_2.[121] This assignment is also consistent with the measured binding energy of the Si 2p line. As the amount of surface Ag in this sample is very small (0.34 atomic %), the ratio of the atomic concentrations O/Si, which is significantly greater than the nominal value of 2, indicates that a significant amount of hydroxyl groups are present on the surface. Hence, Si is likely to be present in the form of an oxyhydroxide (i.e., $SiO_x(OH)_y$).

Ag 3d region

The Ag 3d photoemission regions for the adsorbent materials as a function of the Ag loading are shown in Figure 4-6. Those for Ag, Ag_2O, $AgNO_3$, and AgO standards are shown in Figure 4-5 and are used to aid in the analysis of the silver data for the adsorbent material. Due to the spin-orbit coupling, the Ag 3d region is split into the Ag $3d_{3/2}$ (low energy) and the Ag $3d_{5/2}$ (high energy) bands. In Figure 4-6, the intensity of the Ag $3d_{5/2}$ component increased with increase in the Ag loading as one would expect and is summarized in Table 4-3. The Ag binding energy and FWHM for a 2 wt% Ag/SiO_2 sorbent material was also included in Table 4-3 to explore the effect of supports on the oxidation state of Ag. As is the case for Ag_2O and AgO (Figure 4-5), the Ag 3d region for the Ag/TiO_2 adsorbent materials (Figure 4-6) are shifted lower relative to Ag and $AgNO_3$. Examination of the data in Table 4-3 reveals that the Ag $3d_{5/2}$ binding energies for the Ag/TiO_2 adsorbent materials are within a narrow range of 367.4-367.8 eV. These binding energies are lower than those we measured for Ag and $AgNO_3$ but are in the range of binding energies we measured for Ag_2O (367.9 eV) and AgO (367.5 eV). The anomalous behavior for silver where the oxides have a lower binding energy than the metal has been previously reported[127,128,129] and its origin has been discussed.[125] As pointed out earlier by many authors, it is difficult to differentiate between the various oxides of silver based solely on the binding energy of the Ag 3d lines. However, the FWHM of the Ag $3d_{5/2}$ line and the Auger parameter can be used to assist in chemical state identification. The FWHM for the Ag $3d_{5/2}$ line of Ag, Ag_2O, $AgNO_3$ and AgO are 1.09, 1.25, 1.42 and 2.18 eV, respectively, showing a clear variation with change in oxidation state. The slightly larger FWHM for the $AgNO_3$ relative to Ag_2O despite both having Ag^{1+} is likely due to the difference in local coordination geometry of Ag in these compounds. All of the Ag atoms in Ag_2O are equivalent with each Ag coordinated

with two O atoms at 2.047 Å.[130] On the other hand, Ag in $AgNO_3$ has two non-equivalent sites of Ag with each having multiple Ag-O distances.[131] The significantly broader peak for AgO is due to its bivalent character containing Ag^{1+} and Ag^{3+}.[132] Based on the FWHM of the Ag $3d_{5/2}$ line, Ag in the adsorbent material is present as Ag^{1+}. Though $AgNO_3$ is the precursor used to prepare the sorbent materials, it is not present after calcination based upon the composition and binding energy of the N signal. The surface regions of the adsorbent materials consist of only a small amount of nitrogen (<1 at% for all Ag/TiO_2 samples, and ~2 at% for TiO_2 impregnated with HNO_3), but the N 1s binding energies are in the range of 398.1-399.8 eV, and are significantly lower than that of N in $AgNO_3$, which is 406.5 eV.

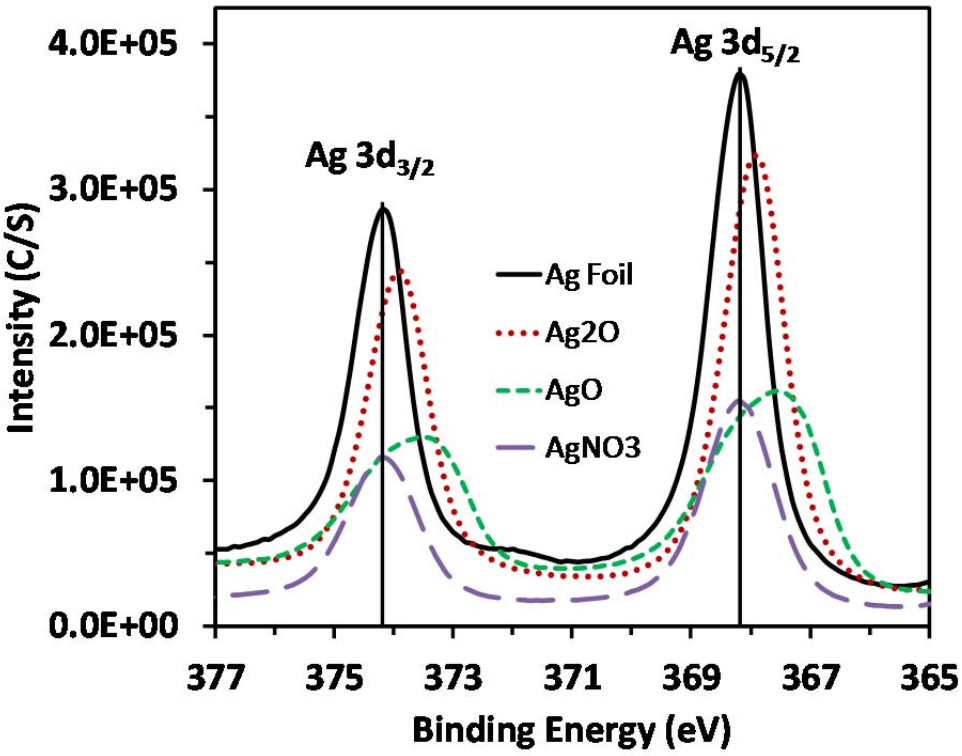

Figure 4-5 Ag 3d photoemission region for the Ag, Ag2O, AgNO3 and AgO reference materials showing the spin orbit doublet of the Ag 3d band
The binding energies for metallic silver are indicated by the vertical lines.

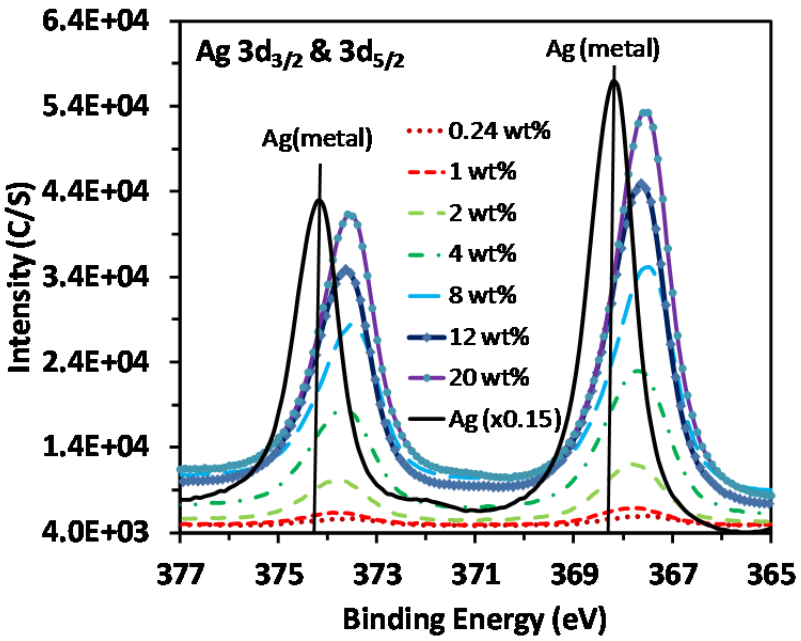

Figure 4-6 Ag 3d photoemission region for the Ag/TiO_2 adsorbent materials as a function of the Ag loading in wt%
The vertical lines indicate the binding energies of the spin-orbit doublet for metallic silver.

Indicative peaks of the X-ray induced Auger MNN lines were also characterized in order to provide further insight into the Ag oxidation state and phases in the adsorbent materials. The Auger regions for Ag, Ag_2O, $AgNO_3$, and AgO references are shown in Figure 4-7. The Ag $3d_{3/2}4d4d$ line for the oxides is shifted to higher energy relative to the metal. The Auger regions for the adsorbent material are shown in Figure 4-8. For loadings in the range of 0.24-4 wt%, the Ag $3d_{3/2}4d4d$ bands are very broad and did not provide further insight as shown in Figure 4-8. However, for loadings of 4, 12 and 20 wt%, the Ag $3d_{3/2}4d4d$ bands are well-defined and are shifted to lower binding energy relative to metallic Ag. Hence, the Auger lines provides further evidence that the silver phase in the adsorbent material is unique as compared to any of the silver references we examined.

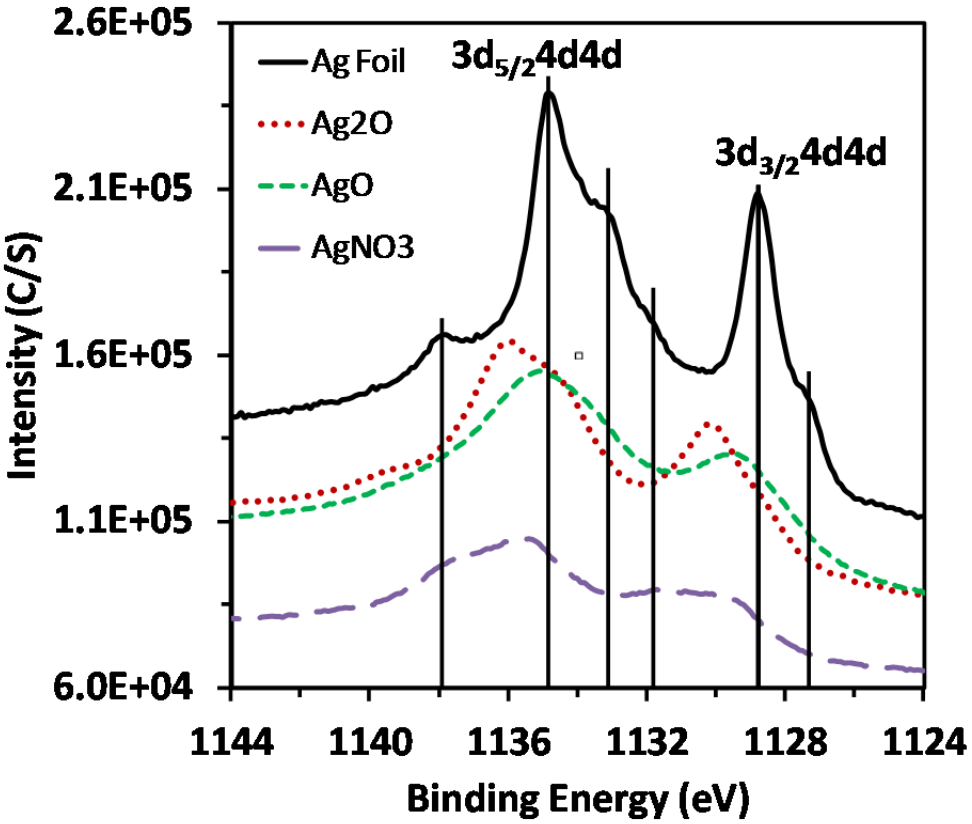

Figure 4-7 X-ray induced Ag 3d4d4d Auger lines for the Ag, Ag2O, AgNO3 and AgO reference materials showing at least 6 components are required to deconvolute the spectra as indicated by the vertical lines for metallic silver

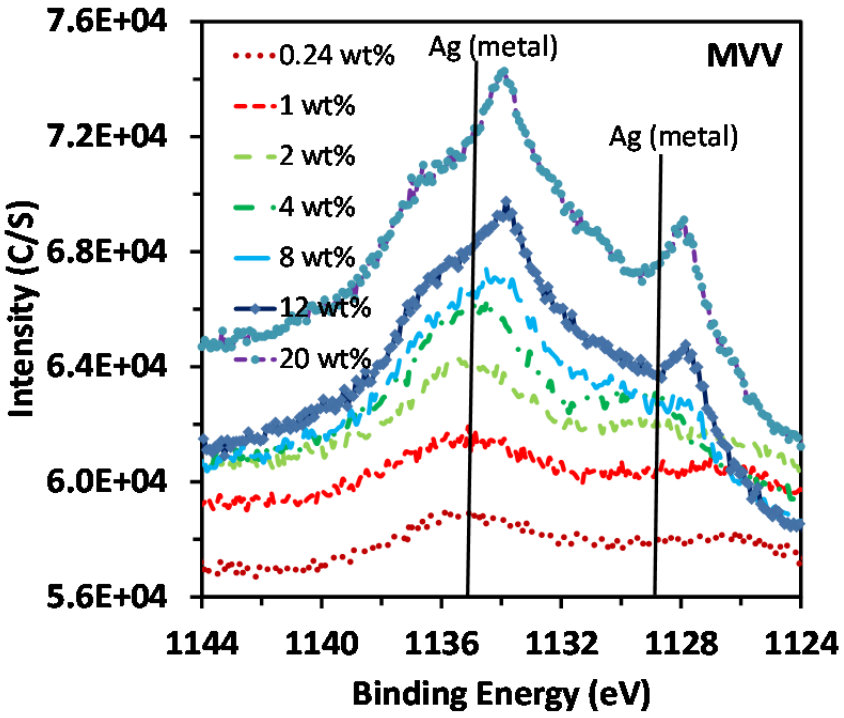

Figure 4-8 X-ray induced Ag MVV Auger lines for the Ag/TiO_2 adsorbent materials as a function of the Ag loading in wt%
The vertical lines indicate the binding energies of the spin-orbit doublet for metallic silver.

Examination of the Ag $3d_{5/2}$ result for the 2wt% Ag/SiO_2 adsorbent material (Table 4-3) reveals a binding energy that is close to those of 2 wt% Ag/TiO_2 and Ag_2O. However, the FWHM for the Ag/SiO_2 material is significantly greater than those of Ag/TiO_2 and Ag_2O indicating that the Ag phase in Ag/SiO_2 differs from the silver phase in Ag/TiO_2 or Ag_2O. Although the Ag $3d_{5/2}$ FWHM for Ag/SiO_2 is comparable to that of AgO, its binding energy is higher than that of AgO. Hence, AgO cannot be present in Ag/SiO_2. The nature of differences in the silver phases will be further explored by X-ray absorption spectroscopy in the next section.

Table 4-3 Summary of deconvolution results of various photoemission lines for the Ag/TiO_2 and Ag/SiO_2 adsorbent materials along with some Ti and Ag reference materials

wt. % Ag in Ag/TiO_2	C 1s BE (FWHM) At%	O 1s BE (FWHM) At%	Ti 2p3/2 & 1/2 BE (FWHM) At%	Ag $3d_{5/2}$ & $3d_{3/2}$ BE (FWHM) At%	Ag ($M_4N_5N_5$) BE (FWHM)
At% Ag		BE (FWHM) At%	BE (FWHM) At%	BE (FWHM) At%	BE (FWHM)
0.24	284.6 (1.72) 10.8 286.1 (1.75) 1.9 288.6 (1.50) 1.6	529.6 (1.45) 52.2 531.1 (1.88) 8.1	458.4 (1.35) 25.2 464.0 (2.22)	367.6 (1.59) 0.17 373.6 (1.59) Δ (Ag 3d) = 6.03	1127.2 (6.25)
1	284.6 (1.67) 9.1 286.0 (1.85) 1.5 288.7(1.65) 1.5	529.6 (1.44) 54.2 531.2 (1.72) 7.3	458.4 (1.35) 26.1 464.1 (2.22)	367.8 (1.57) 0.29 373.8 (1.54) Δ (Ag 3d) = 6.01	1129.5
2	284.6 (1.72) 7.2 286.2 (1.53) 1.3 288.6 (1.74) 1.4	529.3 (1.44) 56.7 531.2 (1.61) 6.3	458.4 (1.34) 26.3 464.1(2.20)	367.8 (1.49) 0.92 373.8 (1.49) Δ (Ag 3d) = 6.04	1129.4
4	286.6 (1.81) 9.6 286.3 (1.63) 1.6 288.5 (1.76) 1.7	529.5 (1.44) 53.2 531.1 (1.65) 6.2	458.3 (1.35) 25.3 464.0 (2.22)	367.7 (1.53) 2.5 373.7 (1.51) Δ (Ag 3d) = 5.99	1129.0
8	284.6 (1.84) 16.6 286.3 (1.68) 1.5 288.5 (1.71) 1.6	529.3 (1.47) 48.6 531.1 (1.62) 5.8	458.2 (1.38) 22.1 463.9 (2.22)	367.4 (1.45) 3.7 373.4 (1.43) Δ (Ag 3d) = 5.98	1129.0
12	284.6 (1.84) 12.1 286.2 (1.95) 1.7 288.6 (1.76) 1.6	529.6 (1.48) 50.2 531.2 (1.64) 5.9	458.3 (1.41) 23.1 464.0 (2.26)	367.6 (1.39) 5.3 373.5 (1.36) Δ (Ag 3d) = 5.97	1127.8
20	284.6 (1.90) 13.7 286.3 (1.51) 1.1 288.5 (1.90) 1.6	529.5 (1.53) 49.9 531.2 (1.56) 5.5	458.3 (1.47) 22.3 463.9 (2.29)	367.5 (1.34) 5.8 373.5 (1.32) Δ (Ag 3d) = 5.94	1127.9
	C 1s	**O 1s**	**Si 2p**	**Ag 3d5/2 &3/2**	**Ag ($M_4N_5N_5$)**
2 wt% Ag/SiO_2	284.6 (2.40) 1.8	532.5 (2.21) 71.1	103.2 (2.21) 26.7	368.0 (2.39) 0.34 374.0 (2.34)	1129.8 (5.58)
	C 1s	O 1s	N 1s	Ag $3d_{5/2}$ & $3d_{3/2}$	Ag ($M_4N_5N_5$)
Ag	N/A	N/A	N/A	368.26 (1.09) 100 374.36 (1.05)	1128.9
Ag_2O	284.6 (1.50) 20.3 285.9 (1.65) 2.7 288.1 (2.04) 3.7	529.3 (1.25) 17.3 530.7 (1.32) 6.2 531.5 (2.16) 4.7	N/A	367.93 (1.25) 45.0 373.92 (1.25)	1130.2
$AgNO_3$	284.6 (1.48) 14.6 286.0 (1.62) 3.0 287.8 (2.08) 2.1	532.1 (1.68) 44.5	403.1 (0.72) 0.2 406.4 (1.24) 10.4 407.3 (2.00) 2.3	368.17 (1.42) 22.8 374.16 (1.32) Δ (Ag 3d) = 5.99	1130.7
AgO	284.6 (1.71) 14.4 286.3 (2.00) 3.5 288.3 (1.76) 3.6	528.8 (1.15) 20.6 530.7 (1.69) 13.1 532.2 (1.76) 3.2 533.3 (2.61) 3.6	N/A	367.52 (2.18) 38.0 373.48 (2.13)	1129.5
TiO_2	C 1s	O 1s	N 1s	Ti 2p 3/2 & 1/2	
	284.6 (2.98) 5.1 286.6 (1.66) 0.7 288.6 (1.66) 0.7	529.7 (1.41) 59.9 531.2 (1.57) 4.6	399.8 (1.84) 2.0 401.7 (1.04) 0.1	458.5 (1.33) 26.9 464.2 (2.20)	N/A

This list includes the binding energies (BE), full-width-at-half-maximum (fwhm), and atomic percent for each component. All binding energies were referenced to adventitious carbon at 284.6 eV.The TiO_2 sample was calcined at 450 ^oC after impregnation with an equivalent quantity of HNO_3.

Table 4-4 is the summary of the Auger parameter (α) for the Ag ($3d_{3/2}$4d4d) X-ray induced

Auger line, the spin orbit splitting for Ti $2p_{3/2}$ and $2p_{1/2}$ lines (ΔTi 2p), the Ag $3d_{5/2}$ and $3d_{3/2}$ lines (ΔAg3d), the difference between the binding energy of the O 1s line for lattice oxygen and the binding energy of the Ti $2p_{3/2}$ line (ΔO-Ti $2p_{3/2}$). Furthermore, the ratios of the atomic concentrations for lattice oxygen to Ti (O_{lat}/Ti), total oxygen to Si (O/Si), surface oxygen to lattice oxygen (O_{surf}/O_{lat}) and Ti/Ag have also been included.

Table 4-4 Summary of Binding Energy Differences and Concentration Ratios

wt % Ag in Ag/TiO_2	α (eV)	ΔTi_{2p} (eV)	ΔO_{1s}-$Ti_{2p3/2}$ (eV)	O_{lat}/ Ti	O_{surf}/O_{lat}	Ti/Ag
0	N/A	5.69	71.24	2.22	0.0761	N/A
0.24	724.7	5.68	71.20	2.07	0.1553	148.2
1	725.0	5.68	71.20	2.08	0.1347	90.0
2	725.4	5.69	71.20	2.16	0.1107	28.6
4	725.2	5.68	71.21	2.10	0.1157	6.8
8	725.8	5.68	71.22	2.20	0.1187	6.0
12	726.2	5.67	71.22	2.17	0.1183	4.4
20	726.2	5.67	71.24	2.24	0.1101	3.8
				O/ Si		Si/Ag
2 wt% Ag/SiO_2	724.8			2.72		78.6
Ag	726.0			N/A		
Ag_2O	724.3			N/A		
$AgNO_3$	724.1			N/A		
AgO	724.6			N/A		

The TiO_2 sample was calcined at 450 ^oC after impregnation with an equivalent quantity of HNO_3.

4.3. XANES/EXAFS Results

4.2.1. **Silver K-edge**

4.2.1.1. **Ag/TiO_2 Silver Analysis**

Phase pure reference materials as well as the adsorbent materials were characterized by XAS. The XANES and EXAFS spectra of the reference materials were used to aid in the identification of the oxidation states and local coordination geometry of Ag in the sorbent material. Figure 4-10 shows XANES spectra for the reference samples and two sorbent

examples at 2 and 20 wt%, all of which show unique character in the XANES region. The X-ray absorption edge energies at half-height for all samples are summarized in Table 4-5. The edge energies for the adsorbent samples are within a narrow range of 25512.6-25513.0 eV, which is very close to that for Ag_2O and is slightly higher than that observed for $AgNO_3$. Figure 4-9 indicates the variations in XANES and the Fourier transforms for reference compounds. However, the edge energies for the adsorbent materials are significantly less than those observed for the Ag metal and AgO indicating that Ag in the adsorbent material is present mostly in the monovalent state. Furthermore, the peak intensity (sometimes referred to as the white-line) for the 20 wt% sample is reduced relative to that of the 2 wt % samples and its position is shifted closer to that of the metal. The shift of the peak intensity toward the metal occurred also in the case of the 8 and 12 wt% Ag samples with the degree of the shift increased with increased loading.

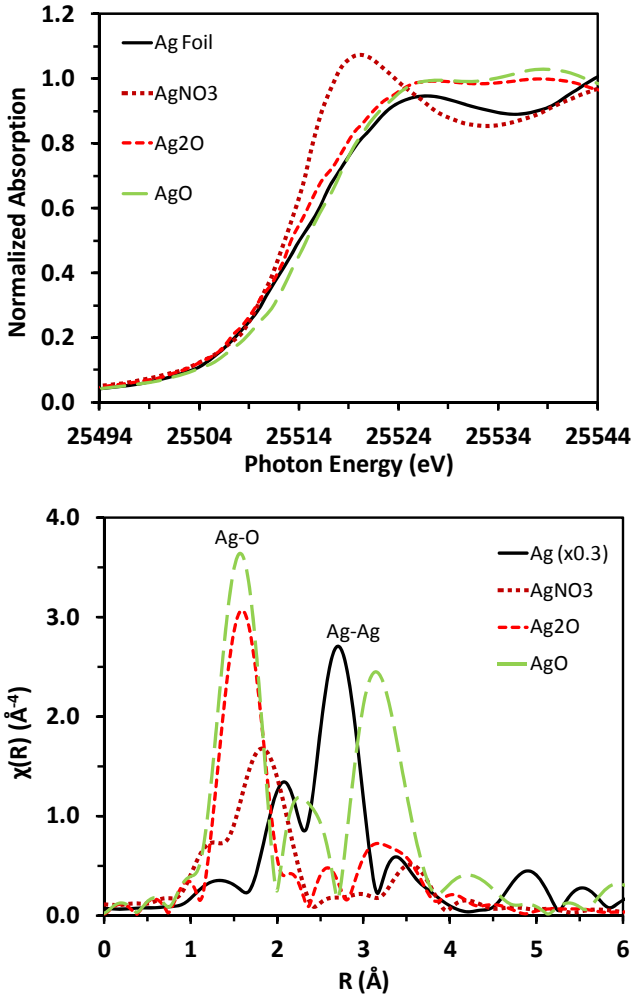

Figure 4-9 Ag K-edge XANES (top) and phase uncorrected Fourier transforms of K^3-weighted EXAFS spectra (bottom) for metallic Ag (scaled by 0.3 for clarity), $AgNO_3$, Ag_2O and AgO reference materials.

Table 4-5 Summary of X-ray absorption edge jumps and energies as measured at half-height

Sample	Edge jump (Δμx)	Edge Energy (half-height) (eV)
1 wt% Ag/TiO_2	0.14	25513.0
2 wt% Ag/TiO_2	0.34	25512.6
4 wt% Ag/TiO_2	0.59	25512.8
8 wt% Ag/TiO_2	0.93	25512.7
12 wt% Ag/TiO_2	1.13	25512.9
20 wt% Ag/TiO_2	1.42	25513.0
2 wt% Ag/SiO_2	0.72	25512.7
Ag	1.02	25514.0

Ag_2O	1.37	25513.0
AgO	1.37	25514.8
$AgNO_3$	1.30	25512.2

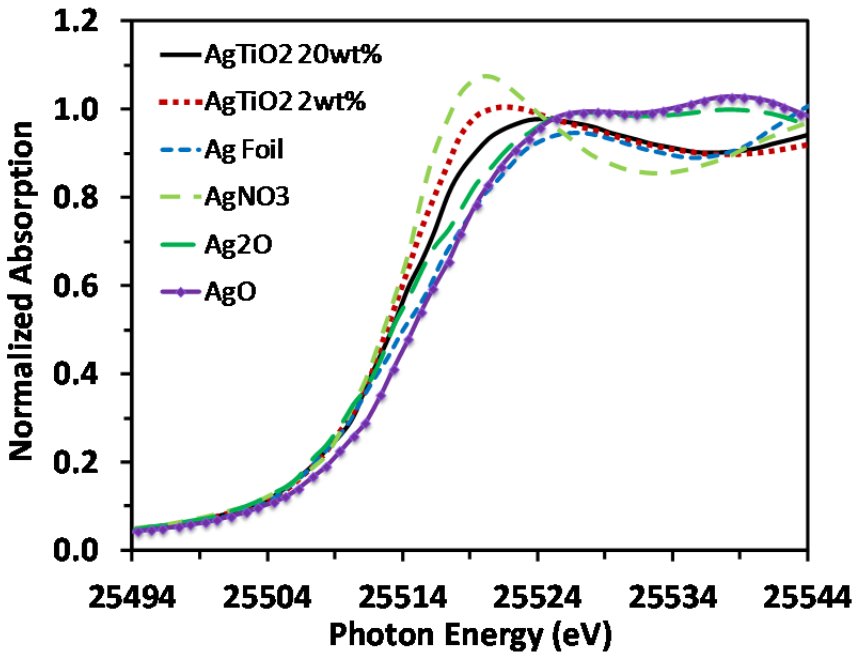

Figure 4-10 Ag K-edge XANES data for 2 and 20 wt% Ag/TiO2 adsorbent materials along with data for Ag, $AgNO_3$, Ag_2O and AgO reference materials

To understand the origin of the peak shift in the XANES data for the adsorbent material toward the metal, the XANES data for the adsorbent material was analyzed as a linear combination of the XANES data for the oxide phase in the 2 wt% Ag sample and the XANES data for metallic Ag (i.e., Ag foil). The linear combination analysis was performed in Athena and provided excellent fits for all samples, as shown in Figure 4-11 for the 20 wt% adsorbent sample. The results show a good correlation between the fit and the data, as the lines lay on top of each other with minimal residual error within the fit. The linear combination analysis for the 20 wt% sample indicates the oxide character contribution is 69%. Similar fits on the other samples

indicate an oxide contribution of 80, 88 and 98%, for 12, 8 and 4 wt% samples, respectively. As will be shown later in the text, due to the highly dispersed nature of the silver particles (N <12), the use of the silver foil (N=12) to account for the metallic character in the linear combination analysis of XAFS spectra for the sorbent materials overestimates the contribution from the oxide phase and underestimates the contribution from the metallic phase.

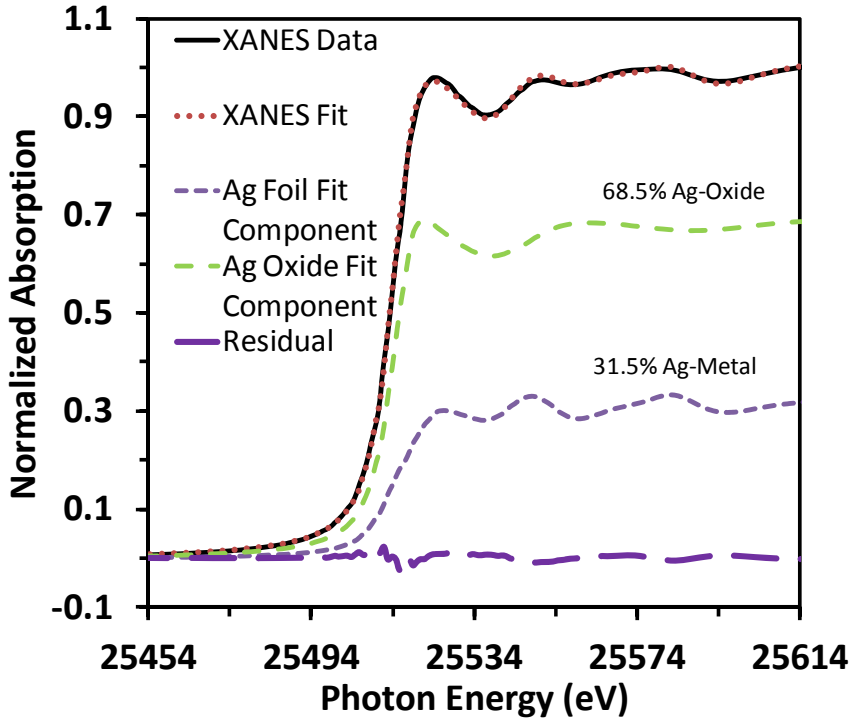

Figure 4-11 Linear combination fit of the 20 wt% adsorbent material showing the contributions from the individual components of the Ag foil and the oxide phase in the adsorbent materials with low loading.

Next, we turn our attention to the EXAFS spectra to examine the local coordination geometry of the oxide phase in the adsorbent materials. The $k^3\chi(k)$ spectra and the Fourier transforms for the 1, 2, 4 wt% Ag/TiO_2 and the $AgNO_3$ reference are compared in Figure 4-12. Clearly, the EXAFS spectra and Fourier transforms for the adsorbent material with loadings in

the range 1-4 wt% are very similar indicating that the local coordination geometry of silver is unchanged in this range of loading. For the sorbent samples, the results indicate that there is a consistent oxide phase, which remains similar in structure and intensity as loading increased up to 4wt%, and that there is no Ag-Ag characteristic present. The slightly lower amplitude for the 1 wt% sample relative to the 2 and 4 wt% samples is due to self-absorption since this set of data was collected in the fluorescence mode rather than the transmission mode, which is the case for all other samples. In addition, the EXAFS oscillations and the Fourier Transforms (FT) for the adsorbent material are distinct from those of $AgNO_3$, which was used as the precursor during sample preparation. While the amplitude of the Ag-O contribution in the FT data for the adsorbent material is somewhat similar to that of $AgNO_3$, its location is shifted to a lower distance indicating, on average, the Ag-O distance in the adsorbent material is about 0.09 Å shorter than that of $AgNO_3$. Furthermore, the EXAFS spectra and Fourier transforms of the 4 wt% adsorbent material are compared in Figure 4-13 with those of Ag_2O and AgO. Clearly, the EXAFS oscillations and the local coordination geometry as depicted in the Fourier transforms of the lower loading Ag/TiO_2 samples are distinct from those of Ag_2O or AgO. That is, the oxide phase in the adsorbent material is not in the form of Ag_2O or AgO.

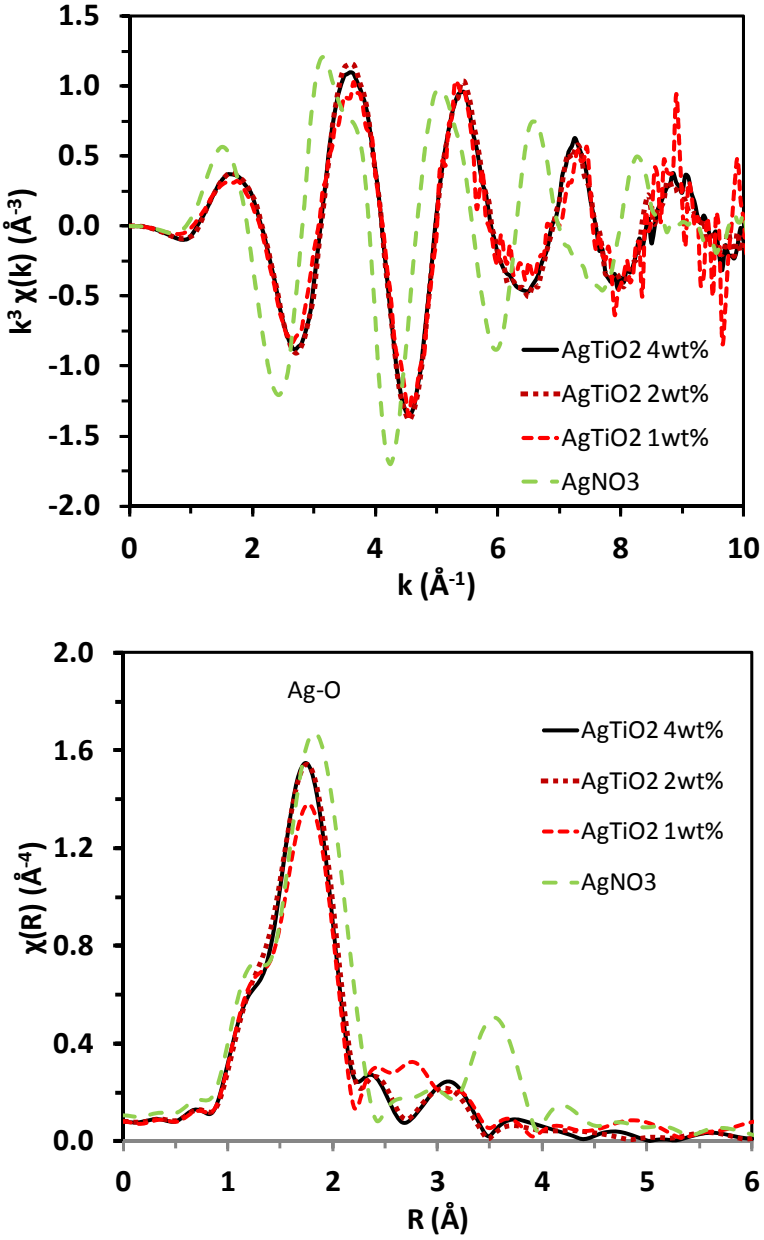

Figure 4-12 Ag K-edge K^3-weighted EXAFS spectra (top) and their phase uncorrected Fourier transforms (bottom) for 1, 2 and 4 wt% Ag/TiO_2 adsorbent materials along with data for $AgNO_3$ reference materials.

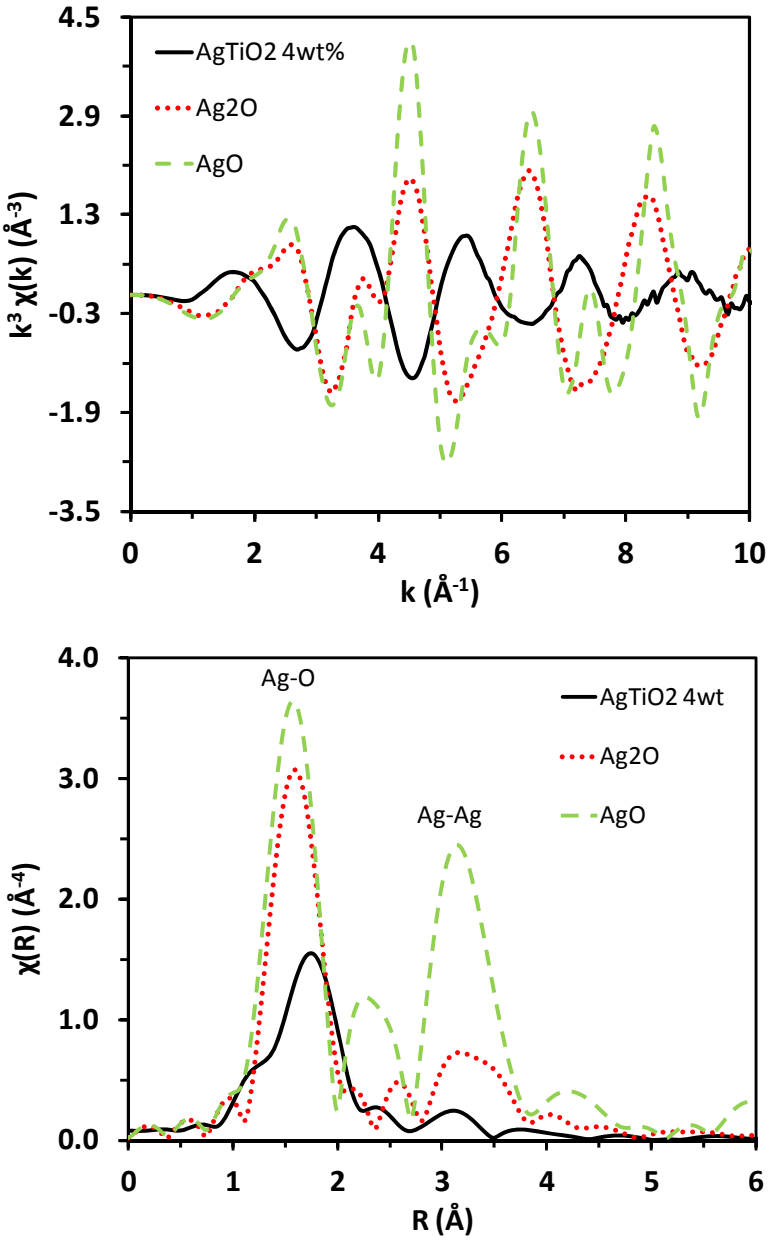

Figure 4-13 Ag K-edge K^3-weighted EXAFS spectra (top) and their phase uncorrected Fourier transforms (bottom) for the 4 wt% Ag/TiO_2 adsorbent materials along with data for Ag_2O, and AgO reference materials.

The EXAFS spectra and Fourier transforms for the Ag/TiO_2 samples at 4, 8, 12, and 20 wt% are compared to those of the Ag metal in Figure 4-14. Both the EXAFS spectra and the

Fourier transforms of the 8-20 wt% samples display the evolution of metallic Ag character with the 20 wt% sample having the highest degree of metallic character. At and above 8 wt%, the results indicate the presence of a metallic phase which grows as the loading increases while the contribution from the oxide phase decreases as the loading increases. This would indicate a growth in the number of metallic Ag particles and/or the size of the Ag particles as the silver content within the adsorbent is increased. Further analyses are required to discern if the origin is due to an increase in the number of crystallites, the size of crystallites or both. The evolution of the metallic character was also confirmed based on linear combination analysis of XANES spectra, which was discussed earlier in this manuscript.

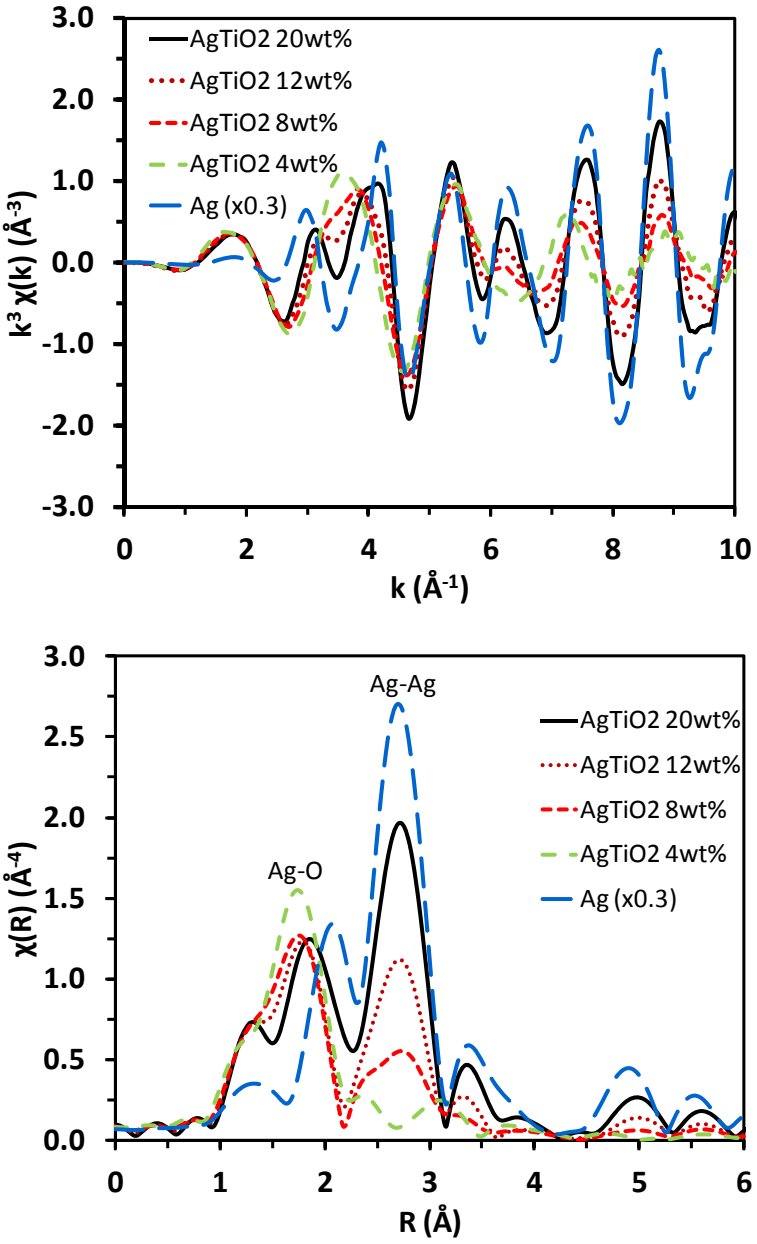

Figure 4-14 Ag K-edge K^3-weighted EXAFS spectra (top) and their phase uncorrected Fourier transforms (bottom) for 4, 8, 12, and 20 wt% Ag/TiO_2 adsorbent materials along with data for metallic Ag scaled by 0.3 for clarity.

To examine the role of support on the structure of the oxide phase, a comparison of the EXAFS spectra and Fourier transforms for a 2 wt% Ag supported on TiO_2 and SiO_2 is shown in Figure 4-15. The EXAFS oscillations are shifted to higher k values in the case of the SiO_2

support, indicating that the Ag-O distance is shorter than that in the case of the TiO_2 support. In both cases, the FT data display a single contribution for Ag-O without a significant contribution from higher coordination spheres, indicating a high degree of structural disorder in the material. The narrower peak in the case of the SiO_2 support indicates a higher degree of order in this case relative to that in the case of the TiO_2, perhaps related to a weaker support interaction.

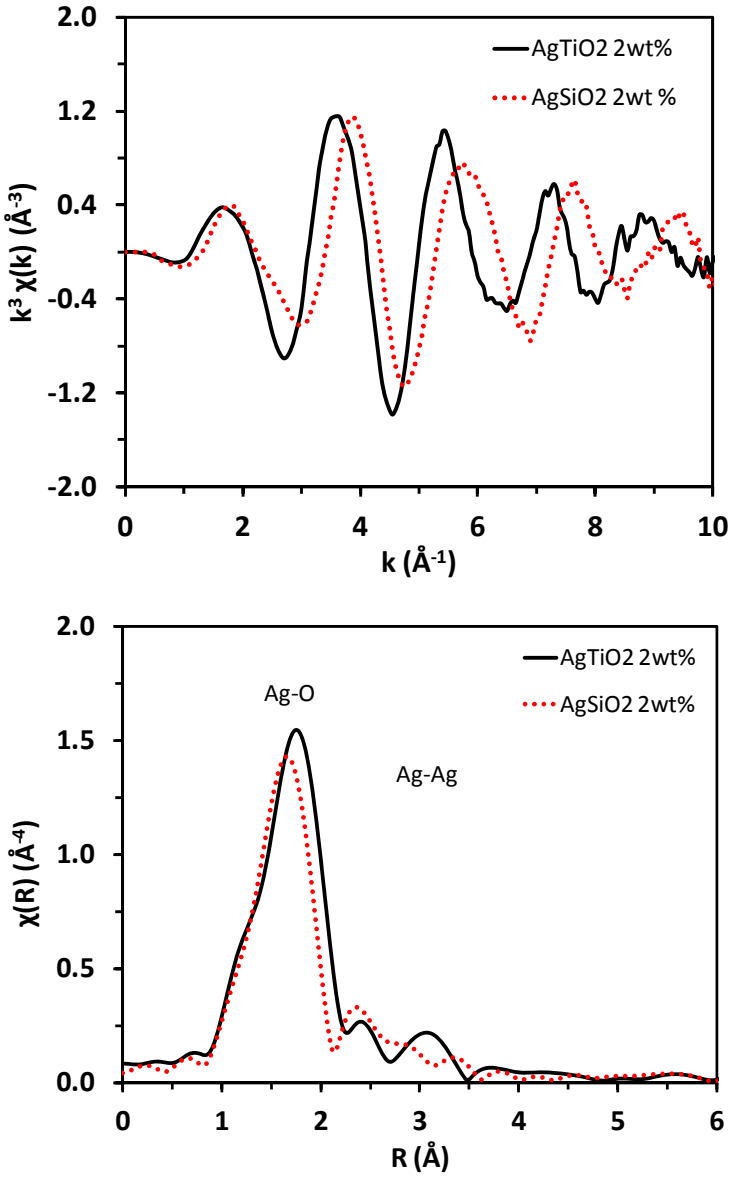

Figure 4-15 Ag K-edge K^3-weighted EXAFS spectra (top) and their phase uncorrected Fourier transforms (bottom) for 2 wt% Ag/TiO_2 and $AgSiO_2$ adsorbent materials.

Fitting of the EXAFS data to the FeFF theory as described in the experimental section is presented in Table 4- 6. AgO is not included in the table, as there was no indicative character associated between its structure and that seen in the sorbent samples. Results for metal, Ag_2O, and $AgNO_3$ are provided and utilize a known coordination to obtain the other parameters. As mentioned before, the amplitude reduction factor (S_0^2) was determined utilizing temperature dependent data for the Ag foil, thereby minimizing the correlation between thermal disorder and S_0^2 providing a better indication of the characteristic disorder associated with the material structure itself. The results indicate that there is a unique bond structure for the oxide form that is present on the TiO_2 support, and its Ag-O bond length is different than those associated with Ag_2O and $AgNO_3$. The Ag-O bond on the sorbent material remains essentially consistent as the metal loading increases and also maintains a consistent coordination number of approximately 4, which also substantiates that the oxide form on the sorbent remains as a surface decoration that must increase in number and size, or both. In contrast, the Ag-Ag metallic structure on the sorbent material, which has a fairly consistent and equal bond length as compared to the Ag metal, shows a growing coordination number as the loading increases, which would indicate a population of crystallites growing in size.

It is also important to note that the type of support influences the structure of the oxide phase. The oxide phase in the case of the 2 wt % Ag/SiO_2 has an Ag-O bond length of 2.22 Å with coordination of two oxygen atoms compared to 2.32 Å with a coordination number of four oxygen atoms in the case of the 2 wt% Ag/TiO_2. Furthermore, the Ag-O coordination shell has a much higher disorder in the case of the TiO_2 support relative to the SiO_2 support, likely due to a stronger support interaction.

Table 4- 6 Summary of EXAFS data analysis results (uncertainty are included in parenthesis)

	x-y	S_0^2	R (Å)	N	$\sigma^2(10^{-3}Å^2)$	F _oxide/metal
Ag Foil	Ag-Ag	0.94(0.2)	2.876	12	10.4 (0.1)	N/A
Ag_2O (XRD)	Ag-O		2.047	2	N/A	N/A
$AgNO_3$ (XRD)	Ag-O		2.412	6	N/A	N/A
Ag/TiO_2-1 wt%	Ag-O	0.94	2.32 (0.01)	4.1 (0.5)	18.8 (1.6)	1.0
Ag/TiO_2-2 wt%	Ag-O	0.94	2.32 (0.01)	4.1 (0.5)	18.8 (1.6)	1.0
Ag/TiO_2-4 wt%	Ag-O	0.94	2.32 (0.01)	4.1 (0.5)	18.8 (1.6)	1.0
Ag/TiO_2-8 wt%	Ag-O	0.94	2.31 (0.01)	4.1 (0.5)	18.8 (1.6)	0.78 (0.07)
Ag/TiO_2-8 wt%	Ag-Ag	0.94	2.872 (0.06)	6.6 (2.0)	16.0 (1.0)	0.22 (0.07)
Ag/TiO_2-12 wt%	Ag-O	0.94	2.30 (0.01)	4.1 (0.5)	18.8 (1.6)	0.67 (0.07)
Ag/TiO_2-12 wt%	Ag-Ag	0.94	2.872(0.06)	8.2 (1.9)	16.0 (1.0)	0.33 (0.07)
Ag/TiO_2-20 wt%	Ag-O	0.94	2.30 (0.01)	4.1 (0.5)	18.8 (1.6)	0.55 (0.07)
Ag/TiO_2-20 wt%	Ag-Ag	0.94	2.872 (0.06)	10.1 (1.9)	16.0 (1.0)	0.45 (0.07)
Ag/SiO_2-2 wt%	Ag-O	0.94	2.22 (0.02)	2.2 (0.4)	11.7(2.8)	1.0

Parameter Definitions:
S_0^2: Many body amplitude reduction factor
R: Path (bond) length
N: Coordination Number
$\sigma^2(10^{-3}Å^2)$: Mean-squared relative displacement
F: Ratio parameter for multiple contributions (samples with metal and oxide)

4.2.1.2. **Ag/TiO_2 Formation Experiments**

The $AgNO_3/TiO_2$ sample was run under the profile as described previously, and the results in Figure 4-16 clearly show that the nitrate still exists when heated to 373 °C. The peak intensity has decreased due to an increase in the thermal disorder within the material, and a change in the relative intensity of the oxide peaks can be observed. This may be due to a loss of oxygen or nitrogen, which has been found to have a mass loss onset around 380 °C.[133] Silver nitrate is known to decompose at temperatures of 420-440 °C.[134] At 450 °C, the peak shape associated with the nitrate precursor is no longer obvious; however, the metallic silver species can be seen, indicated by the peak at 2.88Å.

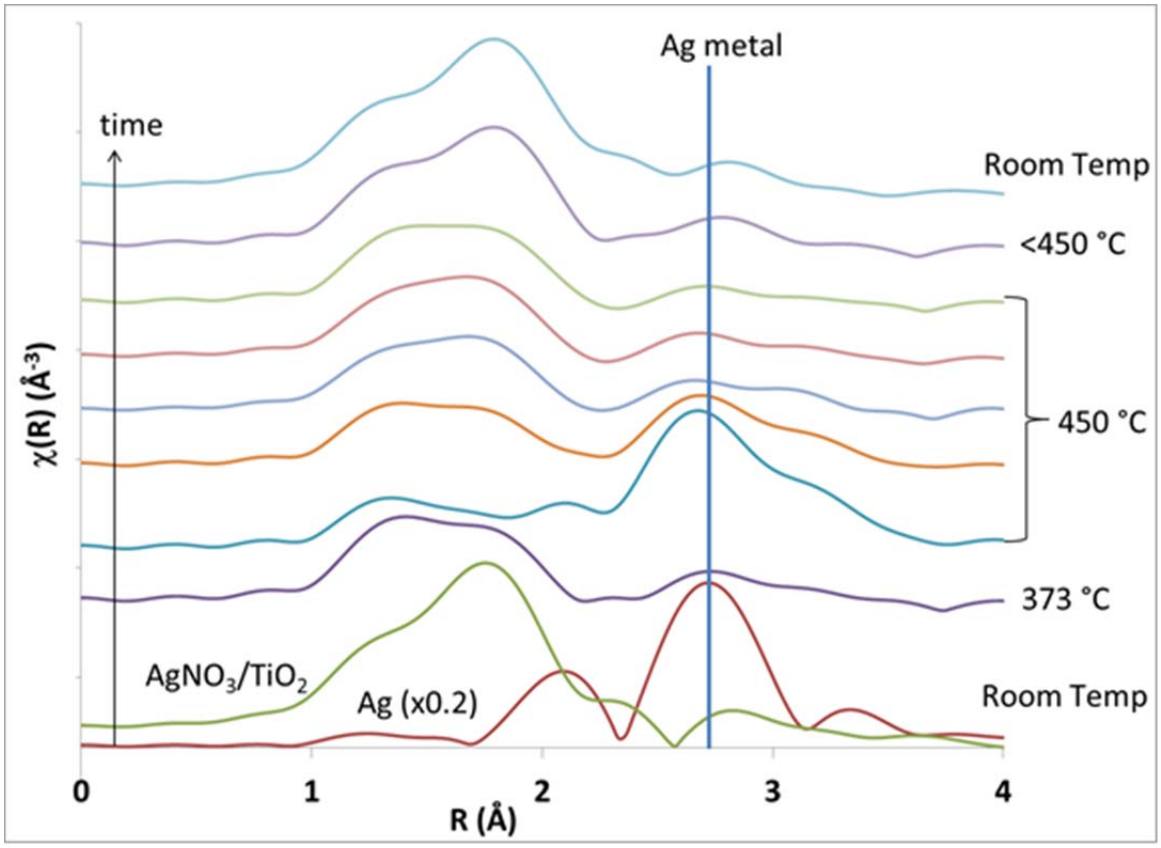

Figure 4-16 Decomposition of $AgNO_3$ impregnated in TiO_2 to silver metal and then redistribution and oxidation to a new oxide phase

The 450 °C calcination temperature is maintained for two hours, and it can be seen that the peak shifts back over that time frame. A contraction in structure can be seen that is indicative of the formation of an oxide phase, but with a weak peak structure indicative of a highly disordered structure. Our K-edge analysis of the structures do not indicate that the silver species is the precursor nitrate, nor is it Ag_2O. These studies also validated the high disorder of the oxide phase via temperature-dependent studies. The final, room temperature scan of the material is consistent with our 2-4 wt% standards, with a calculated Ag-O bond distance of 2.32Å.

The control system studied was $AgNO_3$ wetted to Boron Nitride (BN), as a basis of an inert, oxygen free material to allow the $AgNO_3$ to mobilize and decompose, without any interference or effect from support oxides. This result is shown in Figure 4-17, and indicates that decomposition occurs at a lower temperature. By the time that 350 °C is reached, a substantial metal peak is observed. It is not clear why this occurred, but it is perhaps attributable to the oxygen deficient materials that the nitrate was impregnated onto. While the sample exists at the 450 °C calcination temperature, the metallic peak increases in intensity, implying that the silver metal is mobile and agglomerating into large silver crystals, even under conditions where thermal disorder is substantial. While the Ag foil reference is scaled by a factor of 0.2x in the figure for convenience and appearance purposes, direct comparison of the peak intensity of metallic silver reference versus the silver peak in the BN system at room temperature indicates that the peaks are nearly the same. A nearly identical intensity of the Fourier Transform (FT) peak at 2.88Å implies that the structure of the silver formed in this experiment is nearly fully coordinated with a value of N=12.[135]

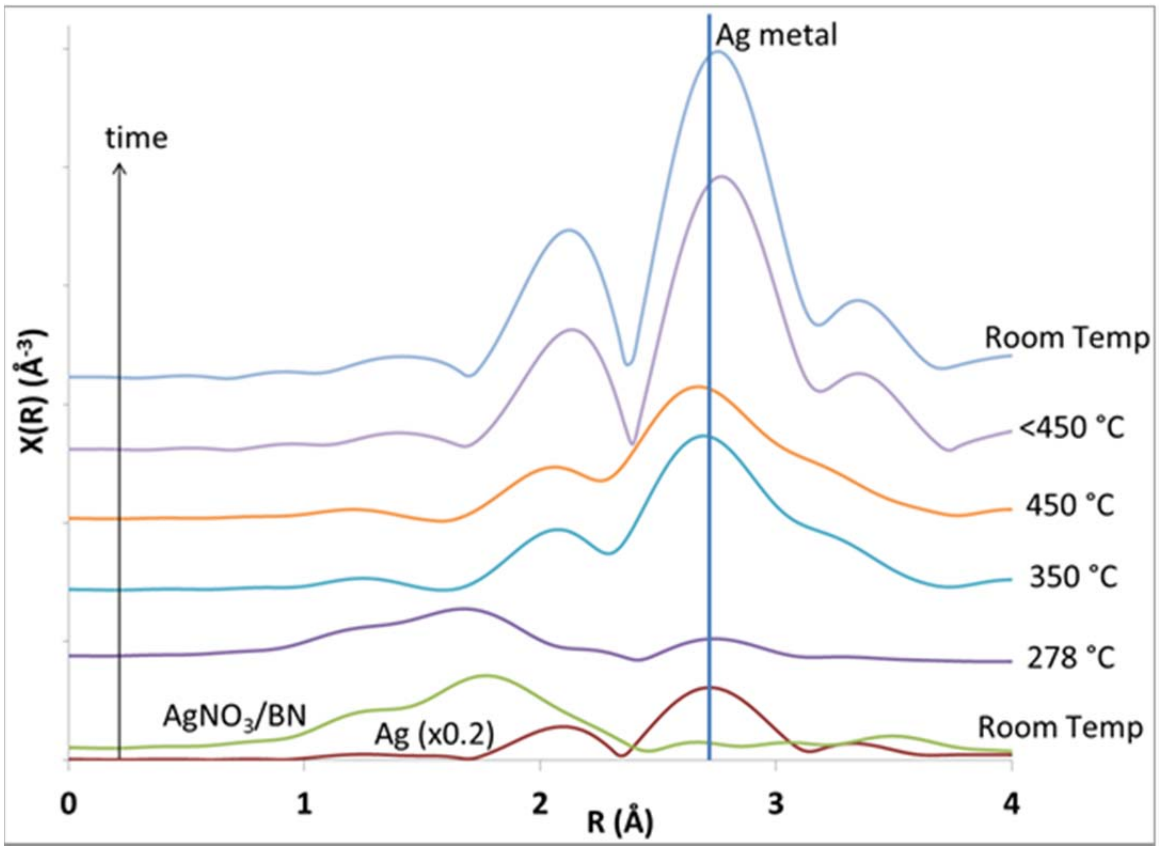

Figure 4-17 Decomposition of $AgNO_3$ impregnated in BN, indicating formation of large metal structures without substantial oxidation products.

Next, we identify the stability of the dispersed silver phase on TiO_2 via a subsequent calcination. While this analysis does not include combustion or other desorption and removal of hydrocarbons as would occur in practice, it does occur in flowing air and should be indicative of the final state of a regeneration process. Figure 4-18 shows the behavior of the adsorbent material over its initial formation and a subsequent calcination. What is observed is a high level of stability, and no major changes during calcination at 450 °C. The peak did not move, and there is no indication of the formation of a silver phase under these conditions.

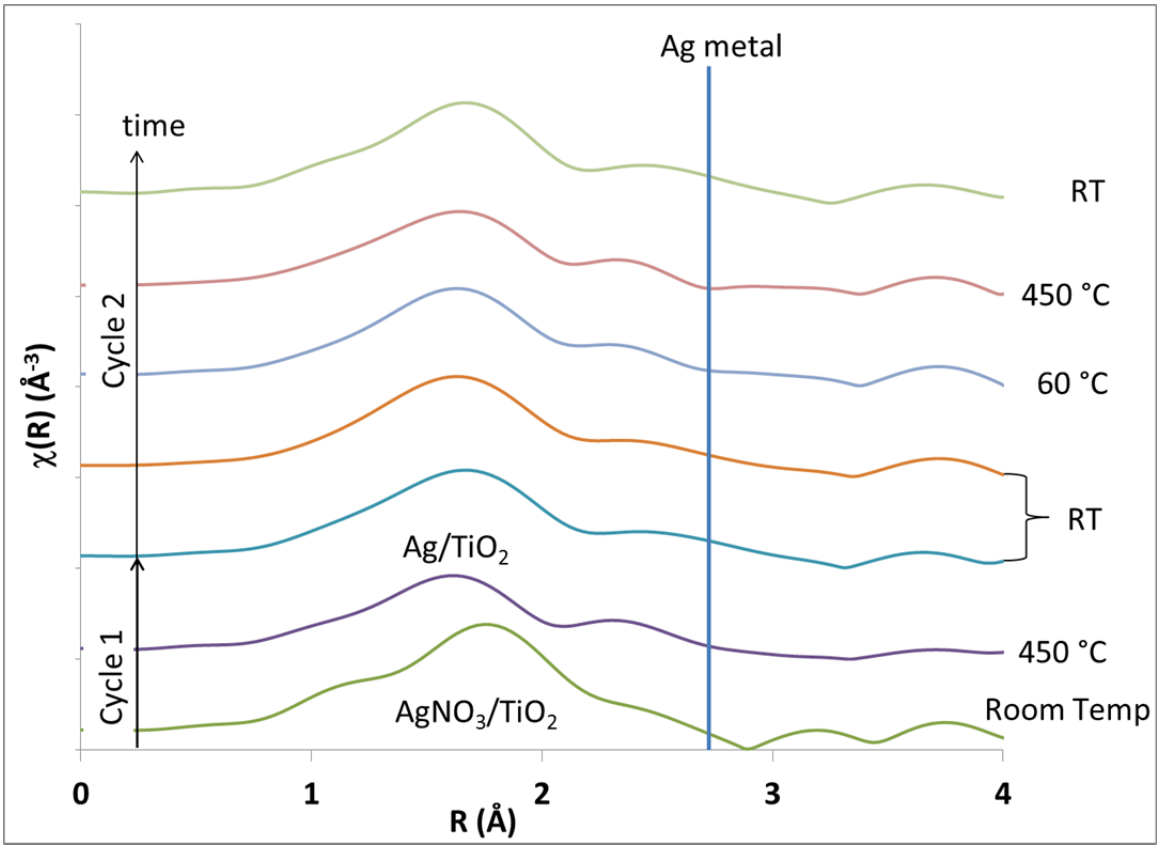

Figure 4-18 Initial formation from nitrate, and second calcination in air for the Ag/TiO_2 system

While the capacity of Ag/TiO_2 is greatest around 4 wt%, the higher loading variants are interesting because of the two distinct silver phases that are observed. TiO_2 was impregnated with $AgNO_3$ solution at a level to create 20wt% silver loading in the sorbent. This material was calcined under the same conditions, and the results are displayed in Figure 4-19. It is clear that the nitrate rapidly decomposes under such loading conditions, and that while some silver disperses to create the observed oxide peak, the substantial structure in the material is the metal peak. While previous analysis has indicated that the metal is not fully coordinated, the peak is still strong, indicating fairly sizable metal formations.

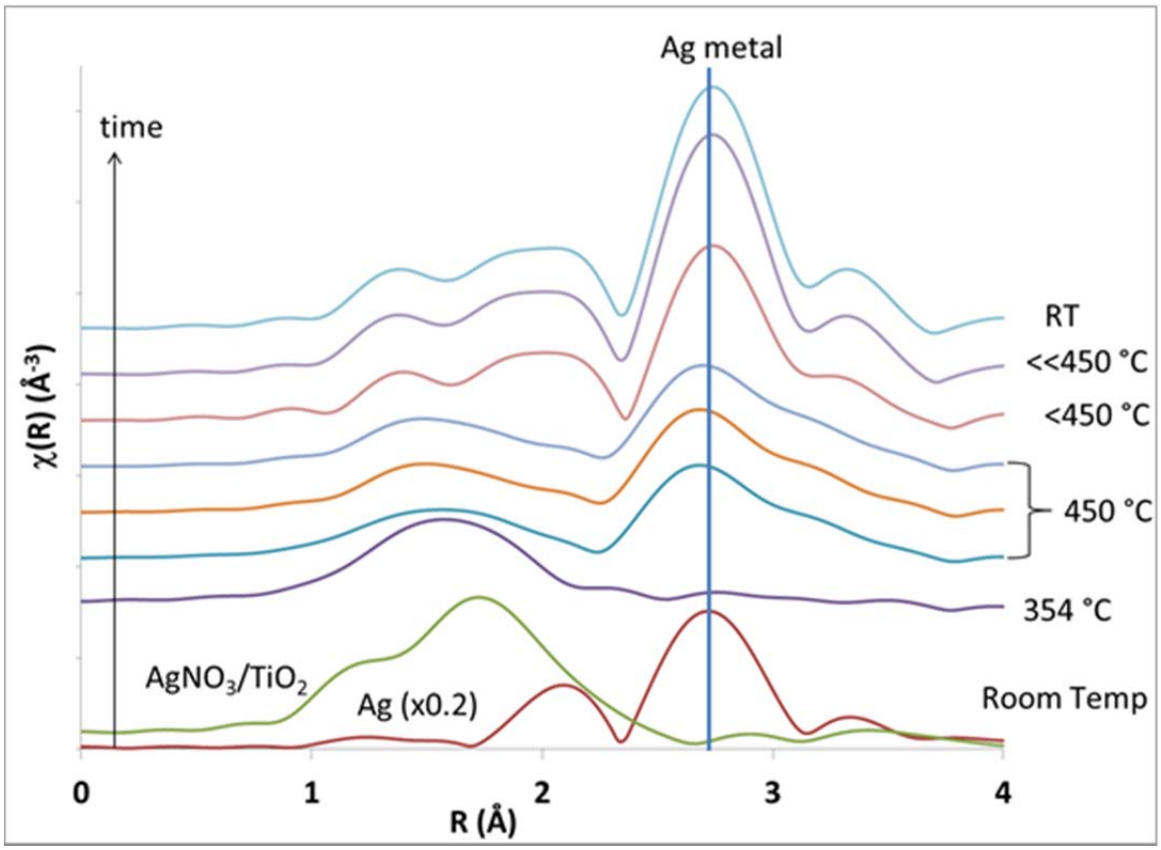

Figure 4-19 Formation experiment for a 20 wt% Ag sorbent material indicating decomposition of the nitrate and formation of the permanent metal structure.

The other condition of interest was the effect of temperature on the formation of the adsorbent materials. To study the potential changes associated with temperature, *in situ* formation experiments were run on 4 and 20 wt% Ag samples, prepared in the same manner as was described. The heating operations were performed in the same manner as for the other formation experiments; the heating was simply increased at the same rate until 550 °C was reached. This temperature was selected because it was considered substantially higher than the decomposition temperature for $AgNO_3$, as well as the temperature for Ag_2O.[136] Figure 4-20 a and b show the progression of Ag/TiO_2 formation under calcination conditions of 550 °C. For the 4

wt% sample, metallic agglomeration is observed, as evidenced by the metallic peak that is formed and remains at room temperature – it is not an intermediate as was observed for normal formation. In the 20 wt% sample, it is clear that under calcination conditions, the remnant of the oxide peak that is seen in the lower-temperature calcination is nearly flat, indicating complete decomposition. Upon cooling, the broadening of the peak prior to the primary Ag metal peak is no longer observed. The peak seen at lower energy is much more distinct, indicating that it is a feature associated with the metal formation, and not broadened due to two species influencing the FT signal in that length range.

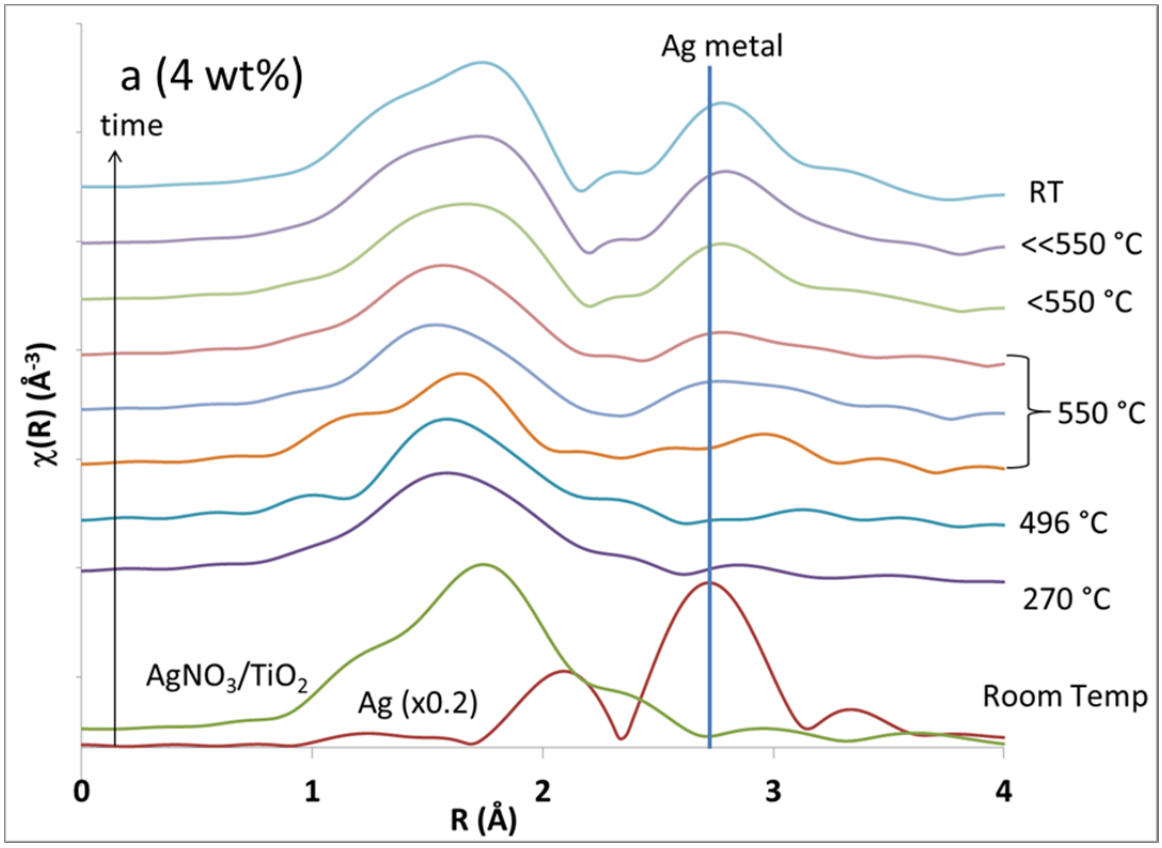

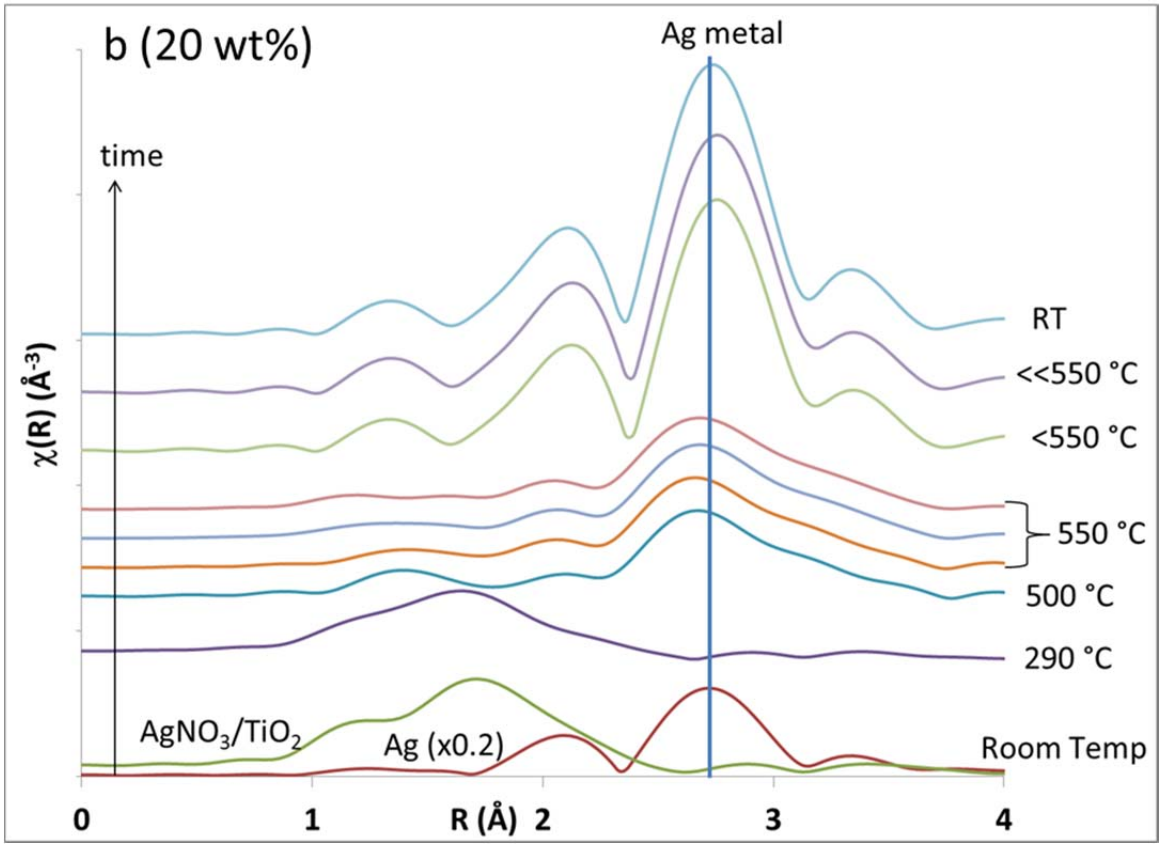

Figure 4-20 (a) Formation of 4 wt% Ag/TiO_2 under high temperature (550 °C) calcination conditions; (b) Formation of 20 wt% Ag/TiO_2 under the same conditions

4.2.2. **Silver L-edges**

Phase pure reference materials as well as the adsorbent materials were characterized by XAS. Figure 4-21 shows the Ag L_3-edge for reference silver foil, as well as the silver oxides, nitrate, and the 2 and 20 wt% Ag/TiO_2. Silver is the most oxidized in Ag(I,III)O exhibits an intense white line and is shifted to the lowest energy point. Both AgO and Ag_2O exhibit a peak, attributable to dipole-allowed $2p_{3/2} \rightarrow 4d$ transitions with differing densities of unoccupied states.[137,138] Most notable however is the presence of a similar though less intense peak in the case of $AgNO_3$ and the Ag/TiO_2 samples.

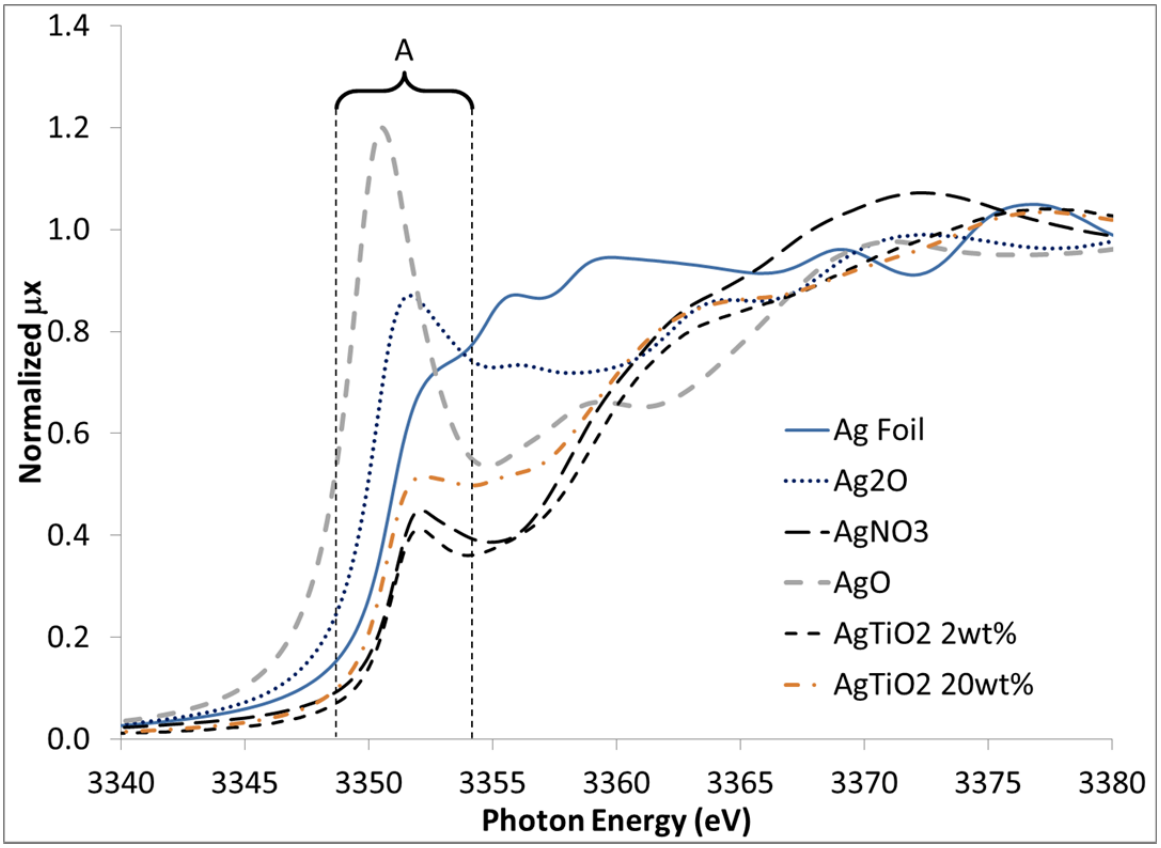

Figure 4-21 Ag L_3 XANES spectra of Ag/TiO_2 and references with principal peak "A" marked

It must be noted that the Ag/TiO_2 samples exhibited a beam reduction that caused a requirement to take great care and special preparatory steps in performing the L-edge studies. Work on the Ag K-edge for these same materials did not show any indication of damage. Thus this damage may be attributable to the significantly higher concentration of X-ray photons at X19A (a focused beamline) relative to X11A (an unfocused beamline). The damage was most notable for the low-loaded Ag/TiO_2, and was less severe on the 20 wt% Ag/TiO_2, due to metal content inherently within the material. Figure 4-22 shows the nature of beam damage for these systems, and also shows the stability as would be expected, for metallic silver. Furthermore, such beam damage was not observed in the case of the oxides Ag_2O, AgO and $AgNO_3$.

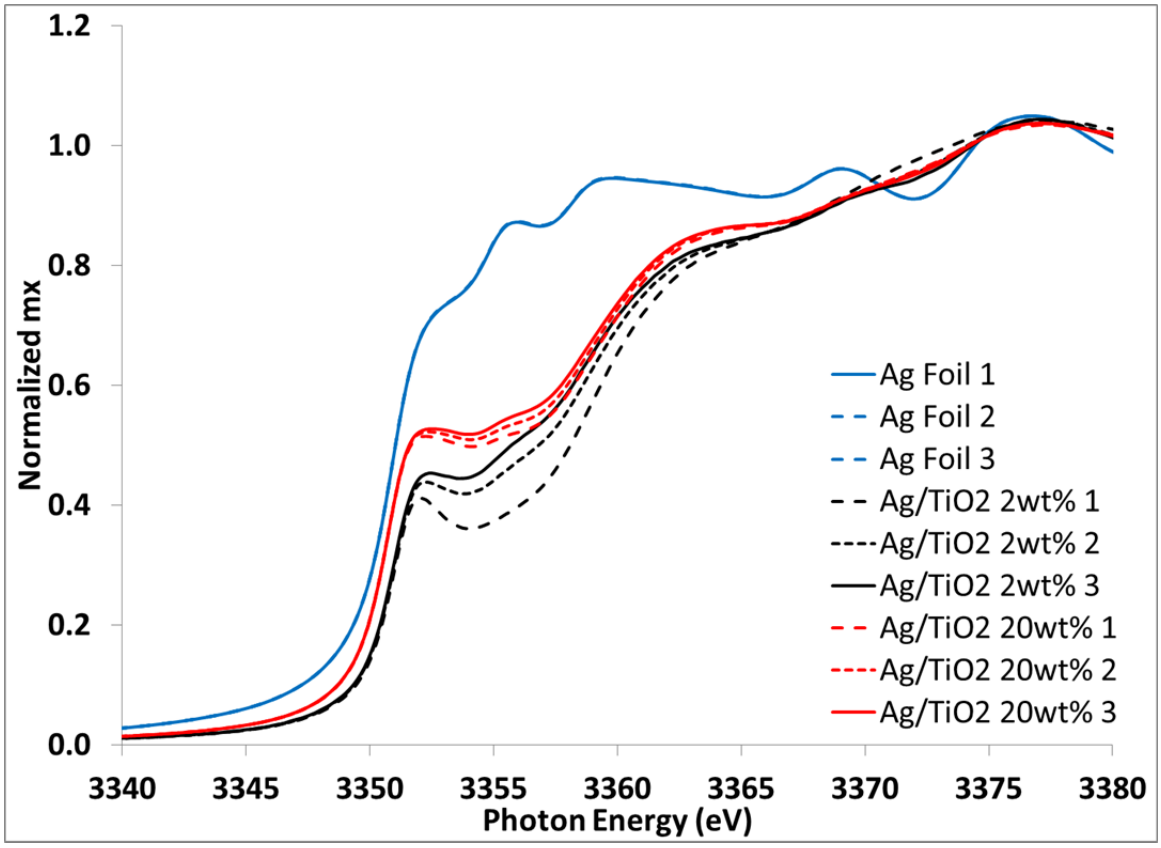

Figure 4-22 Ag L_3 XANES spectra exhibiting beam reduction with amount scaling proportionally to the oxide content

Silver was also studied with respect to L_3-edge changes when exposed to sulfur. It is established that 20 wt% loading has a metallic silver content not seen on the low-loading variants, as well as less surface area, pore volume and capacity.[45] Additionally, it is known that Ag/SiO_2 has a different oxide structure of silver than that observed in Ag/TiO_2, yet a capacity for sulfur that is similar to Ag/TiO_2.[45] Silver loading of 2 and 20 wt% on TiO_2 and 2 wt% on SiO_2 were utilized as a means of comparison in the silver structure when adsorption of sulfur occurs. The results were similar between the fuel samples and the BT reference, and thus the results in Figure 4-23 include only BT on the sorbent for the 20 wt% on TiO_2 and 2 wt% on SiO_2 samples.

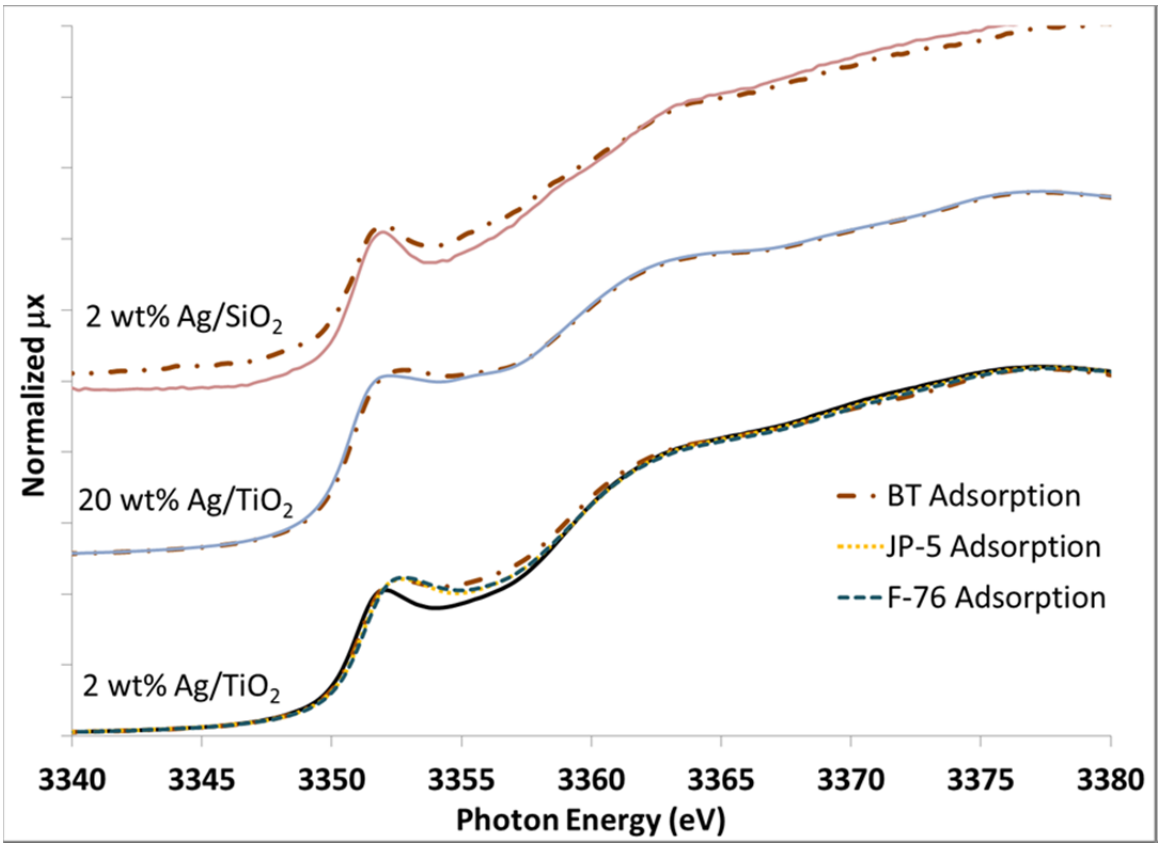

Figure 4-23 Ag L_3 XANES for adsorbent materials contacted with sulfur-bearing hydrocarbons

4.2.3. **Sulfur K-edge**

Figure 4-24 depicts the sulfur K-edge XANES data for a number of reference samples, as well as the fuels that were utilized in the adsorption experiments. These include the elemental sulfur and sulfate references utilized to show the range of oxidation states from 0 to +6, with various other singular compounds included to provide a valuation of the sulfur-heterocycle edge energies. For benzothiophene, its derivatives, and the fuel references, the primary "thiophenic" peak is labeled "B", and its location is marked in Figure 4-24. The JP-5 and F-76 fuels also have a one prior to peak B, which is labeled as peak "A". Their locations will be tabulated and

discussed subsequently. According to the dipole selection rules, the sulfur XANES corresponds to the transition from the 1s core levels to unoccupied states with *p* character. The hydrocarbons and sulfate references exhibit intense white lines while the elemental sulfur edge is much more muted and in this case is due, in part, to self-absorption. The self-absorption effect has been observed in previous sulfur XAFS studies and can be corrected if accurate determination of the area under the white line peak is warranted.[84] If self-absorption is not an issue, changes in the intensity of the white line can be attributed to the fact that the electronic structure of S is $1s^2 2s^2 2p^6 3s^2 3p^4$ and, thus, it can donate from one to six electrons giving oxidation states from 1+ to 6+ or can accept two electrons giving oxidation state of 2-. As sulfur donates electrons, the density of unoccupied states increases and hence the white line area increases. On the other hand, when it accepts electrons, the density of unoccupied states decreases and hence the white line area decreases. Changes in the XANES white line area vs. oxidation state have been observed for other systems, e.g., the Pd L_3-edge of Pd/SiO_2 catalysts.[139]

The XANES shows the distinct spread in edge and peak energy values based upon oxidation state, which is approximately 10.0/9.9 eV (peak energy) 10.1/10.4 eV (inflection point energy) from sulfur to $MgSO_4/ZnSO_4$, respectively. These values compare well with a spread of 10.8 eV (peak energy)[140] between sulfur and Na_2SO_4, and a spread of 10.5 eV (inflection point energy) between sulfur and $NiSO_4$.[141] The sulfur (0) peak is fairly small and gradually sloped, with character seen past 2477 eV being attributable to multiple scattering effects and is consistent with that observed in other studies.[142] The two sulfate samples, Mg and Zn, both show the intense white line with edge that is within 0.4 eV at the inflection point and 0.2 eV at the peak. There are no pre-edge peaks seen with these samples since Mg has no *d*-states in the valence region and those of Zn with electronic configuration of $[Ar]3d^{10}4s^2$ are completely filled.

The hydrocarbon samples shown in Figure 4-24 exhibit an intense white line with inflection edge energy within 0.1 eV of each other. However, JP-5 is shifted approximately 0.7 eV lower relative to the other hydrocarbon samples and also displays a double peak structure at the white line. It should be noted that the peak of the JP-5 white line appears to perhaps be better attributed to two separate Gaussians, as can be seen by the broadening and appearance of a doublet peak structure. This may be an artifact of local coordination from some compounds present in the fuel, perhaps cyclic hydrocarbons with different structure and/or without aromaticity[84,143], or else other sorts of sulfur-bound compounds such as thiols. Generally benzothiophenes with methyl substitutions are established to be the prevalent species within the fuel composition[45], however there clearly is going to be a content of sulfur in the fuels that is not aromatic in nature. The second peak of the JP-5 doublet is within 0.1 eV of the peaks for the other hydrocarbon references and the F-76 fuel sample, so may be assumed to be related to the aromatic sulfur heterocycles.

Similar double-peak structure as was noted for JP-5 has been observed in the XANES profile of compounds with C-S-S-C bonds, such as cystine, as well as in polymerized aromatic sulfides.[144] To better understand the characteristics of the fuels, examination of the first derivative of XANES data (Figure 4-24b) show that the double peak structure in JP-5 also exists in the case of F-76 but their intensities are different from those of JP-5. The peak with the higher energy is much more intense in the case of F-76. Hence, both JP-5 and F-76 may have similar species but their concentrations are different. The relative concentration of sulfur in a form similar to that of BT and/or DBT appears to be significantly higher in the F-76 fuel than in the JP-5 fuel.

The hydrocarbon references in Figure 4-24 all exhibit some weak features at slightly higher energy than the principal peak, associated with EXAFS oscillations. This can be determined by analysis of the variations between substituted and non-substituted compounds, e.g. DBT to 4,6 DMDBT. These are generally shifted approximately 2.1eV from the main peak, which is consistent with previous studies of thiophene compounds.[107] It can be seen clearly that the sulfur in benzothiophene-like sample spectra and the second doublet peaks of JP-5 and F-76 (peak B) has the same oxidation states. Furthermore, sulfur in BT and DBT has the same coordination geometry and sees the same type of atoms since both have similar oscillations above the white line. The first and second peaks generally are attributable to $1s \rightarrow \sigma^*$(S-C) and $1s \rightarrow \pi^*$(C=C) transitions, along with other weaker transitions.[107] However, S in 4,6 DBT display different oscillations above the white line, indicating that its local coordination geometry differs from that of BT or DBT due to the presence of the methyl groups.

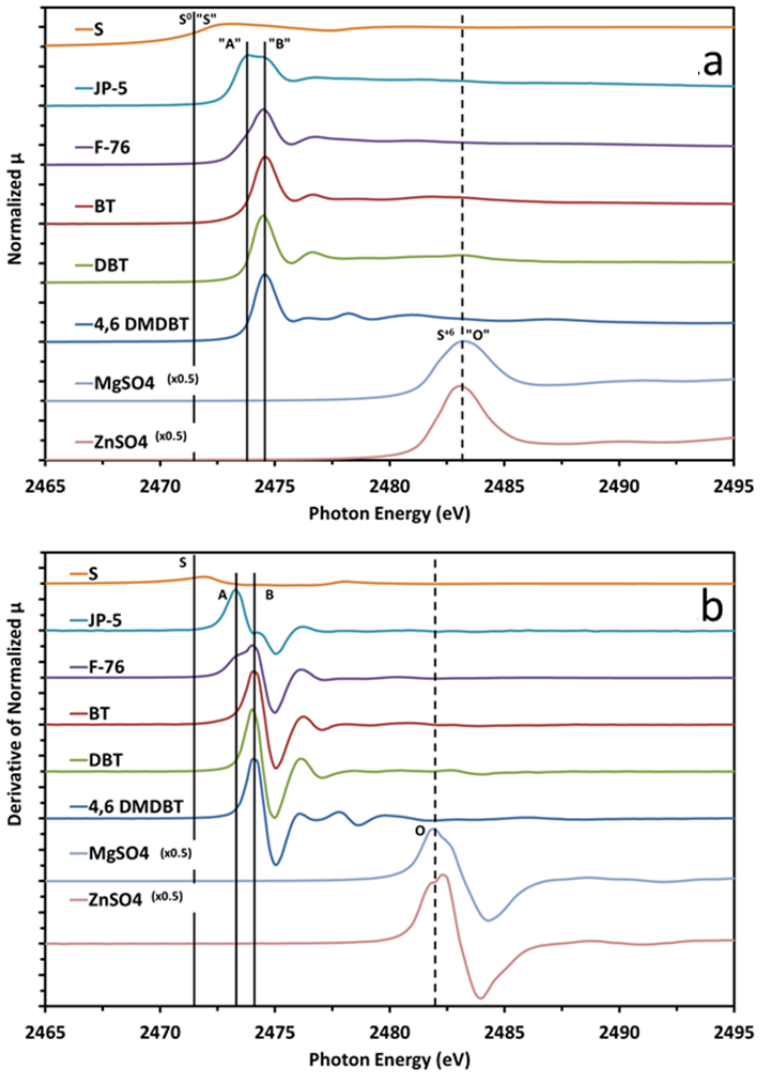

Figure 4-24 XANES spectra of references including elemental sulfur, sulfate, and sulfur hydrocarbon and fuels; b. First derivative of XANES spectra for the same references

TiO_2 without any silver loading was utilized as a control to explore the changes and influences of the support on the sulfur present in the hydrocarbons. It is known that TiO_2 has a demonstrated sulfur adsorption capacity by itself, which is improved upon with the addition of silver.[106] So, any interaction of sulfur with the support would produce a change in the k-edge behavior associated with its local coordination structure. Notionally an interaction with the

support would create a peak shift to lower energy indicating the creation of a TiS_2-like structure[145], or a peak shift to higher energy indicating the formation of an oxidized species.

Figure 4-25 shows the sulfur XANES of BT on bare TiO_2, and 4 and 20 wt% Ag/TiO_2 samples. It is clear that even bare TiO_2 without silver loaded onto it has an affinity for and an ability to substantially change the environment that BT exists in. It is immediately evident that for the BT sample, there is a complete change to the sulfur environment, creating a combination of highly reduced (peak R), and highly oxidized (peak O) sulfur molecules. The reduced sulfur, "R", is in a position roughly appropriate for that of TiS_2[145] or other reduced species. However, for this specific experiment, it should be noted that for the reduced species of TiS_2, there should be a secondary peak at ~9 eV higher energy[145], that may be explained to be associated with the metal 4s and 4p states hybridized with sulfur 3p states.[120] This feature is not observed for this experiment, and indicates that another similarly reduced species may be present, as the shift is significant enough to be indicative of a highly reduced state.[142] A substantial oxide peak, "O" indicative of +6 is notable in the figure, and is present at high energy, 0.6-1 eV above the sulfate references shown in Figure 4-24. This coincides with a complete removal of the main thiophene white line peak "B", at 2474.6 eV. Compared to the results for the supported silver experiments shown in the figure, the intensity of the sulfate peak is substantially higher due to the normalization of fewer features.

For the BT on 4wt% Ag/TiO_2 sample shown in Figure 4-25, it is immediately evident that Peak B' of the BT white line is present at 2472.4 eV, and has not been completely removed. It is at the same location seen on the BT reference (Peak B, shown in Figure 4-24 and the XANES replicated as a small dotted line for each experiment in Figure 4-25), indicating that there is no change in the oxidation state of the portion of BT that contributes to that peak. The second,

weaker peak C', following that edge is shifted approximately 0.3 eV at the inflection and maxima, as compared to the reference EXAFS oscillation in that energy range. Unfortunately this shift cannot be compared to the TiO_2 example shown in the figure, since there was no peak at this location due to the full interaction of BT with TiO_2. Analysis of Peak R at 2468 eV is consistent with the peak seen in the BT/TiO_2 experiment, and exhibits no shift whatsoever. However, the presence of peak B' in this experiment, which also aligns with the second major oscillation of TiS_2, indicates that the nature of a TiO_2 support-adsorbate interaction may be influenced by the loading of Ag (this peak was not present on the bare TiO_2). However, it is not anticipated that the presence of Ag creates its own sulfide, as the Ag-S sulfide edge is seen at a slightly higher energy than the reduced form observed in these experiments.[146]

For the BT on 20 wt% Ag/TiO_2 experiment, it should first be reiterated that this material has much lower BET surface area and pore volume as compared to 4 wt%, and that it has approximately half of the equilibrium sulfur capacity of the 4 wt% samples.[45] However, our analysis of the silver K-edge characteristics of a variety of Ag/TiO_2 samples showed a significant metal contribution, so the intent of this study was to identify any differences in the sulfur arrangement and local structure with metallic silver present in the system versus only an oxide component. Notionally the metal is mostly unavailable, being present in the internal structure of crystallites, however the metal surfaces may have a different type of capacity or functionality than other structures. Judging by the results, it appears that they merely present added metal, without change to the surface hydroxyl groups that perform the interaction. The most notable characteristic is the larger white line in the B' peak, which may indicate a lower amount of reacted sulfur, either in a reduced or oxidized form, and would be consistent with the established knowledge of the 20wt% Ag/TiO_2 system. While the B' peak may be attributable to TiS_2 as

mentioned previously, it is not believed that the additional silver is taking part in the desulfurization, and thus we do not attribute further changes in B' to more reduced species.

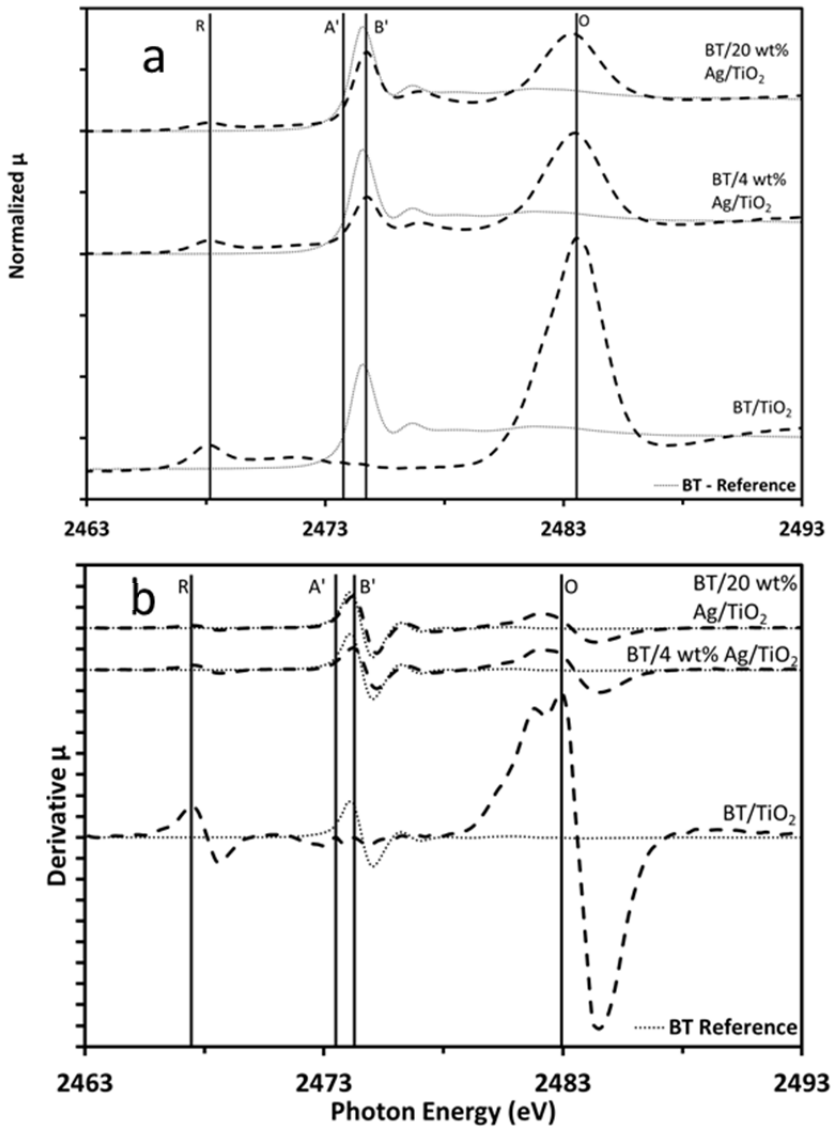

Figure 4-25 a. XANES of BT on the three sorbent materials, with a reference BT spectra; b. First derivative of XANES spectra for the same experiments.

The JP-5 results shown in Figure 4-26 indicate a substantial change in the character of the sulfur local coordination environment, including changes in peaks A and B. The R and O peaks

are at the exact same energy for all three results shown. What is observed is almost complete removal of the lower energy peak in the JP-5 doublet, thus a change from A to C' indicating a slight increase of oxidation state, perhaps to sulfoxide. The location of C' is different than the EXAFS oscillation observed in the local area of C', specifically with the oscillation at 2476.8 eV versus C' at 2476.4 eV.

It can be clearly noted that the intensity of peak B' vs C' change according to silver loading on the adsorbent. The peak associated with thiophene (B and B') grow in intensity with metal loading, while the C' peak that is notionally a higher oxidation state, decreases. For the 4 wt% sample adsorbing sulfur from JP-5, it is notable that the initial thiophenic peak B' is larger as compared to the JP-5/TiO_2 B' peak. At 4% loading, peak B' and C' have about the same intensity, which we believe to be related to the presence of two reduced species changing in concentration based upon the presence of silver, as TiS_2 has a second intense peak in the energy range of B', as discussed previously. The sulfate peak is observed, though the major intensity draws the maxima to lower energy relative to that observed for JP-5 on bare TiO_2 (2482.1 vs. 2482.9 eV). However, this trend appears to be consistent across the various adsorption experiments, where the major contribution to the highly oxidized species on bare TiO_2 appears to be at a higher contribution than on the Ag/TiO_2 samples. This is likely due to the formation of two different oxidized species associated with the support and the dispersed silver.

At 20% loading, the JP-5 XANES is perhaps the most interesting, because peak B'is retained, with the other main markers remaining consistent. However, peak C', is no longer observable as a separate peak; different from the 4 wt% where the peaks were at the same intensity, or the plain TiO_2, where the intensity was higher on C'. Additionally, an extra structure at 2478 eV was observed, which is low in intensity and generally washed out by the

other adsorption edges, but may be attributable to a lesser oxidized sulfur constituent, such as Benzothiophene sulfoxide, which has been reported previously at 2479eV.[147]

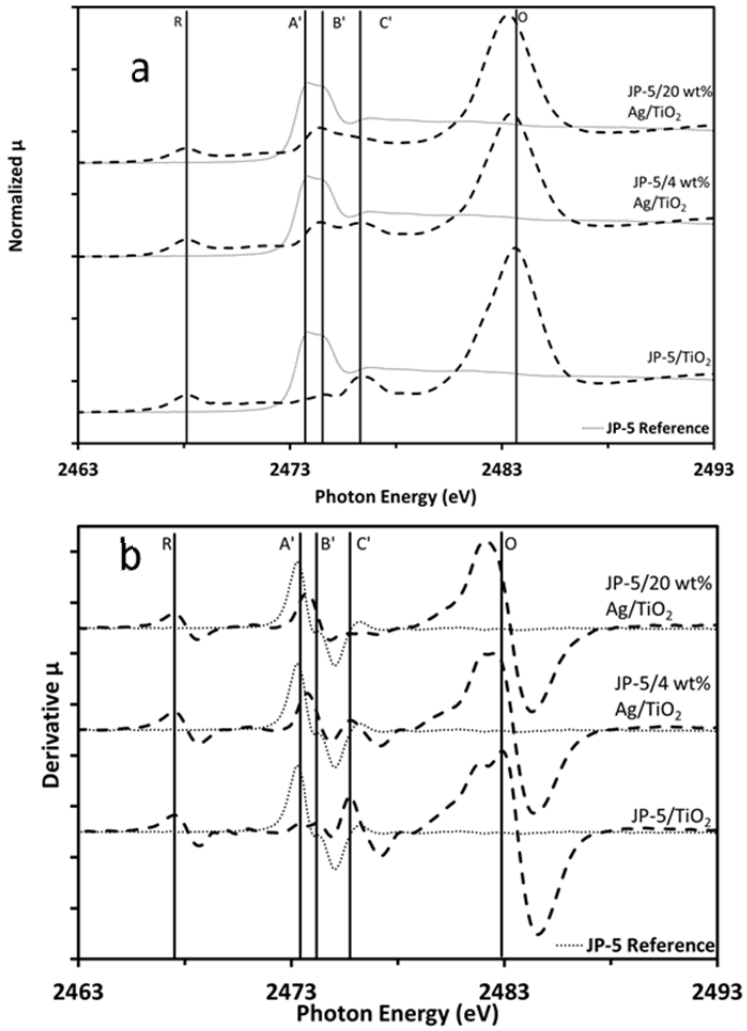

Figure 4-26 a. XANES of JP-5 on the three sorbent materials, with a reference JP-5 spectra; b. First derivative of XANES spectra for the same experiments.

The F-76 results are displayed in Figure 4-27, and also show a change in the character of the sulfur local coordination environment. The F-76 sample shows a similar R and O peak occur as was seen with the other hydrocarbons. The peak B' was reduced in intensity on bare TiO_2, but

still remained in the same location. Given the significantly greater sulfur content in the F-76 fuel relative to the JP-5 fuel, it is reasonable to expect to see the peak B' remain at a reduced level.

The results of F-76 fuel on 4 wt% Ag/TiO_2 show some differences from the blank TiO_2. The primary observation is the weakened C' peak, as compared to the B', which retains a high intensity. Changes in the B' peak, i.e. the increase in B' intensity with Ag loading, may also be indicative of the TiS_2 formation versus alternate reduced species on bare TiO_2, as has been noted for the other experiments. The variation in the C' peak implies a change in the sulfur coordination environment due to the addition of silver as a result of a different type of interaction or more complete conversion to a highly oxidized form. The inflection point energy of peak O for the F-76 experiment is similar in location relative to the case for bare TiO_2.

The 20 wt% Ag/TiO_2 spectra also exhibited differences, with Peak B' retaining strong intensity, either attributable to the lower capacity of 20 wt% Ag/TiO_2, and the fact that the F-76 fuel sample had a substantial amount of sulfur present, or the artifact of the TiS_2 formation associated with Ag loading. Peak C' is further reduced in intensity, indicating that it is either not being formed as a reaction product, or has been further oxidized and thus isn't present.

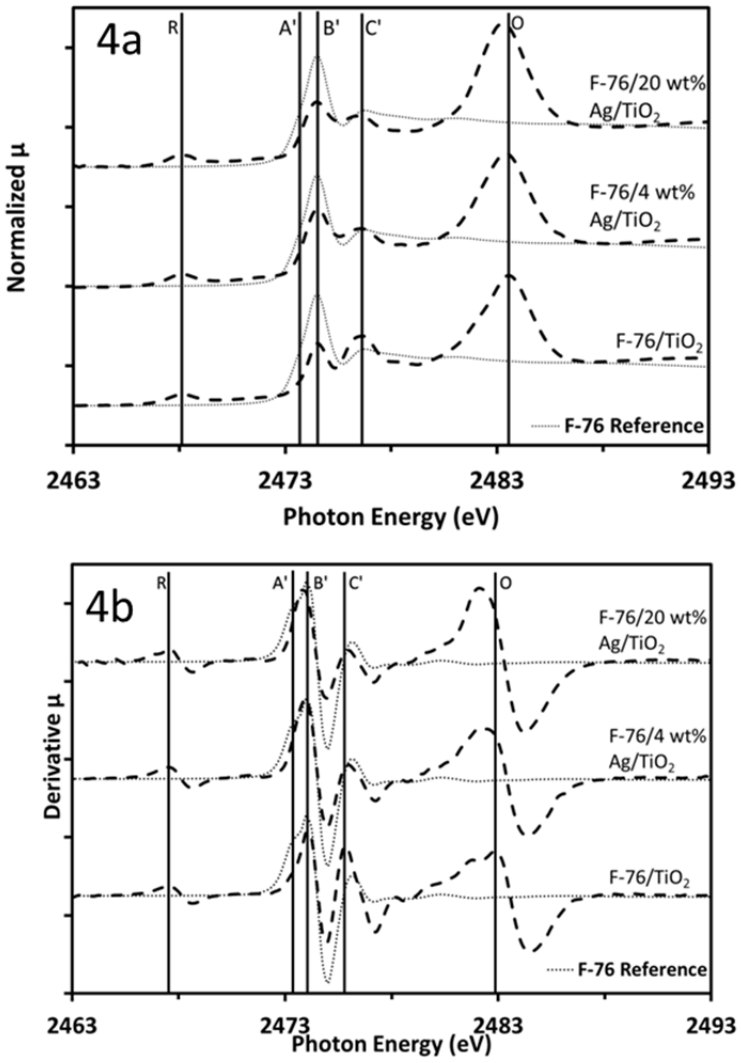

Figure 4-27 a. XANES of F-76 on the three sorbent materials, with a reference F-76 spectra; b. First derivative of XANES spectra for the same experiments

4.2.4. **Titanium K-edge**

Reference materials were prepared and spectra collected in electron yield mode, to probe the surface of the materials to a depth of ca. 100-1000Å.[148] Figure 4-28 shows the XANES spectra for the reference compounds, which were selected to help determine if alternate oxidation states were present in the near-surface area. The XPS Ti 2p studies showed no obvious change in electronic structure of the Ti upon incorporation of the dispersed Ag. However, it was desired to probe further to support both a validation of this observation, as well as the potential to study the potential for changes to Ti upon adsorption of sulfur, to help identify a potential TiS_2 phase

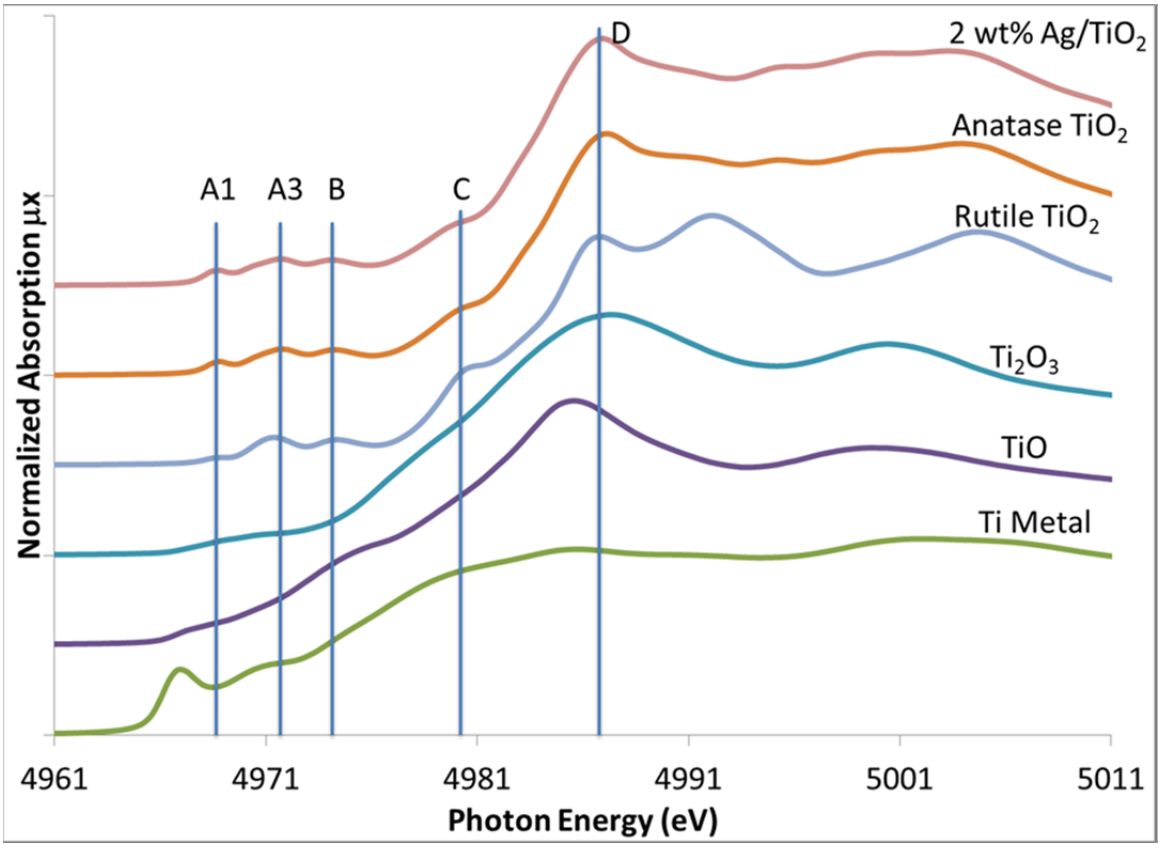

Figure 4-28 Ti K-edge XANES for adsorbent material and reference Ti oxides with pre edge and other features labeled

The spectra shown in Figure 4-29 show that the Ti K-edge XANES appear rather similar, with pre-edge features and peaks all existing in a close range. These features are labeled as A1, A3, B, C, and D (A2 is typically a shoulder on the A3 peak and difficult to discern) in a manner consistent with the peak identification performed by Brydson et al.[149] The spectra for anatase and rutile exhibit similar features in the pre-edge area, with oscillations in the EXAFS being apparent due to the variations in crystal structure. It should be noted that the top spectra, for 2 wt% Ag/TiO_2 appears consistent and highly similar to the Anatase TiO_2 reference. Ti_2O_3 and TiO have pre-edge and subsequent oscillations that are more muted, and exhibit slight shifts.

Ti XANES was collected for Ag/TiO_2 with different levels of silver loading, to identify if the support changes in different ways with the addition of metal. Capacity is highest at ca. 4 wt% Ag[45], and metal structure forms past that, so notionally the greatest utilization of surface oxygen due to the hydration of the greatest number of Ag ions would exist at 4 wt%. However, as shown in Figure 4-29, there is no substantial intensity or peak shifting characteristic with respect to loading, or the creation of a "blank" TiO_2 that was straight from manufacturing versus impregnated with nitrate groups from nitric acid and calcined, similar to the approach for preparing the Ag/TiO_2 sorbent materials.

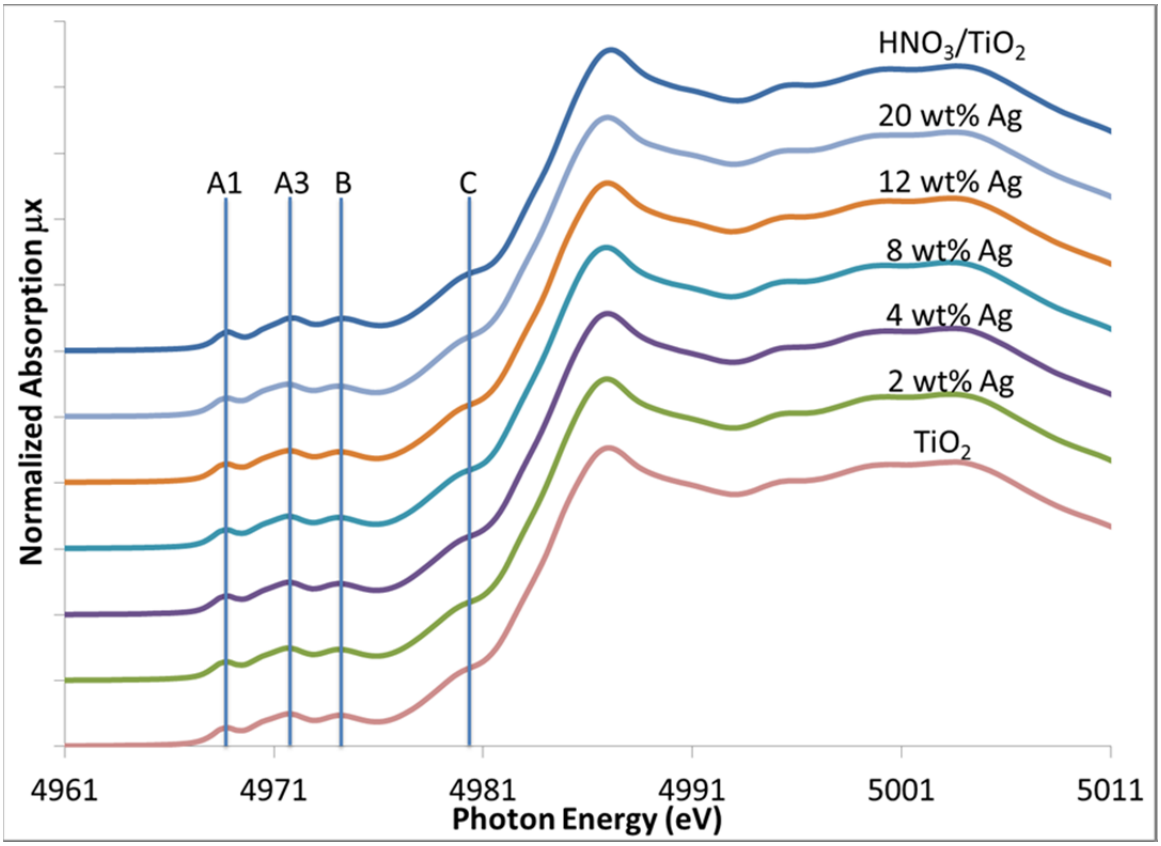

Figure 4-29 Ti K-edge XANES for the adsorbent materials with differing silver loadings. Spectra include TiO_2 as-delivered from vendor, as well as the same TiO_2 after impregnation with HNO_3 and calcined under the same nitrate loading conditions as the Ag-loaded sorbents

K-edge XANES was also studied with respect to the addition of sulfur-bearing compounds. We have postulated from the study of sulfur K-edge on these materials that the support plays a role in the adsorption of sulfur in different ways with and without silver addition. Based upon sulfur K-edge shifts, we identified the potential for S-H reduced sulfur to be present on TiO_2 when silver is not dispersed, and then TiS_2 to be the prevalent reduced form of sulfur when silver was added. Figure 4-30 a-d indicate that there are indeed changes observed with the addition of sulfur to bare TiO_2 and TiO_2 with dispersed silver, and that the results are indeed different. Figure 4-30 shows the entire XANES for both scenarios, and shows the BT reference as well as high sulfur F-76 distillate results. Additionally, JP-5 jet fuel is also shown for the

Ag/TiO_2 system as a means of identifying if any different phenomena are observed. While the spectra appear extremely similar, and there is no change in the edge energy in terms of an overall shift, it can be clearly seen that the spectra differ in intensity at the locations about the key edge features. The most obvious change can be seen in Figure 4-30, where the A2 peak is more pronounced upon contact with sulfur, as compared to the reference for bare TiO_2. Figure 4-30c shows the same characteristic for peak C. It should be noted that these phenomena are not more pronounced for the Ag/TiO_2 sorbent relative to the TiO_2 sorbent. The white line peak is shown in Figure 4-30d, and shows the opposite behavior – the peak is less pronounced upon contact with sulfur, as compared to the unexposed references, and this trend is observed for both materials. Due to the limited amount of hydrocarbon exposed (incipient wetness), and the fact that the BT sample had fully dried its octane solvent prior to collecting spectra, it is not believed that the presence of hydrocarbon or liquid fuel is causing an attenuation effect to cause this.

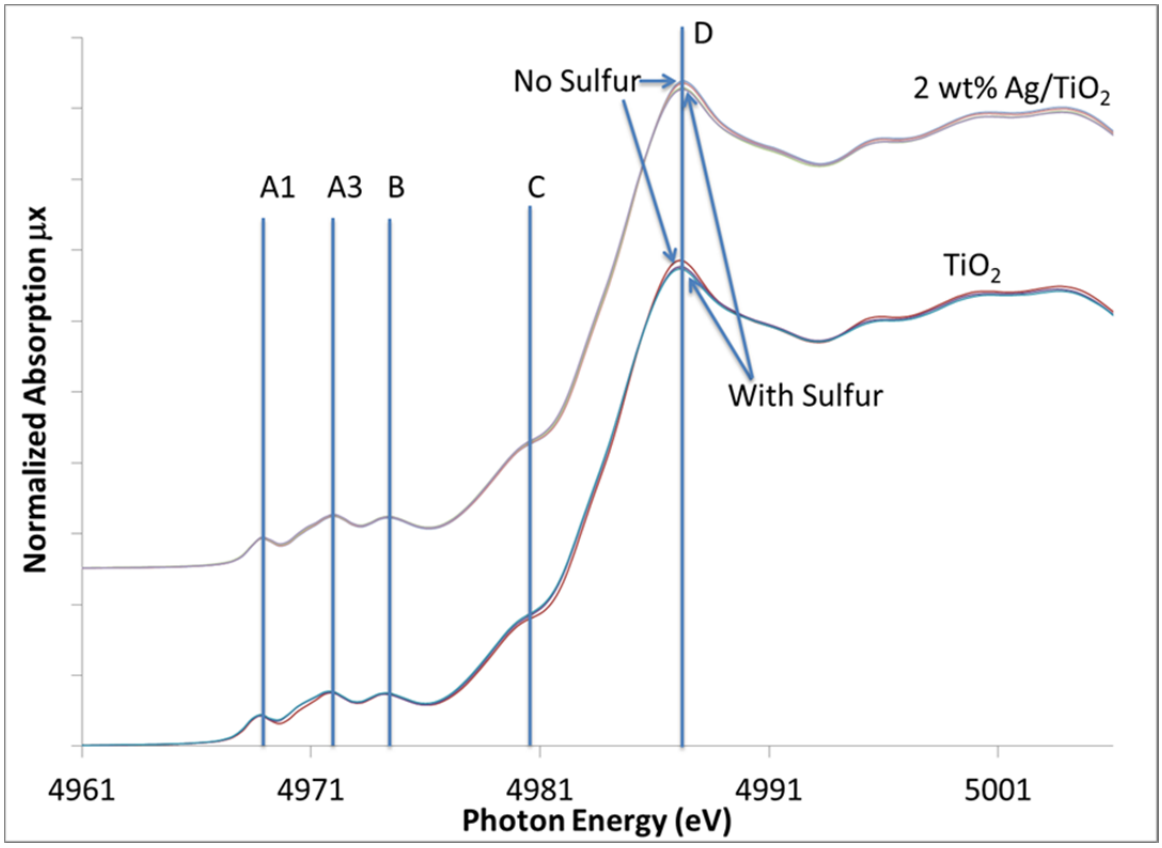

Figure 4-30a-d full Ti K-edge XANES, with peak notations listed (A2 omitted to better show the changes in the TiO_2 spectra). Each area of observed change is shown in greater detail in b-d

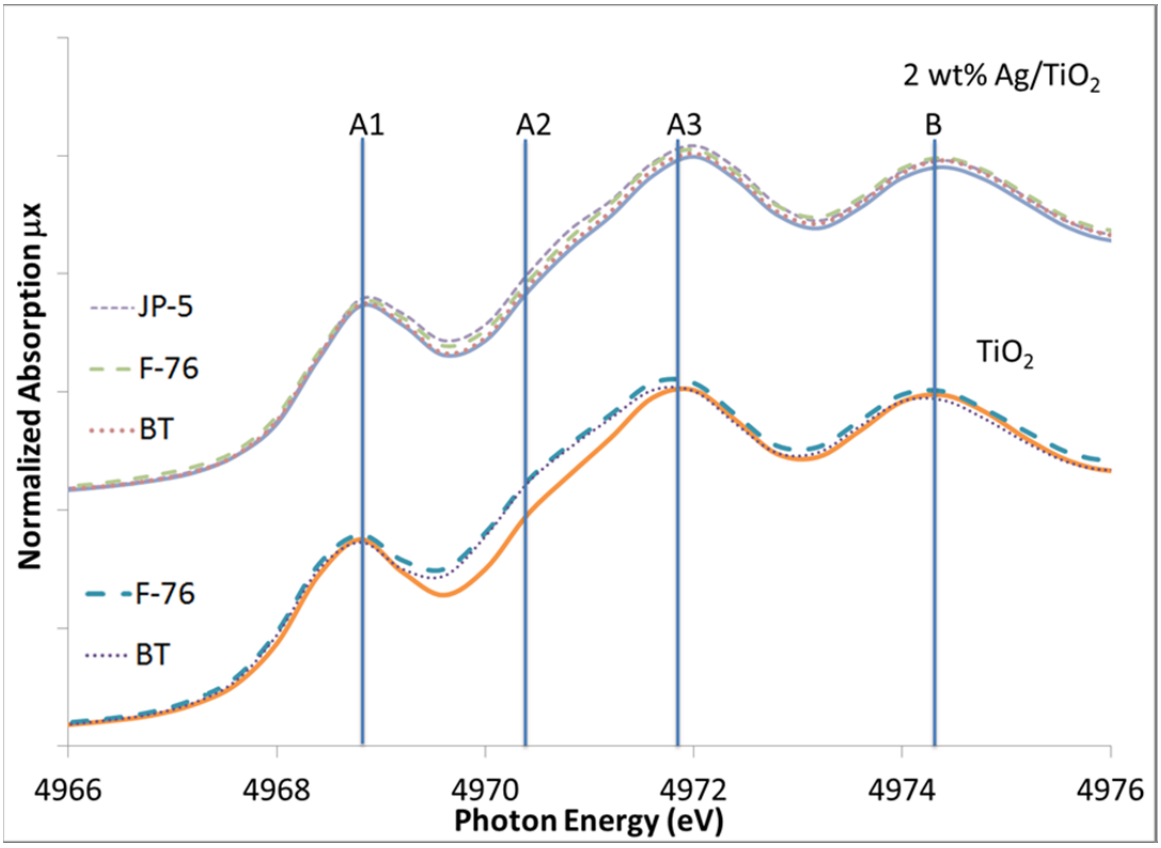

Figure 4-30b Ti K-edge XANES of the pre-edge features of TiO_2 and Ag/TiO_2 upon contact with various sulfur

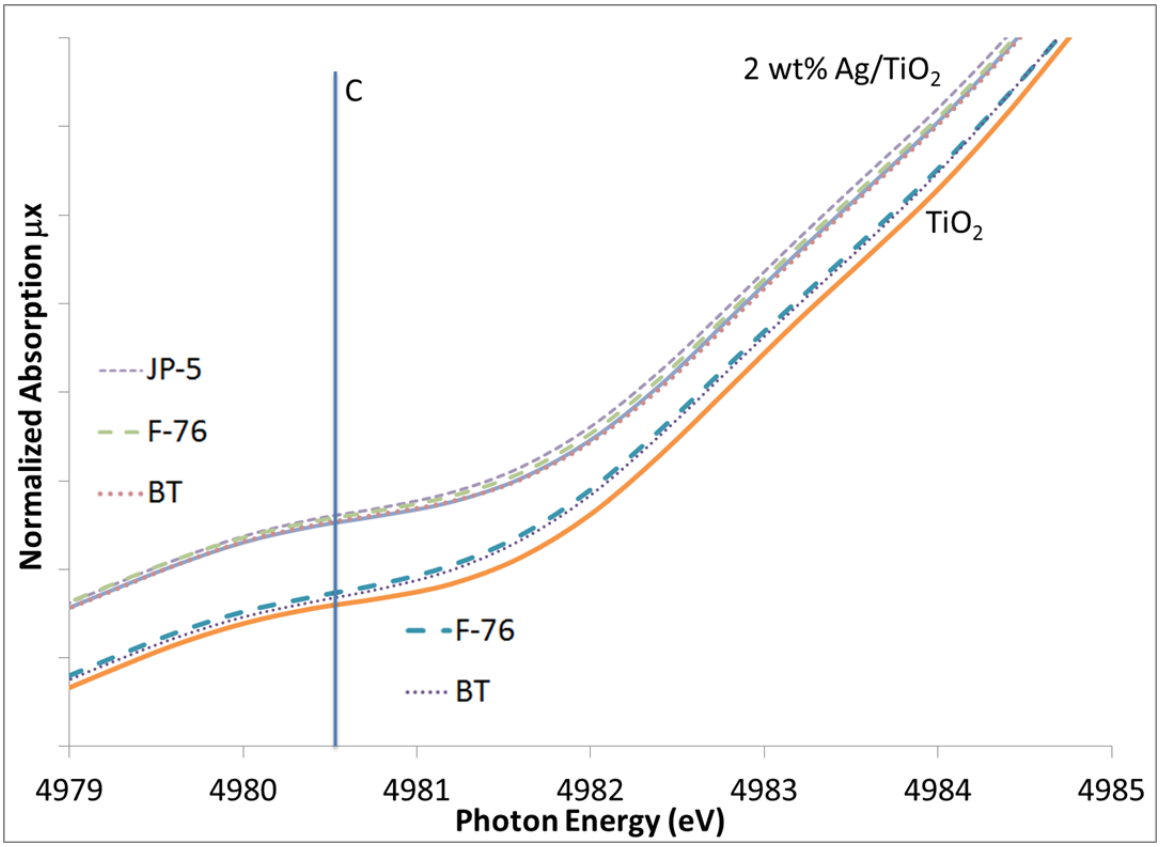

Figure 4-30cTi K-edge XANES of the Peak C features for the adsorption experiments

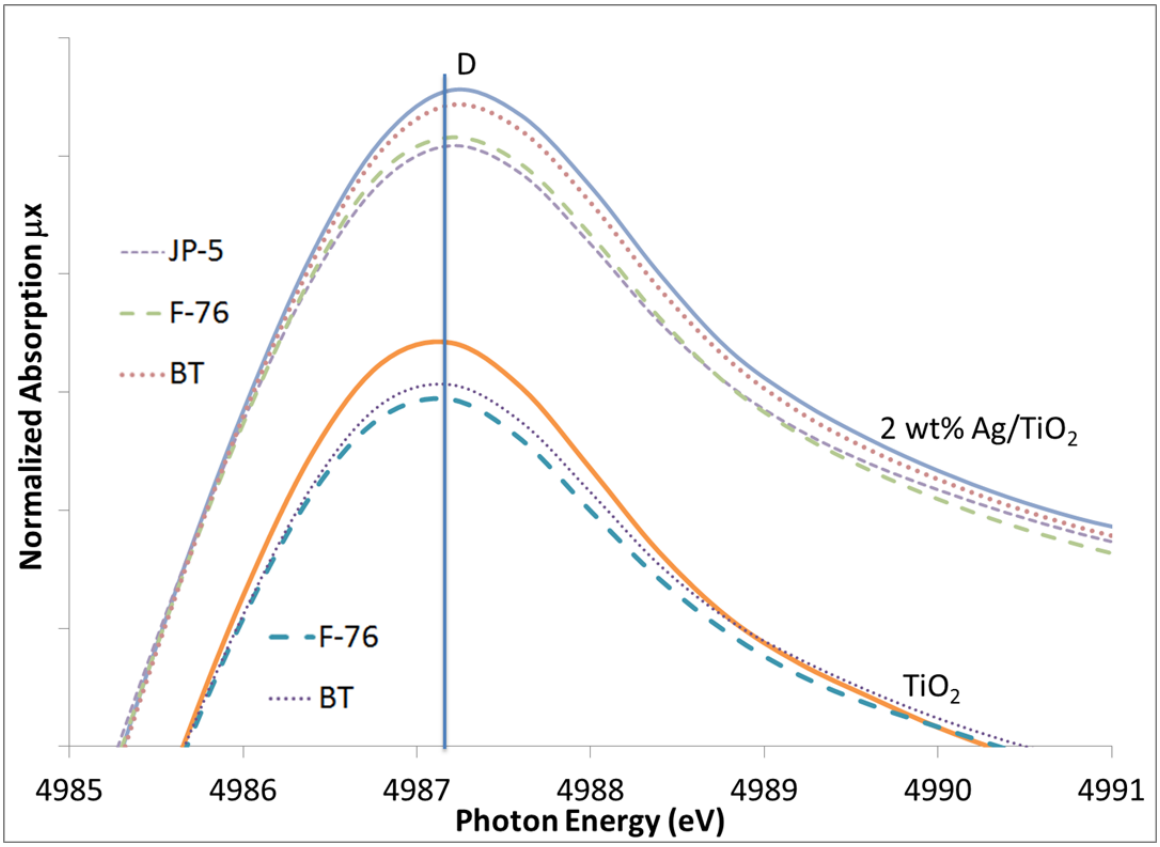

Figure 4-30d Ti K-edge XANES of peak D for the adsorption experiments

5. Discussion of Results

The use of EXAFS as a tool to identify the nature of the silver component of Ag/TiO_2 adsorbents is performed for the first time with supporting information provided by XPS and XRD. Detailed study of the Ag/TiO_2 system as produced with a range of silver loading levels indicate the presence of a unique form of silver oxide that is not like its precursor ($AgNO_3$) or assumed oxide form (Ag_2O). This form of Ag-O is consistent with respect to mass loading, while the metallic silver species increases in coordination, indicating growth of silver crystallites. From these results, coupled with capacity results established previously, one may conclude that the active phase is a type of silver oxide crystallite, which either serves as the adsorbing species or else facilitates adsorption in conjunction with other active moieties that are the actual interfacial sites. Thus it appears likely that crystals of silver oxide exist in a form that is likely fine and highly dispersed due to known capacity and molar ratios of adsorbed sulfur to silver atoms. Then, at higher loadings, silver metal cluster size increases, as evidenced by growing coordination number for the metallic phase. This silver metal has an oxide shell, as determined from the XPS studies, though it is not clear that this oxide, which is likely only a very small component on a number of atoms basis, has any real influence upon adsorption performance, as compared to what would notionally be a far higher number density of small oxide clusters dispersed throughout the TiO_2 surface. The oxide shell may be present on all sides of the oxide particle, or may only be present on the exposed outer surface. Figure 5-1 graphically depicts the potential forms of silver on Ag/TiO_2 adsorbent materials as seen in this study.

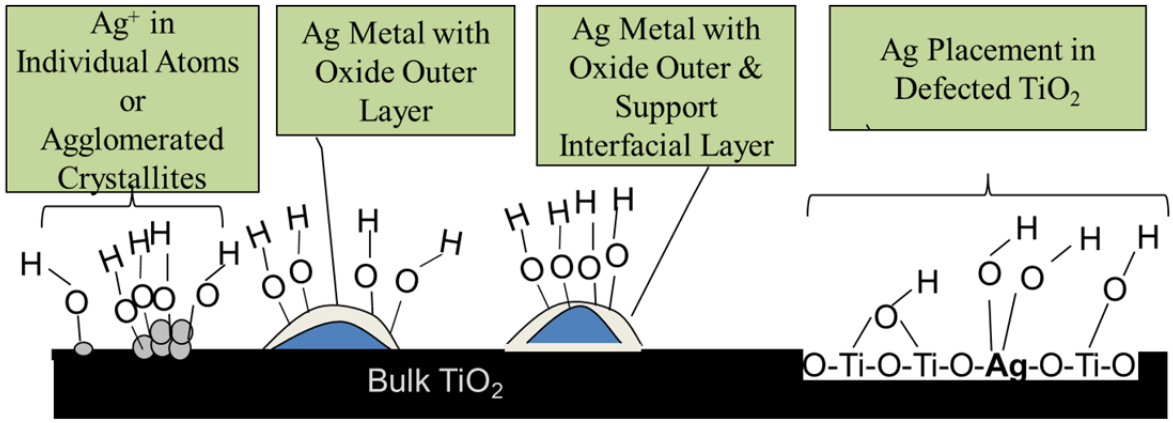

Figure 5-1 Theoretical Forms of Ag on TiO_2 support

Given the previously observed capacity of TiO_2, and the monotonic enhancement in capacity observed from TiO_2 loaded at ≤4 wt% silver for selective desulfurization, one might conclude that the fine oxide particles catalyze the creation the adsorptive species on the surface of TiO_2. Based upon findings, the effects and proposed mechanisms will be discussed further.

5.1. Silver

- Silver K-edge

We conclude from the analysis of the EXAFS results at different loading levels of Ag on TiO_2 (and also contrasted with reference materials and a variant of Ag on SiO_2 support), that the form of silver when supported on TiO_2 as a sorbent material is a unique variant. The oxide form is not Ag_2O, AgO or $AgNO_3$. For loadings up to 4 wt%, the silver is in an oxide form with an Ag-O bond distance of 2.32 Å, with a consistent coordination number of N≈4 and a high degree of structural disorder. The structure of the oxide phase that forms on theTiO_2 support is also distinct from the structure of the oxide phase that forms on the SiO_2 support. As noted in Table 4- 6, the Ag-Ag distance for all loadings in the range 8-20 wt% is consistent with that of metallic

Ag but the coordination number increases as the loading increases from 8 to 12 wt%, indicating the growth of metal crystallites and evolution of more consistent metallic structure, while the structure of the oxide component remains unchanged. As the loading on the TiO_2 support increased to 8, 12, and 20 wt%, the mole fractions for the oxide phase decreased to 0.78, 0.67, and 0.55, respectively, while those of the metallic phase increased appropriately so that the sum of the fractions of the oxide and metallic phases adds up to one for each loading. The mole fraction for the oxide phase was determined by dividing the measured coordination number for the oxide when the metal is present by that for the oxide when that metal was not present. It is to be noted that the mole fractions for the oxide phase and the metallic phase determined based on the coordination numbers are more accurate than those determined based on the linear combination analysis of XAFS spectra. This is because in the linear combination analysis the silver foil was used to account for the metallic character in the sorbent materials which would have been fine if the size of the silver particles in the sorbent materials is larger than 10 nm. As indicated in Table 4- 6, the Ag-Ag coordination number for the silver particles could be well below that of the silver foil which is 12. On this basis, the linear combination analysis of XAFS spectra overestimates the mole fraction for the oxide phase and underestimates the mole fractions for the metallic phase.

TiO_2 is well known to have a defected surface structure and these defects have been attributed to various characteristics associated with adsorptive capacity.[150] Previous efforts[151,152,153,154,155] have indicated that 3D islands form as silver metal along step edges on the TiO_2 planes and related studies[155] have indicated that the silver clusters are larger than those of other metals loaded on TiO_2.[155] The previous work reported that no interaction was seen, though

XPS exhibited a strong peak shift for smaller clusters.[156] While XPS shifting is consistent with the results shown in Figures 2-5, the EXAFS results show a consistent oxide phase which is unique as compared to reference samples. It also appears to be unique as compared to various reactive intermediate silver oxides reported previously[157], and has a constant presence at all loading levels ≤4wt%. While the presence of Ag metal may be consistent with the structures reported previously, the adsorption capacity benefits that have been seen with Ag loaded onto TiO_2 are greatest at ca. 4wt% loadings,[45] not elevated loading levels. This implies that the established Ag metal is not an active constituent in the desulfurization operation. Thus the species of interest under this analysis is indeed the Ag-O coordinated structure, which is otherwise unknown and not discussed in detail in other studies of adsorbent materials or dispersed silver. Other analysis has theorized the presence of Ag^{+1} on the surface of the TiO_2 support[47] with coordination into the oxygen structure of the TiO_2 support. Optimized fitting of the EXAFS results was performed by utilizing a procedure accounting for the first oxygen shell theory from $AgNO_3$,[130] which indicates that a central Ag scatterer will have six coordinated oxygen atoms present in the nearby structure. For the $AgNO_3$ theory utilized, these oxygen atoms are all present at roughly ~2.41Å (as the exact coordinates for the oxygen atoms are not well defined), which is greater than the estimated Ag-O distance for the supported Ag/TiO_2 materials based on EXAFS spectra. Review of the XANES data would indicate that the behavior of Ag_2O is similar between the supported materials and the Ag_2O reference at energies associated with the lower half of the edge; however the structure at the upper half of the edge and beyond is substantially unique, as is the case when compared to $AgNO_3$, the silver species precursor. Ag in Ag_2O, however, is linearly coordinated with two oxygen atoms at 2.04Å[114], a far shorter distance than that of the oxide phase in the sorbent material. These results would in

total confirm the presence of Ag^{+1} as the form of silver present within the oxide phase, but one that is unique from either the $AgNO_3$ or the Ag_2O forms that might be expected given the conditions for preparation, and the thermodynamic stability of the bulk compounds.

Based on surveys of the literature, it appears that for solid phase silver, the observed Ag-O bond distance of 2.32Å is unique. However, similar Ag-O distances have been observed under fully hydrated aqueous conditions based on X-ray absorption spectroscopy. Specifically, silver perchlorate[111,158] and silver nitrate[111,158,159] have been studied at various concentrations and temperatures to identify the hydration characteristics of Ag^+ in solution. The findings for perchlorate in solution at room-temperature indicate a coordination number in the range of 4.3-4.5 with a bond length in the range of 2.31-2.32 Å.[159] The findings for $AgNO_3$ in solution at room temperature indicated a coordination number in the range of 3.4-4.4 with a bond length in the range also 2.31-2.32 Å.[159] These studies show that the hydrated Ag^+ ion exists with a fourfold coordination with water. However, more recently, further analysis has shown that it is not possible to distinguish between distorted tetrahedral structures and other forms of collinear O-Ag-O structures.[111]

As prior studies of the Ag/TiO_2 system indicate a substantially increased surface acidity with the addition of Ag as compared to a bare TiO_2 surface[63], the substantial increase in titer uptake would be consistent with a large number of hydroxyl groups coordinated with the Ag present. This would form the O-Ag-O type arrangement that is identified by this bond distance, and indicative of a hydrated species dispersed as a solid on TiO_2. The uptake and large number of Ag-O bonds would imply that the silver notionally facilitates the creation of geminal hydroxyl

groups that interact with the sulfur heterocycles. This would explain too why the Ag-O bond length of 2.32Å is observed in a highly disordered structure – silver disperses into defect sites where the surface oxygen structure is changed, and then truncates with other hydroxyl groups in a manner that allows it to obtain a coordination of optimal stability. This results in highly dispersed, highly disordered O-Ag-O type bonding associated with interaction with the support's surface oxygen and additional oxygen present in the surface hydroxyls on the TiO_2 and Ag itself. Thus it can be postulated that dissociated water, present as hydroxyl groups on the metal surface, causes a local coordination structure similar to a fully hydrated Ag ion, and the facilitation of increased surface hydroxyl groups is key to the performance of the sorbent. While plain TiO_2 will truncate with surface hydroxyl groups, it is the tendency of the dispersed silver to associate with multiple groups to form its stable fourfold coordinated structure that facilitates the increase in capacity.

- Silver L-edge

The L-edge further identifies that the oxide form of silver dispersed on TiO_2 is not Ag_2O, AgO or $AgNO_3$. Figure 4-21 shows the similarities and differences between the $AgNO_3$, 2 and 20 wt% Ag/TiO_2, and metallic Ag. Utilizing a linear combination fitting approach to simulate the 20 wt% Ag/TiO_2 sample from spectra of the metal and 2 wt% Ag/TiO_2 Ag oxide, the mole fraction for the oxide was found to be 73%, which is roughly comparable to the value found via K-edge analysis of 69%, using different samples from the same production lots. In our previous analysis, we had accounted for coordination number being less than 12 for the metallic silver fraction within the sorbent, and calculated an actual mole fraction for the oxide phase of 0.55. This was due to the fact that the linear combination analysis of XAFS spectra overestimates the mole fraction for the oxide phase and underestimates the mole fractions for the metallic phase.

This would hold true for this case as well, but the linear combination at the L_3-edge appears to validate that the oxide and metal fractions are approximately correct.

The XANES shown in Figure 4-21 is ripe with information on the oxide phase in the 2 wt% sorbent material. Though similar in appearance to the $AgNO_3$ reference, it should be noted that the 2 wt% sample has a more distinct but less intense peak A. This peak, indicative of the $2p \rightarrow 4d$ transition, has an intensity associated with the degree of covalency.[138] Ag_2O, for example, has substantially higher covalency than $AgNO_3$, and the difference in the feature of Peak A can be attributed to this.[138] In addition, these difference, are undoubtedly related to differences in local coordination geometry with Ag in Ag2O has linear coordination with R = 2.04 Å) while Ag in $AgNO_3$ has octahedral coordination with R = 2.41 Å). The intensity of the feature for the 2 wt% sample is lower than that for $AgNO_3$, and thus it can be attributed to a greater ionic character than even that for the nitrate exhibits as a result of different coordination geometries; similar to the basis of the K-edge absorption. It should be noted that this feature is not anticipated for materials with a closed d^{10} shell, and its presence can be attributed to unexpected vacancies in the 4d states proportional to the degree of covalency.[138] Thus we can better attribute the ability to desulfurize to the acidic character of the sorbent surface, and the importance of electrostatic forces in creating the disordered ionic structure[138] that facilitates adsorption via active surface moieties.

Under adsorptive conditions, subtle changes to the Ag L_3 spectra can be observed, as shown in Figure 4-23. From the sulfur perspective that we have shown and will discuss further, there was no indication of a reduced sulfur species that would indicate Ag_2S on the surface. Thus we postulated that the reduced sulfur observed was attributable to S-H groups and TiS_2. In the figure we show that there is a slight change observed in the A feature of the spectra for 2

wt% Ag/TiO_2, which differs in behavior from the higher loaded Ag/TiO_2 and the Ag/SiO_2 samples shown for comparison. The peak intensity appears greater upon first glance; however the distinct character of peak A is less than the 2 wt% reference. It appears that the states contributing to the rising edge at higher energies of 3355 eV and greater cause the peak to wash out and potentially shift slightly overall to higher energy. Because there is no basis to assume an Ag_2S species is formed on the surface, one must attribute this behavior to what was postulated from the analysis of the sulfur K-edge. Specifically, that silver will tenaciously attempt to maintain its fully hydrated structure, and facilitate the creation of a titanium sulfide species to maintain its own hydration, thereby preventing the sulfur fragments from associating with surface hydroxyls to create oxidized sulfur species (which are also observed in the sulfur XANES). When silver is not present, the S-H groups solubilize into the hydrated TiO_2 surface, but with silver added to the surface, this does not occur due to the tenacity of the silver to its local hydration. The A peak is washed out and possibly less influential due to higher energy interactions which draw the edge to slightly higher energy, when sulfur is added because it forces a higher level of hydration and ionic character on the surface Ag by further filling of the few unoccupied d states.

The results seen on 2 wt% Ag/TiO_2 are different from those seen on the 20 wt% and the Ag/SiO_2. The 20 wt% sample shows minimal differences with and without sulfur for two reasons. First, there is less total capacity, due to lower surface area, pore volume, and dispersion.[45] Therefore the ability of the sorbent to adsorb sulfur is reduced, and so any changes would be less obvious. The second reason is because of the high loading variant's tendency to create larger metal crystals as opposed to dispersed surface oxides. While efficient to minimize surface free energy, it is not a desired effect for a viable adsorbent material. Thus this metallic

silver resides with the core of the particle and is less able to be involved in the adsorption reactions. However, its presence still provides a metallic silver bias to the spectra. This means that minor changes to the spectra from the signal associated with desulfurization adsorption reactions are overcome by the metal signal and are more difficult to discern. For SiO_2, the A peak appears to also be slightly washed out by higher energy features. However, there is no shift of the overall edge to higher energy, and the feature intensity may be questionable due to a higher normalized baseline in the experiment with BT.

5.2. Sulfur

It is clear from a cursory review of the XANES results, that the thiophenic sulfur present in the fuels and BT sample change to other forms upon contact with the adsorbent materials. The baseline capacity of TiO_2 is established from prior analysis[45,70], and it is postulated that the addition of silver enhances the capacity via coordination with more or different surface hydroxyls.[63] Review of the results in Table 5-1 indicates that a reduced form of sulfur is created, along with a highly oxidized form, and that the constituents that are formed vary according to the presence and loading of silver. The peaks observed around the assumed value for a thiophenic compound (ca. 2474) clearly offer a substantial amount of information as references and under the adsorption conditions, with formation of lesser oxidized species as well as considerations for the reduced species. Figure 5-2 indicates graphically the known and assumed oxidation state of sulfur for the various observed peaks, to show the sensitivity of the XANES to oxidation state, and a basis for the accuracy of our claims. It should be noted that the most reduced peak location does not fit the observed trend, and would mathematically fit best if a "3-" structure were possible. All of the other peaks fit the trendline of known oxidation states

extremely well.[84,160] This discussion attempts to provide insight into the sulfur chemistries in the fuel and changes during adsorption, based upon analysis of XANES spectra.

Table 5-1 Tabulation of the main identified peaks from the XANES spectra and its first derivative maxima, assumed to be the inflection point of the edge

Peak #	R		S		A or A'		B or B'		C or C'		O	
Type	Inflection	Peak	Inflection	Peak	Inflection	Peak	Inflection	Peak	Inflection	Peak	Inflection	Peak
Loc (est.), eV	2467.5	2468.2	2471.9	2473.2	2473.3	2473.8	2474.0	2474.5	2476.1	2476.7	2482.2	2483.2
Δ from S	-4.4	-5.0	0.0	0.0	1.4	0.6	2.1	1.3	4.2	3.5	10.3	10.0
Est. Ox	-2		0		0.x		0.x		2		6	
S	ND		2471.9	2473.2	ND		ND		ND		ND	
BT	ND		ND		ND		2474.1	2474.6	2476.2	2476.7	2480.9	2481.7
DBT	ND		ND		ND		2474	2474.5	2476.1	2476.6	2482.7	2483.1
4,6-DMDBT	ND		ND		ND		2474.1	2474.6	2476.1	2476.5	ND	
JP5	ND		ND		2473.3	2473.8	2474.2	2474.4	2476.2	2476.8	ND	
F76	ND		ND		2473.3	2473.8	2474	2474.5	2476.1	2476.8	ND	
MgSO4	ND		ND		ND		ND		ND		2481.9	2483.3
ZnSO4	ND		ND		ND		ND		ND		2482.3	2483.1
TiO2 BT	2467.5	2468.2	ND		ND		ND		ND		2482.9	2483.55
4% AgTiO2 BT	2467.5	2468.2	ND		ND		2474.2	2474.8	2476.5	2477	2482.1	2483.5
20% AgTiO2 BT	2467.5	2468.2	ND		ND		2474.2	2474.7	2476.4	2476.9	2482.1	2483.4
TiO2 JP5	2467.5	2468.2	ND		ND		2474.2	2474.7	2475.75	2476.4	2482.9	2483.6
4% AgTiO2 JP5	2467.5	2468.1	ND		ND		2473.7	2474.4	2475.8	2476.4	2482.1	2483.4
20% AgTiO2 JP5	2467.5	2468.1	ND		ND		2473.8	2474.4	ND		2482.1	2483.3
TiO2 F76	2467.5	2468.2	ND		ND		2474	2474.5	2475.8	2476.7	2482.9	2483.55
4% AgTiO2 F76	2467.5	2468.1	ND		ND		2473.9	2474.5	2476	2476.6	2482.1	2483.4
20% AgTiO2 F76	2467.5	2468.1	ND		ND		2473.9	2474.5	2476	2476.4	2482.1	2483.3

Average values were calculated and the distance from elemental sulfur was calculated based upon this average for a rough estimate of shift in the edges.

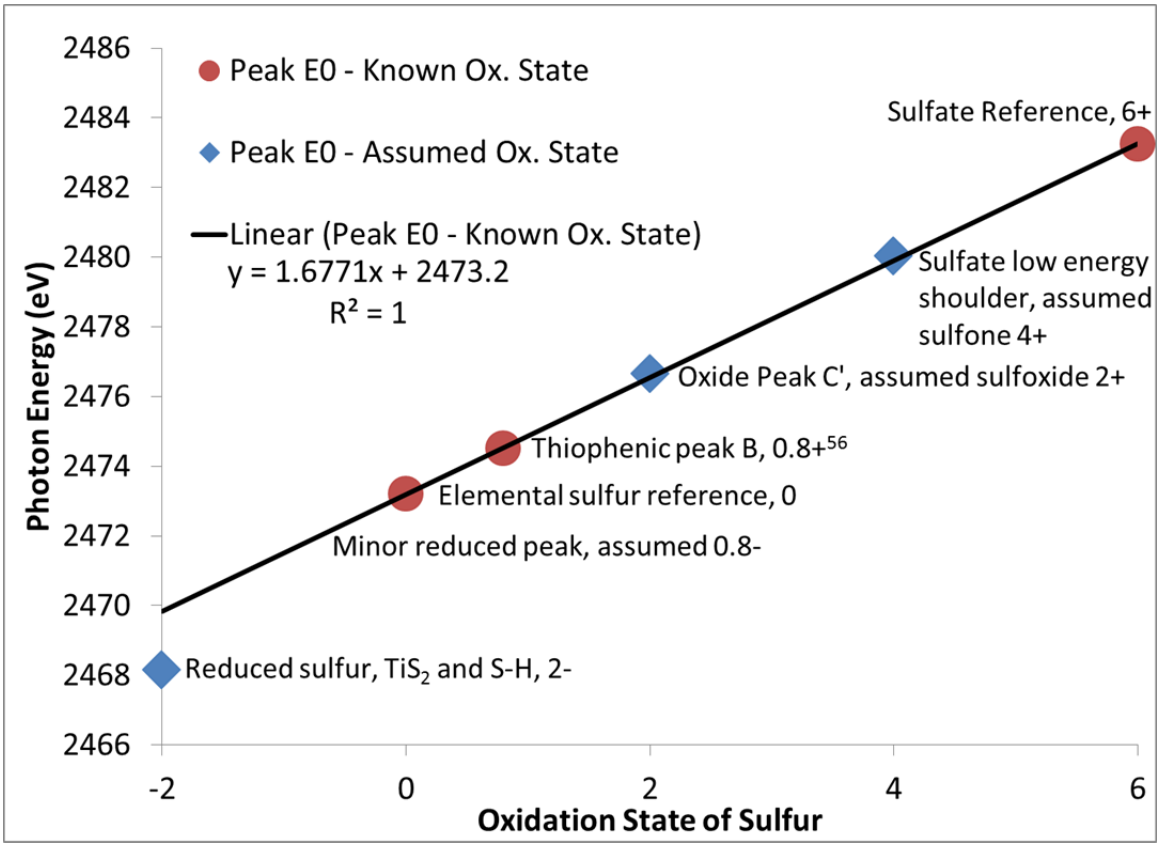

Figure 5-2 Plot of oxidation state versus photon energy associated with peak maxima

The results on TiO_2 indicate that there is formation of oxidized sulfur, which is consistent with DFT calculations performed previously.[70] However, the oxidation state observed on the sulfur is not necessarily consistent with previous calculations, and the XANES informs of the formation of the highly oxidized sulfate. The experimental results also clearly indicate the formation of a reduced species in the form of possibly TiS_2 and/or an S-H group in addition to the sulfate. For the oxide, studies previously reported and referenced above seem to indicate a threefold coordination of sulfur, between one surface and two bridging oxygen atoms. The oxidation state observed indicates additional oxygen present in the coordination of the sulfur molecules with the surface. This may be explained by additional hydroxyl groups that truncate titanium sites in a highly hydrated structure as is discussed in this work, which may not be

accounted for in the DFT studies. It is also possible that the results seen are the result of a chain reaction. It is known that thiophene can be photocatalyzed to multiple products including sulfones and SO_4^{2-} in a chain reaction fashion.[161] However, these mechanisms typically have an SO_3^{2-} intermediate which is known to be stable on TiO_2 surfaces.[162] This type of mechanism is not consistent with the observed oxidation states seen in the XANES, as we do not observe a substantial white line associated with an intermediate oxidation state, which should be intense at higher oxidation states.

For all experimental adsorption samples, a peak labeled R was noted upon addition of sulfur, with an inflection at 2467.5 eV and peak at 2468.1-2 eV. It is well known that reduced sulfur in the 2- oxidation state would exist at a point below the elemental sulfur edge, and that the range for which the reduced sulfur edge exists can be quite broad.[163,164] The location of the peak has been noted to be shifted towards lower energy as the covalent nature of the bonding decreases[165], however typically the range of location for reduced sulfur is close to the sulfur edge itself. The location of the reduced species identified for these samples is at a location of approximately -4.4 and -5 eV at the inflection and peak energies, respectively, which is a distance far extended from what would normally be expected for a reduced sulfur form. Thus, we must consider the effect of some other coordination or structure that causes such a peak to exist. This would include the possibility of a sulfide structure (TiS_2, TiS_3, Ag_2S), or a sulfur group of the form S-H, associated with a hydrated TiO_2 surface.

It is clear that on bare TiO_2, a large peak appears at higher energy with a similar intensity as the main thiophenic peak, indicating that there is a reaction occurring. From the XANES and first derivative spectra, it appears that the sulfur is being oxidized, with some also being reduced. However, careful observation of the BT on TiO_2 experiment will indicate that there is no B' peak

created. This is important to note because it indicates that there are potentially two surface-sulfur interactions occurring, which are discussed above. The reaction to TiS_2 need not be mutually exclusive of the creation of a reduced by highly hydrated species. Instead, it appears that treatment to the support, in this case addition of silver, causes a situation where the final reduced product may differ depending upon the exposed sorbent surface species.

For reduced crystalline Ag_2S[146] and TiS_2[145], both show a doublet peak at their position, which we do not see in the XANES spectra collected. However, for adsorbed fuel, it is not appropriate to assume an ordered structure exists, and thus the doublet may be washed out due to lack of crystallinity. TiS_3 is also known to exist[166], and exhibits a single peak structure. The Ag_2S edge is not sufficiently distanced with respect to the elemental sulfur edge and therefore is not likely; previous sulfur k-edge studies indicate it to be only 0.9 eV lower energy than sulfur.[146] The TiS_3 spectra reported previously lack detail due to the S-S bridging bonds suppressing the observability of many final states. Review of the XANES shows that TiS_3 is located at a higher energy than TiS_2, and thus is very close to the elemental sulfur edge. Therefore TiS_3 is not a candidate for applicability to the XANES spectra as observed in our experiments.[166] Studies of the TiS_2 edge indicate spacing between the observed peaks[167] that this would be consistent with our observations. Specifically, the lowest energy peak observed at low energy that can be attributed to the splitting of the 1s orbital to $3d^1$, and specifically into the t_{2g} and e_g states, related to the sulfur *3p*-titanium 3*d* antibonding states.[145,168] These XANES spectra exhibit this low-energy peak as defined and discussed as peak R, however these also have a second major feature that is approximately 6-9 eV distanced from the low energy peak. It should be noted that various normalized spectra show the intensity of the lower energy peak as anywhere from a minor component (e.g. 14% of the subsequent peak[168]) to approximate parity in

terms of the intensity of all peaks over the entire spread[145]. Thus the viability of a produced TiS_2 peak is contingent upon identification of a structure in the range of ca. 2474 eV. The presence of the two peaks in coordination with each other is a meaningful fingerprint to identify the formation of TiS_2 versus other reduced species, and also in explaining the presence and changes in the B' peak amongst spectra.

For certain cases, such as the BT/TiO_2 spectra, peak R is observed, however the structure at higher energy, which would be expected based upon previous studies of TiS_2 XANES, does not appear. With a still obvious peak R, the question of a second reduced sulfur form becomes important. The basis of the S-H group concept is from systems consisting of low-Fe glasses with variable SiO_2 content, where an unidentified structure has been observed at around 2466 eV, and it is claimed that the structure is correlated to SiO_2 content itself.[169] Further analysis in glassy samples have indicated that the peaks observed at low energy (2466 eV) in hydrous silicate melts, specific to unique sulfide environments.[170] The presence of the 2466 eV structure in other systems is generally observed at a condition when sulfur in the 6+ form is not seen, under low oxygen partial pressure conditons, and notionally related to sulfur dissolution.[171] This peak in that system is believed to be associated with an SH^- species, due to some form of solubilized H_2S or other R-SH^- species, which has also been noted via Raman spectroscopy techniques.[171,172] Other studies of hydrous silicate glasses indicate a variation in a peak observed at 2466.5 eV with respect to water content, and attribute this to an S^{2-}-H_2O complex formation.[173] Overall, the S-H bonding characteristic and local coordination is reasonable, because it is consistent with other observed phenomena such as what is seen in XPS, where the second lowest observed XPS binding energy is sulfur in mercaptan (with S-H type of bonding) with S 2p binding energy of 162-163 eV. The most reduced state of Sulfur is in the form of Na_2S with S 2p binding energy at

161-162 eV, consistent with the fact that Na is highly electro-positive; however it is not relevant to the constituents present in our system. Thus S-H at a far-shifted energy level is reasonable, given the possibility of mercaptan being present in the fuels themselves, and the potential of cracking of sulfur-bound molecules to make fragmented organic R-S-H or other S-H species under adsorption.

The formation of dissociated water in silicates[174] and its importance in the formation of this H_2S/SH^- dissolution is analogous to the importance of water truncating as hydroxyls on TiO_2[175,176], and its proposed utility in the desulfurization of fuels[63]. Thus we can postulate that the presence of the edge at 2467.5 eV can be attributed to a similar phenomenon in a TiO_2 system. SiO_2 and TiO_2 have both been shown to have an affinity for sulfur[106], and this work described in this document has attributed the form of Ag seen dispersed on TiO_2 to be associated with a fully hydrated local structure on the TiO_2 surface. Thus the overall scenario appears to be in alignment, in that water and surface acidity associated with water on the TiO_2 support provides a mechanism for which adsorbed sulfur dissolves as a reduced form into the moisture on the surface of the support as an S-H group. This exhibits a similar peak at a similar energy range, due to the relatively similar surface acidity and moisture conditions present in the referenced silicate systems and our TiO_2 system of interest.

Study of the BT experiments are essential, because the baseline experiment of BT on TiO_2 shows a clear removal of the peak associated with the thiophenic compounds, yet the experiments with Ag loaded on the TiO_2, retain the peak structure with the intermediate peaks remaining. Explanation of why this occurs, given that the capacitive maxima should exist around the 4 wt% sample should be related to the function of different types of adsorption sites and their mechanisms on sulfur compounds other than BT. Thus, it is reasonable to associate the

structure to a mechanism associated with the support itself, instead of the supported silver component, because the peak is observed for the support even when silver is not present. The presence of similar peak R under bare versus dispersed Ag scenarios is thus based upon the silver facilitating sulfidation of the support versus a bare hydrated TiO_2 surface merely solubilizing and complexing with the sulfur groups. Because no peak B' is observed under BT/TiO_2 experimentation, yet appears under BT/TiO_2 experimentation, we may assume that the form of the reduced species changes, and the S-H variant is associated with the hydrated support surface.

The observation of peak C' could be attributed to a sulfoxide formation. While stable thiophene sulfoxides are known to exist[177], analysis of the intensities of the A and B peaks indicate a mechanism set where the lower energy (oxidation state) components (peak A) go to sulfoxide (peak C'). Sulfoxides of formal oxidation state 0 have been reported in the ca. 2476 eV range[179], and would be indicative of the formation of product C'. While the energy range of C' is similar to the first oscillation after the aromatic thiophene (peak C), its intensity and placement identify it as a unique structure, with its energy consistent with a single oxygen atom associated to the sulfur. In other words, sulfur perhaps associated with a terminal hydroxyl group on the sorbent.

There appear to be multiple mechanisms that are observed in the materials studied and reported in this paper. Besides the reduced sulfur form discussed above, there is a substantial oxidation that is observed for all samples. This oxidation is at an edge energy level indicative of a sulfate, with sulfur present in the 6+ form. However, it is essential to review the derivative spectra associated with these experiments, because they help to provide additional insight into the scenarios being observed. When studying the derivative charts, it can clearly be seen that in the case of the bare TiO_2 experiments, a distinct double peak can be observed in the spectra in

the ca. 2483 eV range. While careful observation of the spectra at this energy level shows little difference or divergence in the peak shape (e.g. a shoulder or other shape characteristic), the derivative spectra shows it consistently. Studying the derivative spectra with respect to the loading of silver also shows that the dual peak changes as the silver loading increases, indicating changes in the proportions of contributing signal. Thus, it is not merely a doublet peak associated with two nonequivalent sulfur locations or distorted tetrahedral structures with equivalent structures as are observed in our sulfate references.[178] This portion of the spectra is also observed with a broadening of the peak, perhaps associated with a sulfone species.

The observed doublet in the derivative spectra suggests a shifting character such that the slightly lower energy peak appears to increase influence based upon loading. This appears to indicate that a second species is formed with the inclusion of silver that is not as prevalent on the bare TiO_2. The lower energy feature has a first derivative maxima at 2481.7 eV (not included in table), with the doublet first derivative peak at 2482.9 eV, as can be easily observed in the case of the BT/TiO_2 experiment due to the high intensity of the sulfate peak. It is clear that the inclusion of silver causes the first derivative at the lower energy side of the range to increase while the higher energy side decreases. This may indicate a greater tendency to produce a sulfone (as proposed based upon observations from work by Samokhvalov et. al[47]), or alternate sulfate form. A spacing of 1.2 eV is smaller than the other reported spacing between sulfone and sulfate[179], so we assume that only broadening on the low-energy shoulder of the peak contains signal associated with the sulfone. Notionally the changes may be due to the interaction of different kinds of hydroxyl groups, which may create different coordination structures which cause subtle changes in these peaks. Also, the typical wide-spread in energy between various compounds also comes into play in terms of identification of specific structures or states. A

second explanation could be the formation of a sulfate ester, which also has a slight shift to lower energy as compared to sulfate[179], but may somehow serve as an intermediate in the cleavage of sulfur from its organic structure in the creation of the SO_4 species.

These changes are difficult to observe due to the intensity and broadness of the spectra in the normalized XANES, though with close observation, a slight broadening can be seen for the samples. Still, these differences emphasize the necessity of utilization of both the XANES and its derivative spectra for identification of structures and unique components within the samples studied.

For the energy range associated with thiophene, it is clear that JP-5 has two separate components, A and B. Observation of the peak structure charted as the first derivative provides indication that the F-76 sample also consists of the two different types of compounds, but the lower energy portion at a substantially lower amount. The lower energy structure has slightly less oxidative nature than the benzothiophene type compounds, given its placement; this can be attributed perhaps to less aromaticity, or an alkane structure that has less affinity for lone electrons on the sulfur atom.

The derivative spectra are very telling for the thiophenic region in the JP-5 experiments. It is very obvious that all of the sulfur is changed such that its approximate oxidation state increases, as is evidenced by the shift in the spectra far to the right. The reduced sulfur peak is apparent and has a similar normalized intensity across the bare TiO_2 and the silver loaded samples. For the bare TiO_2, it is obvious that the initial derivative peaks from the reference JP-5 are completely displaced and shifted to higher energy. A two-peak structure is observed for all JP-5 experiments, as viewed in the XANES spectra, but the relative intensity and location shift

with an increasing amount of silver. Even for the 20 wt% sample though, the peak is shifted to higher energy as compared to uncontacted JP-5. The observed behavior on bare TiO_2 may indicate a similar adsorptive character as occurred when BT was adsorbed in on bare TiO_2. The fundamental difference may be that given the nature of compounds and increased complexity of the compounds in JP-5 versus a pure BT sample; other reactions occur during adsorption which results in the formation of a different peak that is discerned via the derivative spectra. This may mean that different positions on the molecules tend to be cleaved, or molecules/fragments appear based upon the final chemistry upon the surface. The different end states have different local coordination based upon the reactivity and surface conditions, associated with treatment and metals loading. Alternately, and the presence of the peaks in a similar yet shifted location may actually be attributed to pre-edge features of the sulfone/sulfate structure, rather than remnants of the thiophenic signal. This would also be indicative of a substantial cracking reaction occurring, as opposed to straight adsorption of complete molecules.

The F-76 experiments have a challenge associated with them in that the fuel itself has such high sulfur that capacity can be exhausted as compared to the other experiments. Thus there is a greater potential for unadsorbed sulfur to be present in the fuel present in the sorbent pores. Though the reported capacity of the adsorbent material is in excess of the minimum 3mg S/g sorbent for all challenge (jet) fuels as reported[45], F-76 fuel is a heavier cut with the potential for far heavier and larger sulfur molecules. Given the sorbent pore volume reported (0.27cc/g), the fuel present in the pores at incipient wetness (0.23g) would provide approximately 2mg of sulfur per gram of adsorbent. The experiment is to equilibrium capacity, which is higher than a breakthrough value typically reported. Thus it is anticipated that the sulfur would be adsorbed fully, but the chance still exists that unaccounted sulfur is present in the liquid within the pore

volume. This unadsorbed sulfur will still present a signal consistent with the reference F-76 fuel, though a fraction of the sulfur is indeed adsorbed. The strong white line that fits in the same location and is just a fraction of the intensity of the reference signal may be indicative of this, though we believe it is more associated with the formation of TiS_2.

5.3. Titanium

The TiO_2 studies did not show a notable change to the spectra upon addition of any content of silver. This may be attributable to the probing depth of the electron yield detection method, which probes the structure within several hundred Angstroms from the surface , however some subtle changes were seen when sulfur was added. Because the amount of sulfur loaded on the sorbent was less than the quantity of silver dispersed onto the support, we believe that the observations must be attributed to other phenomena. We postulate that the lack of change with addition of silver is due to the fact that the silver exists in the hydrated surface, amongst the hydroxyl groups present, and not in lattice defects or other places where the Ag has a meaningful interaction with the TiO_2. This itself is important as it highlights the importance of control of the surface chemistry itself, and its influence on the dispersion that occurs during the calcination and subsequent formation of surface oxide. It also seemingly highlights the importance again of the hydrated surface structure and its effect upon sorbent capacity.

For the Ti K-edge results, emphasis should be made on the findings associated with the addition of sulfur to the sorbent materials, as shown in Figure 4-30. Most interesting is the increased intensity of peak A2 on the bare TiO_2 upon contact with sulfur. Disparity in the results on bare TiO_2 versus dispersed silver variants for the various sulfur compounds was an area of substantial analysis in the sulfur K-edge study. The main consideration is of the changes that

occur between the hydrated TiO_2 surface and its interaction with reduced sulfur species when it is bare versus when silver is dispersed, as the results indicated differences in the final products. The results shown from the Ti K-edge basis indicate that the chemistry is more interesting on bare TiO_2 then when the silver is dispersed. While we postulated that TiS_2 was formed when silver was dispersed on the support, there is no substantial change to the spectra for Ag/TiO_2 to be indicative of another species.

The A2 peak is a characteristic that is not as well discussed and attributed as compared to the A1, A3 and B peaks. This is because of the difficulty to observe it due to beamline resolution.[180] This pre edge feature is dipole forbidden and tends to be weakened in symmetric environments as a result. Thus, it is associated with surface characteristics, which is an important consideration for this study.[180] The A2 peak has been attributed to specific $3d \rightarrow 4p$ transitions[181], 1s transitions to t_{2g} and e_g[182], but has also been merely attributed to a superposition of multiple Lorentzians associated with A1 and A3 in the simulation of the spectra.[182] Growth of peak A2 has been observed in the creation of hydrothermally produced titanate nanotubes, and is associated with an anatase-like structure in oxygen-rich titanate materials.[183] It is clear from our spectra that A2 distinctly appears in the case of bare TiO_2 contacted with sulfur, without any observable change in A1 or A3, implying that it is indeed a distinct transition. This would be a sensible conclusion given its attribution to the surface species, which is where our reduced sulfur compounds are interacting. Further, the creation of S-H complexes with water are proposed to create high localized hydrogen fugacity, and thus it is required to have a good sink of hydrogen in order to allow the reactions to proceed.[184] This aligns with our understanding of TiO_2, which assumes that it serves as a sink for hydrogen under other adsorption conditions, due to the low

activation energy for migration into the bulk.[185] Additionally, the intensity of peak A2 appears to be related to the size of the TiO_2 crystallites, which may imply the formation of a new surface structure that breaks up the TiO_2 into smaller crystallites. This would cause A2 to intensify[180], as would other distortions in the Ti-O bonding distances.[186]

Peak C changes are also increased in the case of sulfur on the bare TiO_2. It is attributed to 1s → 4d transitions in anatase simultaneous with the creation of a hole in the highest occupied ligand orbitals.[149,187] Its increase would indicate that sulfur ligands are interacting with some surface TiO_2 in a coordinated manner, perhaps associated with the formation of complexes that were postulated previously for the S-H species on bare TiO_2.

For both the bare and dispersed silver sorbent experiments, peak D decreases as sulfur is adsorbed. This feature range has been attributed to the Ti-O extended structure of next nearest neighbors in rutile TiO_2.[188] The decrease in peak D may thus be associated with the disturbing of otherwise consistent surfaces when sulfur adsorbs, breaking up some portion of the Ti-O structure by varying the next-nearest coordination on the surface. This would occur regardless of the form of sulfur that is on the surface when adsorbed onto bare or dispersed Ag sorbents. This peak area is associated with dipole-allowed 3s → np transitions, which become increasingly difficult to discern with smaller TiO_2 clusters.[180] Thus again its intensity may be related to a reduction in the quantity and quality of coordinated TiO_2 structures on the surface after sulfur causes disruption, even if the sort of disruption changes according to surface treatments and resultant sulfur species (i.e. TiS_2 vs. S-H complex).

Though a TiS_2 reference spectrum was not collected, the XANES was studied for similarity to other reported spectra.[189] The spectra collected for this work are difficult to compare to phase-pure TiS_2 samples, in that these substantially retain the characteristic of anatase. The TiS_2 spectra show fewer pre-edge characteristics than anatase, which makes it difficult to deconvolute the spectra, given the overwhelming anatase signal. TiS_2 exhibits a pre-edge peak in the area of A1-A2 (ca. 4970 eV), which is potentially seen for both samples. However, the main edge for TiS_2 exhibits a white line peak at an energy of ca. 4977 eV, which is an area overwhelmed by the rising edge of anatase, making it especially difficult to identify. Notionally the increase in peak C, coupled with reduced peak D maxima could imply that the individual constituents that form the overall spectra are indeed changing with respect to one another, and that TiS_2 is a possibility.

What is not necessarily understood is why the features on the Ag/TiO_2 are not as pronounced, based upon our previous postulation that TiS_2 is more of a formation phenomenon associated with Ag/TiO_2 than the bare TiO_2. It may mean however, that the relative concentrations vary in a way that was not identifiable by study of the sulfur K-edge XANES. This was due to the intense white lines observed in the sulfur XANES due to the density of unoccupied states. The intensity was sufficiently great that it was not possible to characterize concentrations of products at one oxidation state versus another. The result seen here may imply that the bare TiO_2, through solubilization of the reduced sulfur form, allows more of it to exist, while the presence of silver, while facilitating the formation of TiS_2, really does support the oxidation of sulfur to sulfate, which is easily observed upon adsorption of sulfur.

5.4. Description of Mechanism

Based upon the results as discussed thus far, it is evident that the TiO_2 support plays a substantial role in the desulfurization performance, and that it facilitates the formation of a reduced, as well as an oxidized species of sulfur. Thus, the TiO_2 support cannot be discounted in terms of its importance in the desulfurization of liquid fuels. Based upon the XANES spectra, we hypothesize that the adsorption is actually a cracking reaction which creates sulfur fragments that reduce and oxidize. The hydroxyl groups may initially interface with the hydrocarbon via the sulfur atom itself or the electron cloud associated with the aromaticity of the ring structures. The interface with sulfur was identified by DFT[70], and interactions between both bridging groups as well as singular hydroxyls to both the aromatic density as well as sulfur was observed on acidic hydroxyl-dense silica and alumina surfaces.[190] Radical ion formation at Lewis acid sites have been observed in the literature, and associated with nucleophilic attack on aromatic density[191], as well as cracking and bond cleavage.[192] In aqueous conditions, interaction of hydroxyls with thiophene have been observed to principally attack the 2 position, which is claimed to be most reactive, and ultimately cause a cleavage.[193] The cleavage has been compared in aqueous and hydrogen-rich systems, and it has been observed that cleavage occurs under H-atom-rich conditions[194]. For the Ag/TiO_2 system, this indicates that the actual reaction may be related to the loss of hydrogen from hydroxyl groups, and the creation of the oxidized species.

The observed XANES results indicate that the hydrated surfaces offer ample opportunity for the sulfur and the aromatic portion of the molecule to be adsorbed, and the resultant multi-adsorption literally rips the molecules apart. The highly hydrated surface of the adsorbent enables sulfoxide, sulfone, and four-coordinated oxygen conditions to exist as the sulfur

interacts. The interaction on the larger molecules causes cracking to occur, with some fraction cracking totally to form a reduced sulfur-hydrogen species, or else a mercaptan with the same end group. This may be due to the attack at the most reactive position on the ring, or attack at the other end of the molecule totally, but a stretching and weakening of bonds that result in breakage. Based upon analysis of the blank TiO_2 versus Ag-loaded TiO_2, it appears that the TiO_2 surface itself, known to have substantial surface water, directly complexes with the sulfur fragments to make the S-H species discussed. We conclude this based upon the lack of XANES structure in the ca. 2474 eV range, which would be indicative of the second set of major peaks in TiS_2. However, with addition of silver, this situation changes, and while the peak location and rough intensity remains the same, one can observe the B' peak presence, and in some cases, increasing with addition of silver. This indicates that the addition of silver creates a competition for surface moisture and related functional groups. Thus with a lack of hydration, the S-H groups react with surface Ti atoms to create TiS_2, which then leaves the surface hydroxyls to be associated with the surface silver atoms. In other words, the addition of silver facilitates the sulfidation of the support, adding capacity for silver atoms. We believe this is due to a hydrophilic characteristic of the dispersed Ag - it desires to remain in a hydrated form, and thus preferentially accepts and retains hydroxyl groups, thereby forcing sulfur at the surface to directly interface with the TiO_2, and ultimately create a surface sulfide.

Obviously a large amount of the sulfur does not reduce, but rather oxidizes as its final state. This may be due to solubility of the reduced sulfur in the support, overall presence of oxygen on the surface, or even a competitive allocation of available hydrogen (from hydroxyls, particularly those reacting with the sulfur to produce sulfone or sulfate) between cleaved end groups and the support itself. The reduced sulfur species truncated as an S-H bond, where the H

may be associated with surface water, or ultimately a surface TiS_2 species. This cracking also creates sulfur fragments which are suitably oxidized to be sulfate or if a fragment of the hydrocarbon remains, then as a sulfate ester. It is known from our studies of the silver loading that the well hydrated system causes a fourfold coordination of oxygen with silver, which is in a 1+ oxidation state. Of course sulfate is a 6+ oxidation state on the sulfur atom, but the TiO_2 surface is predisposed to this type of fourfold oxygen coordination. Thus it appears that the attack on the sulfur and rings causes the cracked sulfur fragments to coordinate in a similar way. It appears that the inclusion of silver facilitates the cracking[78], or simply adds more hydroxyl groups that also participate in the fourfold coordination. This increase in hydroxyl groups supports the formation of solvated oxidized sulfur and/or sulfur complexes, which undergo hydrolysis to become fully oxidized, and then solvated into the bulk phase.[72]

Based upon observations of sulfur, our overall proposed mechanism is as follows:

$$A \rightarrow C' \quad (1)$$

$$B \rightarrow B' + R + O \quad (2)$$

Equation 7

Where equation 7 (1) indicates that the non-thiophenic or non-aromatic constituents turn to a slightly more oxidized species as observed by the presence of the C' peak in the XANES. Equation 7 (2) indicates the aromatic thiophene constituents that crack and adsorb as a reduced 2- form and the oxidized sulfate in 6+ form. Due to the variability of peak B', it is proposed in the mechanism. We have established that upon adsorption, an element of B' is associated with an EXAFS oscillation of the TiS_2 reduced species, however it is plausible that B' also is indicative of some remnant or associated hydrocarbons. Figure 5-3 shows an example of a peak

fitting which considers multiple absorption edges coming from multiple different chemical species.

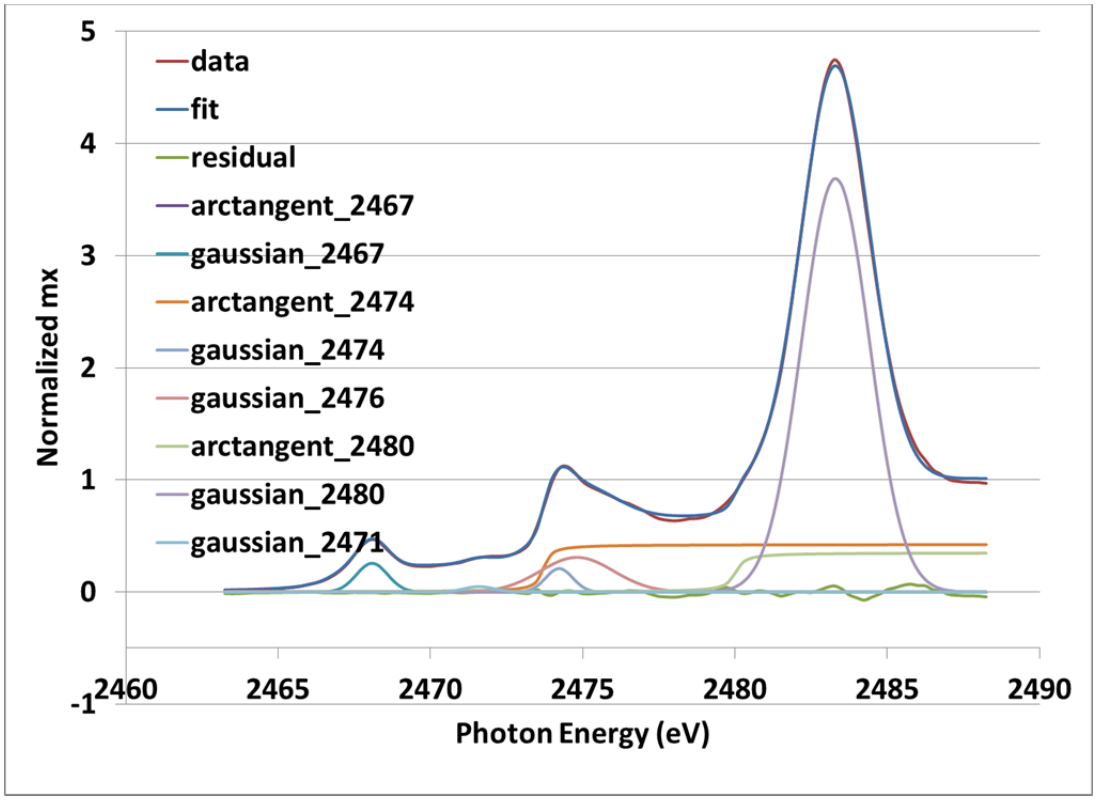

Figure 5-3 Sample XANES Fitting Utilizing Gaussian-Arctangent Curves to describe multiple states

As the reactions proceed under adsorptive conditions, two conditions can occur that limit the adsorbent reactivity and capacity. Competitive adsorption is well known and established, even for this sorbent system with model compounds versus real fuels.[106] Thus there is a stable organic-surface interaction that exists. Previous studies on zeolites have indicated that the interaction of the sulfur with hydroxyls is less stable than the interaction of aromaticity with hydroxyls.[190] Given aromatic content of fuel, as well as the potential for some quality of adsorbed compounds to remain as complete molecules, some will remain and remove useful surface and surface hydroxyls. Also, as sulfur coordinates with the surface and takes up four

surface oxygen atoms, the available surface oxygen reduces, and ultimately there is insufficient surface and reagent to crack and adsorb the molecules and the sulfur.

6. Connection to Research Proposal and Effort's Contribution to Engineering Science

The work performed as proposed to the Dissertation Committee has provided a substantial basis of learning and knowledge of the application of XAFS techniques. Specifically, the use of XANES to identify oxidation state character, EXAFS to study overall structure and perform data analysis, as well as linear combination and fitting based upon theory associated with multiple scattering paths. The efforts as described within this document reflect the focus upon the use of X-ray techniques to create a new, detailed understanding of the Ag/TiO_2 system, with references and comparative samples included to support the analysis

The intent of studying this Ag/TiO_2 system is to better understand the nature of the interaction of sulfur with the adsorbent material. **The ability to probe all of the key atomic entities as both pure references and under in situ conditions is a major new area of knowledge and insight with respect to this adsorbent system and the field of liquid phase desulfurization technology.** It is known that adsorption performance does not improve past a certain loading of silver, despite an increase in active metal surface area, due to a loss in pore volume and dispersion[45]; but that an optimized loading offers capacity significantly greater than plain TiO_2.[61] Given the capacity of TiO_2, and the enhancement of capacity with a silver dopant, it was possible to formulate a hypothesis which postulates a variety of potential active sites and mechanisms. These were defined and explained under the preliminary exam, and examples of these mechanisms are shown in Figure 6-1, without change from prior presentation.

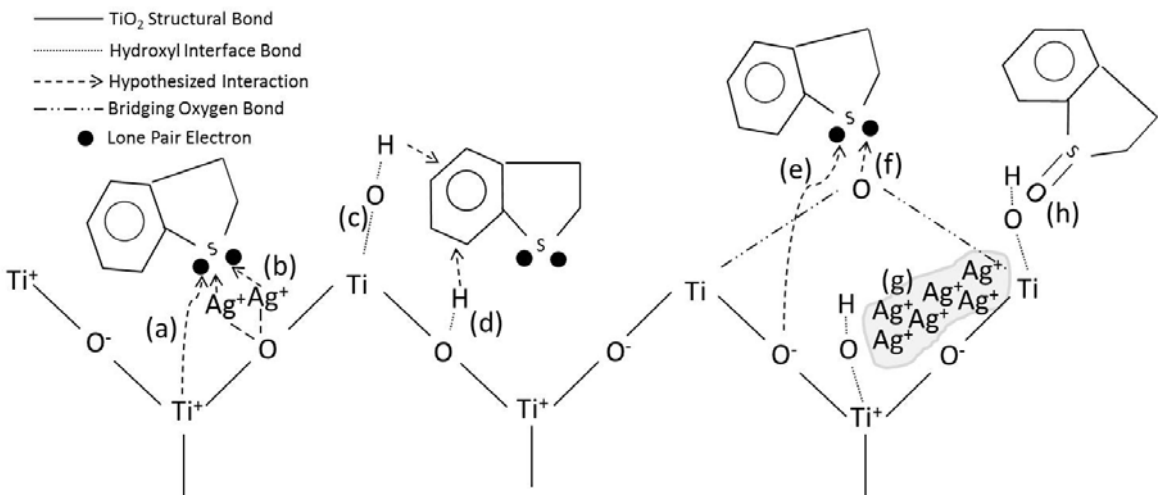

Figure 6-1 Potential mechanisms of sulfur heterocycle adsorption on Ag/TiO_2 system

The mechanisms postulated in Figure 6-1 all consider aspects of the system which may affect adsorption performance. It was proposed that the actual desulfurization activity may actually be a combination of approaches, either working individually or in concert with one another. Based upon the studies performed, it appears that this is the case. For the purpose of reiterating the initial basis, I quote the preliminary exam document. "**I hypothesize that the actual mechanism of sulfur adsorption is a combination of scenarios (d), (f), (g) and (h), which in summary indicates that adsorption is a combination of pi-complexation with defected surface hydroxyls, which compete for surface with a dissociative chemisorption facilitated by hydroxyl mobility induced by the small silver oxide clusters."** Details of the hypothesized scenarios as they were defined previously are provided in Appendix A.

The efforts performed expand knowledge and capability of the techniques of EXAFS, and utilize it in practical ways that support chemical engineering knowledge in a meaningful way. The application has been applied in multiple ways, using multiple techniques and emphasizes in situ experimentation with real components that are indicative of operations that would be practical. This helps to support the development of a mechanism based upon those documented.

To reiterate the hypothesis, it was believed that there is a competitive scenario where pi-bonding or other interaction of hydroxyl groups with the aromatic compounds (including non-sulfur aromatics) is competing with a catalyzed or otherwise facilitated dissociative or cracking reaction. The studies performed have provided sufficient insight to successfully identify this to be the case. The research performed to draw this conclusion was through efforts in the following key areas:

- Advanced data analysis and fitting of EXAFS spectra
- Studies of the pre edge regions, and XANES data for adsorbent materials
- Studies of the Silver L-edges
- Studies of the Titanium K-edge
- Studies of the Sulfur K-edge *in situ*
- *In situ* EXAFS for adsorbent materials during formation, calcination and regeneration

Completion of this work has provided full characterization of the system under the application of EXAFS, which should produce substantial insight given its range, power and sensitivity, which excels where other techniques fall short. To address the desulfurization approaches previously hypothesized, identification of relevance based upon experimentation is shown in Table 6-1.

Table 6-1 Resolution of Proposed Hypotheses from Preliminary Exam

Hypothesis	Description	Observed?
a	Locally positive Ti interacting with local negativity of electron lone pair at S	Y - Indication of TiS_2 observed.
b	Locally positive Ag from Ag_2O-stoichiometry form looking for local negative S for negative charge or to form sulfide	N - No indication of Ag_2S formation
c	Equivalent hydroxyls (bridging O based) interface with pi electrons	Y - Fourfold coordination for Ag and S requires surface Oxygen interaction
d	Non-equivalent hydroxyls (TiO_2 oxygen) interface with pi electrons	Y - Fourfold coordination for Ag and S requires hydroxyl group interaction of oxygen
e	TiO_2 oxygen interface with lone pairs	M - Formation of sulfate and other oxidized species implies significant oxygen interaction, so surface TiO_2 species may donate oxygen
f	Bridging oxygen interface with lone pairs	Y - Surface anatase structure appears to be upset upon adsorption, indicating disruption of bridiging oxygen and lattice structure at the surface
g	2D Ag islands inducing or decorating vacancies, potentially catalyzing oxygen or hydroxyl group formation/mobility	N - 2D or 3D formation of silver on surface appears well coordinated and metal structure does not appear to be involved in desulfurization
h	Catalyzed (via (g)) or reagent-limited replacement of hydroxyls that react with thiophenic sulfur oxide	Y - Sulfate and other oxide species observed distinctly in sulfur XANES

7. Conclusions

The studies performed have helped to facilitate learning and provide experience in utilization of the techniques associated with analysis of materials surfaces and structures. Specifically, a focus was made on the utilization of X-ray Absorption Spectroscopy. This includes advanced learning of XAS experimentation and beamline operations, analysis, fitting results to theory, and analyzing the results of multiple techniques to identify actual mechanisms and characteristics of the Ag/TiO_2 system both by direct and differential analysis of the results. The use of multiple EXAFS techniques enables mastery in a powerful set of tools that allows substantial characterization of chemical systems under real and relevant conditions. Knowledge gained from this effort will support engineering developments in the areas of fuel processing, desulfurization, fuel cells, power generation and analytical physical chemistry and surface science.

To recap, the efforts performed within this body of work include:

1. XRD evaluation of sorbent materials to verify dispersion of small crystals
2. XPS analysis to better understand surface chemistry and effects of the dispersed silver phase
3. EXAFS of silver (K-edge), with full analysis of the structure and identification of the behavior of the surface silver species.
4. XANES of silver (L-edge) to better understand the influence of ionic behavior of dispersed silver, and change in occupied states upon adsorption of sulfur.
5. XANES of titanium to identify influence of silver dispersion and sulfur adsorption, as well as better understand the potential for sulfide formation.

6. XANES of sulfur to identify changes in oxidation state during desulfurization adsorption conditions.
7. In situ studies of the formation and calcination of the adsorbent material, to provide unique insight into the intermediate steps in the formation process as well as the thermal stability of the system.
8. Identification of mechanisms associated with the desulfurization process forming multiple products of various oxidation states.
9. Application of the techniques and studies to previously proposed hypothesized desulfurization approaches.

The work performed provides unique insight into the desulfurization process and the effect of surface chemistry upon adsorbent capacity. The application of the techniques and combination of results to better identify how the system operates and performs is the major development and finding under this research. The major uniqueness of this work is that it allows for direct probing and insight of the key components, including under in situ conditions. This offers superior insight that is customized to the system.

Overall findings suggest that surface hydration of the TiO_2 support plays a major influential effect upon the development of sulfur capacity and the sorbent performance. The sorbent material derives capacity not from one specific surface feature or material component, but rather multiple approaches that together offer better capacity as compared to any one by itself. Perhaps most interesting was the finding that upon adsorption, some sulfur becomes reduced, while other sulfur becomes completely oxidized to the fullest extent. Also interesting and related is the degree of ionic character associated with the silver and sulfate species on the TiO_2 surface.

Based upon the findings in this work, further studies could be performed to help develop higher performing sorbent materials. While the surface acidity and support influence of multiple materials has been studied, further work must be performed to help facilitate the defected surface and overall hydrated ionic characteristic. This requires materials which offer superior surface area, retained acidity and stability, and have the ability to better disperse greater amounts of silver and water. While the practicality of particles and particle processing is a major consideration, follow-on work should focus upon approaches to provide greater surface area and surface hydration. This may include nanotubes or other nanostructures of Ti oxides that better disperse. New and novel means of processing or treatment with steam, water, or other compounds that may produce hydroxyls would also be beneficial. Because of the importance of the hydroxyl groups, further study should also be performed to better identify the type of hydroxyl groups, so that conditions can be optimized to support the formation of that specific type (e.g. germinal hydroxyls) to support desulfurization. Additionally, techniques that better probe the hydroxyl groups under various conditions would be helpful. While in situ XAS (including possibly the application of UV beamlines to study oxygen) is useful, IR has been also shown to have a beneficial utility. Either of these techniques, as well as XPS shouldbe utilized on materials that have a true adsorbed species with all other compounds evacuated. This may require adsorption and subsequent drying or treatment in vacuum to ensure that only fully adsorbed compounds are retained. This may help build insight into which sites and compounds are most tenacious, and better understand what kinds of sites need to be increased in number, while what other active sites may not be desirable. In situ XAS of the material under multiple desulfurization and regeneration cycles would also be an interesting approach, which was not possible under our experimentation due to the fragile nature of the kapton windows in the *in situ*

furnace. Overall, this area of research is ripe with opportunity, and the need for ever-cleaner fuels, produced at the lowest possible cost will drive the development of novel desulfurization processes going forward.

Appendix A

Mechanism (a) suggests that titanium is involved in the adsorption of sulfur heterocycles, (which will generically be called Benzothiophene (BT) within these explanation paragraphs). It is well known that water will dissociate on a TiO_2 surface, as the local negativity of two lone pairs of electrons within the water structure[195] interface with the local positive character of the Lewis acid type Ti^+ surface sites, which are deficient of oxygen.[196] While this is a mechanism for creation of hydroxyl groups on the surface of TiO_2, a similar characteristic is assumed for (a). Thiophene is considered aromatic, however there is a lone pair of electrons present in a p-orbital, which may exhibit character analogous to the water interaction described above.[197] Thus, the lone pair of electrons on BT may directly interface with local positive structure on the surface of TiO_2. This behavior would support the overall mechanism by providing an approach for sulfur to interface with readily available surface Ti. If this is plausible, a local coordination structure of Ti-S would be identifiable on the Ti K-edge when analyzed in electron yield mode. The bond length of Ti-S is 2.413Å[198], versus a Ti-O bond length of 1.94Å[199],and so should be readily discernible if present in that form as a final equilibrium state.

Mechanism (b) is similar to (a), however it accounts for the interaction of silver directly with BT. The image implies a structure similar to Ag_2O, based upon initial EXAFS analysis. However, it is known that silver preferentially binds and retains sulfur as compared to oxygen.[200] Given the relatively small number of Silver atoms that would notionally be exposed, this would

only be able to account for a small amount of the capacity, however it is known that Silver only enhances the capacity already present.[45] Given this small value, and the fact that not all of the exposed atoms would be involved in interfacing with sulfur, it is possible that study of the Silver edge EXAFS may not be indicative. However, increased sensitivity of the L-edges for Silver may provide additional information that can be used to discern differences that would be indicative of Ag-S versus Ag-O.[200] The Ag-S bond is approximately 2.518Å[201], which may interfere with some Ag-O coordination shells as calculated from the results to date, but indication may also be discernible by comparative technique given a peak broadening of the EXAFS Fourier transform. A double check may be possible via analysis of the Sulfur K-edge.

Mechanism (c) and (d) are the same, except for the assumptions associated with the formation of hydroxyl groups. Consistent with the hypothesis provided by Nair[202], surface hydroxyl groups may play a role in the adsorption of BT onto TiO_2.[203],[204] The scenario that differentiates the two scenarios (which likely both occur), is the effect of defects on the TiO_2 surface. The types of defect, or lack thereof, may affect the nature of and coordination of surface hydroxyls that are formed on the TiO_2.[156,196] On a defected TiO_2 surface, oxygen will be missing in the bridging positions (between two Ti atoms), and so a hydroxyl group will take the place of a defect space, with the proton being donated to a nearby bridging oxygen atom, creating two equivalent and neighboring sites, which is what is indicated as (c). On a clean, non-defected surface, two different hydroxyl groups will be formed, one in a random position associated with a Ti atom, and the proton will be donated to a nearby oxygen position that is either a bridging atom or part of the bulk structure[156,196], which is indicated as (d) in the above figure. One thing that should be noted regarding the concept of hydroxyl group interaction is related to the findings

of Takeda et. al, who found that the hydroxyl formation quantity and thus adsorptive capacity is dependent upon the electronegativity of the support, and showed that SiO_2 (Si has an electronegativity of 1.90[205]) had less carbon uptake than TiO2 (Ti=1.54) which had less than ZrO2 (Zr=1.33), indicating that higher electronegativity yields fewer hydroxyl groups on the oxide surface, and thus less adsorptive capacity.[206] Given that Silver has a higher electronegativity than Titanium (1.93 vs. 1.54), if the capacity was purely due to hydroxyl groups, the capacity should be reduced. However, the nature of the surface type and fault characteristics may make a substantial difference with respect to both the presence of nanoparticles (i.e. Silver)[207] and catalytic activity[208], particularly with specific minority structures where asymmetry and surface relaxation create substantially larger oxygen displacements than other structures, and thus may affect the ability for certain molecules to interface.[209] Regardless, utilization of Ag K and L-edge studies as well as Ti K-edge analysis should provide indication if the local structure changes, and particularly if the backscattering amplitude and peak width of oxygen bond structures change due to the high level of sulfur and nonsulfur aromatics present in the fuels.

Mechanisms (e) and (f) are similar in concept, but differentiate based upon the type of oxygen location on the TiO_2. The (e) variant assumes adsorption activity at the bulk oxygen level, while (f) assumes the same from the bridging oxygen positions, which may or may not be positively charged.[210] Previous work on fuel processing has indicated the potential for an exchange of a reactive Oxygen for Sulfur within a thiophene type molecule on an oxide supported catalyst, with oxidized variants offering higher performance associated with anion vacancies.[211] While this study was performed on a sulfide catalyst, the oxygen-sulfur transfer

and vacancy characteristics offer some similarity. For the Ag/TiO_2 system, notionally the sulfur would interface between the sulfur lone pair on the BT and a positively charged bridging oxygen[210]; however the sulfur might also interface in the place of an oxygen vacancy, or near a silver island where there is a locality of positively charged silver with insufficient local oxygen coordination. The interface may actually appear between the sulfur and oxygen, coordinating to a positively charged area where the higher electron density may be oriented. Study of the Sulfur K-edge should provide insight into the formation of sulfur-oxygen bonds, and the oxidation state variations that occur on the Sulfur atom. Given the breadth of sulfur oxidation states, a study of the XANES structure should be especially insightful to characterize the difference between raw fuel and reacted fuel that is wetted into the Ag/TiO_2 sorbent material.

Mechanism (g) is related to the form of the silver present on the TiO_2 surface. Previous work has found Silver on TiO_2 to be 3D structures formed at step edges.[156] However, it is not clear if this is the case for the low-loading Ag/TiO_2 system of greatest interest, though it may be plausible for the high loading variants, where coordinated metal is seen. The form of silver within this effort is instead thought to likely be very small decorations on the surface and within defect locations, where there is still substantial oxygen density, with growth of larger crystals, as the loading increases, as was indicated in Figure 4-1.

Through the analysis of coordination of the silver EXAFS data, some insight may be obtained as to how large of atomic groups are present under different conditions. Recent technique development and analysis has indicated that certain methods allow fairly accurate characterization of crystallite size and morphology through some basic structural assumptions,

and application of these techniques may provide insight into the nature of the silver forms. With an improved understanding of the nature of the dispersed Silver and its characteristics through study of the Ag L-edges, more insight can be provided to support the basis for the actual mechanism that occurs during sulfur adsorption.

The final proposed mechanism, (h) is different in that it assumes more of a reactive characteristic. This assumes a complete, hydroxyl facilitated reaction of the sulfur to be occurring, which has the potential to be either stably oxidized and adsorbed on a reagent limited basis[212], or catalytically regenerated on a continuous basis[213] (potentially in this case having hydroxyls mobilized from or by the Silver). Oxide and dioxide forms of thiophene structures have been identified[214], with the dioxide form losing its aromaticity.[215] Sulfur dioxide is known to photooxidize on TiO_2 in the presence of hydroxyls and surface water.[212] However, if an adsorbent should be loaded sufficiently with hydroxyl groups with sufficient mobility, such that the hydroxyl groups and not the surface is the rate limiting step, a potentially reactive/dissociative adsorption, or else just cracking could be performed, with higher oxides of sulfur being the byproduct.[213] If this were the case, it opens new opportunity even for the compact implementation of oxidative desulfurization and continuous processes. The extent that this occurs can be identified through the analysis of Sulfur K-edge XANES for change in oxidation state. The end state for this mechanism would differ from (e) and (f) in that the oxidation reactions of the sulfur as a multi-oxide form, particularly if performed multiple times via a catalyzed or facilitated transport mechanism, should yield SO_4 as the final product.[213]

References

[1] Song, C. Fuel processing for low-temperature and high-temperature fuel cells: Challenges, and opportunities for sustainable development in the 21st century. *Catal. Today* **2002**, *77*, 17-49.

[2] MIL–PRF–16884M Fuel, Naval Distillate (NATO Code F–76). Retrieved 3 September 2013 from http://www.everyspec.com/MIL-SPECS/MIL-SPECS-MIL-DTL/MIL-DTL-16884M_43460/

[3] MIL-DTL-5624V, DETAIL SPECIFICATION: TURBINE FUEL, AVIATION, GRADES JP-4 and JP-5 (11-JUL-2013). Retrieved 3 September 2013 from http://www.everyspec.com/MIL-SPECS/MIL-SPECS-MIL-DTL/MIL-DTL-5624V_47197/

[4] James Larminie, Andrew Dicks. Fuel Cell Systems Explained. West Sussex : Wiley, 2003.

[5] Song, C**.** Catalytic fuel processing for fuel cell applications. Challenges and opportunities. *Am. Chem. Soc. Div. Fuel Chem. Prepr.* **2001**, Vol. 46, pp. 8-13.

[6] Samokhvalov, A.; Nair, S.; Duin, E.C.; Tatarchuk, B. Surface characterization of Ag/Titania adsorbents. *Appl. Surf. Sci.* **2010,** *256,* 3647-3652.

[7] John Heinzel, Ian Peek, John Kuseian, Donald Hoffman. Advances in Logistic Fuels Desulfurization. San Francisco, **2006**. 232 National Meeting of the American Chemical Society.

[8] John Heinzel, Steven Miller, Ian Peek, Edward House, and Donald Hoffman. Fuel Processing Models For Navy Fuel Cell Applications. Salt Lake City, **2007**. American Institute of Chemical Engineers.

[9] D.L. Trimm, Z.I. Onsan. Onboard fuel conversion for hydrogen-fuel-cell-driven vehicles. *Catal. Rev.-Sci. Eng.* **2001**, 43, 31-84.

[10] Subir Roychoudhury, Dennis Walsh, Deryn Chu, Erik Kallio. PERFORMANCE OF A DIESEL, JP-8 REFORMER. Fort Belvoir : Defense Technical Information Center, **2006**. ADA481763.

[11] R. Sanderson, S. Abens, J. Hunt, M. Lukas, W. Keil, R. Kopp, G. Steinfeld. High Temperature PEM Fuel Cell System Palm Springs, **2009**. Fuel Cell Seminar.

[12] Song, C. S. An overview of new approaches to deep desulfurization for ultra-clean gasoline, diesel fuel and jet fuel. *Catal. Today* **2003**, *86(1-4)*, 211–263.

[13] Song, C., Ma, X. New design approaches to ultra-clean diesel fuels by deep desulfurization and deep dearomatization. *Applied Catalysis B: Environmental* **2003**, 41, 207-238.

[14] X. Ma, K. Sakanishi, I. Mochida, Hydrodesulfurization reactivities of various sulfur compounds in diesel fuel, *Ind. Eng. Chem. Res.* **1994**, 33 (2), 218–222.

[15] T. Kabe, A. Ishiharam, H. Tajimal. Hydrodesulfurization of sulfur-containing polyaromatic compounds in light oil. *Ind. Eng. Chem. Res.* **1992**, 31, 1577-1580.

[16] B.C. Gates, H. Topsoee. Reactivities in deep catalytic hydrodesulfurization: challenges, opportunities, and the importance of 4-methyldibenzothiophene and 4,6-dimethyldibenzothiophene. *Polyhedron* **1997**, 16, 3213.

[17] X. Ma, K. Sakanishi, T. Isoda, I. Mochidal. Hydrodesulfurization reactivities of narrow-cut fractions in a gas oil. *Ind. Eng. Chem. Res*. **1995**, Vol. 34, pp. 748-754.

[18] Wang, Y.; Yang, R.T.; Heinzel, J.M. Desulfurization of jet fuel by π-complexation adsorption with metal halides supported on MCM-41 and SBA-15 mesoporous materials. *Chem. Eng. Sci.* **2008,** *63,* 356-365.

[19] Heinzel, J., Cervi, M., Hoffman, D. and Nickens, A. U.S. Navy Sorbent Development for Liquid-Phase Removal of Sulfur From Logistics Fuels for Fuel Cell Applications. San Antonio, **2006**. Fuel Cell Seminar.

[20] Babich, I V, and J A Moulijn. Science and Technology of Novel Processes for Deep Desulfurization of Oil Refinery Streams: A Review. Fuel **2003**, Vol. 82, pp. 607-31.

[21] Hsu, S.; Mochida, I. *Chemistry of Diesel Fuels*; Song, C., Eds.; Taylor & Francis: New York, 2000.

[22] Torrisi, S., Street, R. The challenging chemistry of ultra-low-sulfur diesel. *World Refining.* December 2002.

[23] Ito, E.; Veen, J.V. On novel processes for removing sulphur from refinery streams. *Catal. Today* **2006**, *116,* 446–460.

[24] Knudsen, K.G.; Cooper, B.H.; Topsøe, H. Catalyst and process technologies for ultra low sulfur diesel. *Appl. Catal. A* **1999**, *189*, 205-215.

[25] Stanislaus, A.; Marafi, A.; Rana, M. Recent advances in the science and technology of ultra low sulfur diesel (ULSD) production. *Catal. Today* **2010,** *153,* 1-68.

[26] Francisco, M., Arce, A., Soto, A. Ionic Liquids on Desulfurization of Fuel Oils. *Fluid Phase Equilibria* **2010**, 294, 39-48.

[27] Gao, H., Luo, M., Xing, J., Wu, Y., Li, Y., Li, W., Liu, Q., Liu,H. Desulfurization of Fuel by Extraction with Pyridinium-Based Ionic Liquids. *Industrial & Engineering Chemistry Research* **2008**, Vol. 47, pp. 8384-38.

[28] Gao, H., Xing, J., Li, Y., Li, W., Liu, Q., Liu, H. Desulfurization of Diesel Fuel by Extraction with Lewis-Acidic Ionic Liquid. *Separation Science and Technology* **2009**, 44, 971-82.

[29] Oxidative Desulfurization of Fuel Oils. Jiang, Z., Lu, H., Zhang, Y., Li, C. *Chinese Journal of Catalysis* **2011**, 32, 707-15.

[30] Gatan, R., Barger, P., Gembicki,V. Oxidative Desulfurization: A New Technology for ULSD . *ACS Division of Fuel* Chemistry **2004**, 49, 577.

[31] Gasoline Desulfurization by Catalytic Alkylation over Silica-supported Heteropolyacids: From Model Reaction to Real Feed Conversion. Arias, M., Laurenti, D., Geantet, C., Vrinat, M., Hideyuki, I., Yoshimura, Y. *Catalysis Today* **2008,** Vol. 130, pp. 190-194.

[32] Guo, B., Wang, R., Li, Y. The Performance of Solid Phosphoric Acid Catalysts and Macroporous Sulfonic Resins on Gasoline Alkylation Desulfurization. *Fuel Processing Technology* **2010**, 91, 1731-35.

[33] Desulfurization. Guo, B., and Li, Y. Analysis and Simulation of Reactive Distillation for Gasoline Alkylation *Chemical Engineering Science* **2012**, 72, 115-125.

[34] Shiraishi, Y., Hirai, T., Komasawa, I. A Novel Desulfurization Process for Fuel Oils Based on the Formation and Subsequent Precipitation of S-Alkylsulfonium Salts. Desulfurization and Simultaneous Denitrogenation of Vacuum Gas Oil. *Industrial and Engineering Chemistry Research* **2001**, 40, 3398-405.

[35] Peek, I., Heinzel, J., Kuseian, J., Hoffman, D. Pervaporation Membrane Analysis for Logistics Fuel Separations for Navy Platforms. Philadelphia : American Institute of Chemical Engineers, 2008.

[36] Mitra, D. Desulfurization of Gasoline by Pervaporation. *Separation and Purification Reviews* **2012**, Vol. 41, pp. 97-125.

[37] Heinzel, J. *Fuels Fractionation and Separation.* Philadelphia : U.S. Navy, 2008.

[38] New Sorbents for Desulfurization of Liquid Fuels by π-Complexation. Yang, R., Takahashi, A., Yang, F. *Industrial & Engineering Chemistry Research* **2001**, 40, 6236-239

[39] Wang, Y., Yang, F.H., Yang, R.T., Heinzel, J.M., & Nickens, A.D. Desulfurization of high-sulfur jet fuel by π-complexation with copper and palladium halide sorbents. *Ind. Eng. Chem. Res.* **2006**, 45, 7649-7655.

[40] Hernández-Maldonado, A.J.; Yang, R.T. New sorbents for desulfurization of diesel fuels via π-complexation. *AIChE J.* **2004**, *50(4),* 791-801.

[41] Velu, S.; Ma, X.; Song, C. Selective adsorption for removing sulfur from jet fuel over zeolite-based adsorbents. *Ind. Eng. Chem. Res.* **2003**, *42*, 5293-5304.

[42] Chen, H.; Wang, Y.; Yang, F.H.; Yang, R.T. Desulfurization of high-sulfur jet fuel by mesoporous π-complexation adsorbents. *Chem. Eng. Sci.* **2009,** *64,* 5240-5246.

[43] Wang, Y.; Yang, R.T.; Heinzel, J.M. Desulfurization of jet fuel by π-complexation adsorption with metal halides supported on MCM-41 and SBA-15 mesoporous materials. *Chem. Eng. Sci.* **2008,** *63,* 356-365.

[44] Watanabe, S.; Ma, X.; Song, C. Characterization of Structural and Surface Properties of Nanocrystalline TiO2-CeO2 Mixed Oxides by XRD, XPS, TPR, and TBD. *J. Phys. Chem. C* **2009**, *113*, 14249-14257.

[45] Nair, S.; Tatarchuk, B. Supported silver adsorbents for selective removal of sulfur species from hydrocarbon fuels. *Fuel* **2010,** *89,* 3218-3225.

[46] Samokhvalov, A.; Duin, E.C.; Nair, S.; Tatarchuk, B. An *in situ* temperature-programmed XPS study of the surface chemical reactions of thiophene with Ag/titania. *Surf. Interface Anal.* **2010**, *42*, 1476-1482.

[47] Samokhvalov, A.; Duin, E.C.; Nair, S.; Tatarchuk, B. Adsorption and desorption of dibenzothiophene on Ag-titania studied by the complementary temperature-programmed XPS and ESR. *Appl. Surf. Sci.* **2011,** *257,* 3226-3232.

[48] Samokhvalov, A.; Duin, E.C.; Nair, S.; Bowman, M.; Davis, Z.; Tatarchuk, B. Study of the Surface Chemical Reactions of Thiophene with Ag/Titania by the Complementary Temperature-Programmed Desorption, and X-ray Photoelectron Spectroscopy: Adsorption, Desorption, and Sorbent Regeneration Mechanisms. *J. Phys. Chem. C* **2010**, *114*, 4075-4085.

[49] Samokhvalov, A.; Nair, S.; Duin, E.C.; Tatarchuk, B. Surface characterization of Ag/Titania adsorbents. *Appl. Surf. Sci.* **2010,** *256,* 3647-3652.

[50] Nair, S.; Tatarchuk; B.; Yang, H. Silver-based sorbents. US20080283446 A1, November 20, 2008.

[51] Duraiswamy, K.; Woods, R.R. Multi-stage sulfur removal system and process for an auxiliary fuel system. US7452404 B2, November 18, 2008.

[52] Duraiswamy, K.; Woods, R.R. Multi-stage sulfur removal system and process for an auxiliary fuel system. US7452405 B2, November 18, 2008.

[53] Hernández-Maldonado, A., Yang, R., W. Canella. Desulfurization of Commercial Jet Fuels by Adsorption via π-Complexation with Vapor Phase Ion Exchanged Cu(I)−Y Zeolites. *Ind. Chem. Eng. Res.* **2004**, *43*, 6142-6149.

[54] Yang, R.; Hernández-Maldonado, A.; Yang, F. Desulfurization of Transportation Fuels with Zeolites Under Ambient Conditions. *Science* **2003**, *301*, 79-81.

[55] Hernández-Maldonado, A.; Yang, R. Desulfurization of Liquid Fuels by Adsorption via π Complexation with Cu(I)−Y and Ag−Y Zeolites. *Ind. Eng. Chem. Res.* **2003**, *42*, 123-129.

[56] Hernández-Maldonado, A.; Yang, R. Desulfurization of Commercial Liquid Fuels by Selective Adsorption via Pi-Complexation with Cu(I)-Y Zeolite. *Ind. Eng. Chem. Res.* **2003,** *42*, 3103-3110.

[57] Hernández-Maldonado, A.; Yang, F.; Qi, G.; Yang, R. Desulfurization of transportation fuels by π-complexation sorbents: Cu(I)-, Ni(II)-, and Zn(II)-zeolites. *Appl. Catal., B* **2005**, *56*, 111-126.

[58] Sentorun-Shalaby, C.; Saha, S.; Ma, X.; Song, C. Mesoporous-molecular-sieve-supported nickel sorbents for adsorptive desulfurization of commercial ultra-low-sulfur diesel fuel. Appl. Catal., B **2011**, *101*, 718-726.

[59] Wang, Y.; Yang, R.; Heinzel, J. Desulfurization of Jet Fuel JP-5 Light Fraction by MCM-41 and SBA-15 Supported Cuprous Oxide for Fuel Cell Applications. *Ind. Eng. Chem. Res.* **2009**, *48*, 142-147.

[60] Wang, L.; Sun, B.; Yang, B.; Yang, R. Effects of aromatics on desulfurization of liquid fuel by π-complexation and carbon adsorbents. *Chem. Eng. Sci.* **2012**, *73*, 208-217.

[61] Guo, J.; Watanabe, S.; Janik, M.; Ma, X.; Song, C. Density functional theory study on adsorption of thiophene on TiO2 anatase (0 0 1) surfaces. *Catal. Today* **2010**, *149*, 218-223.

[62] Nanayakkara, C. E., Pettibone, J., & Grassian, V. H. Sulfur dioxide adsorption and photooxidation on isotopically-labeled titanium dioxide nanoparticle surfaces: Roles of surface hydroxyl groups and adsorbed water in the formation and stability of adsorbed sulfite and sulfate. *Physical Chemistry Chemical Physics*, **2012**, *14*(19), 6957-6966.

[63] Nair, S., Shahadat Hussain, A. H. M., & Tatarchuk, B. J. The role of surface acidity in adsorption of aromatic sulfur heterocycles from fuels. *Fuel*. **2012**, 105, 695–704.

[64] Vuk, A. Š., Ješe, R., Orel, B., & Dražč, G. The effect of surface hydroxyl groups on the adsorption properties of nanocrystalline TiO 2 films. International Journal of Photoenergy, **2005**, 7(4), 163-168.

[65] Matsumoto, Y., Nagai, H., & Sato, E. Photocatalytic oxidation of sulfur on titanium dioxide. *The Journal of Physical Chemistry*, 1982, *86*(24), 4664-4668.

[66] Hebenstreit, E. L. D., Hebenstreit, W., & Diebold, U. Structures of sulfur on $TiO_{2\ (110)}$ determined by scanning tunneling microscopy, X-ray photoelectron spectroscopy and low-energy electron diffraction. *Surface science*, **2001**, *470*(3), 347-360.

[67] Li, S. C., & Diebold, U. Reactivity of TiO2 rutile and anatase surfaces toward nitroaromatics. *Journal of the American Chemical Society*, 2009, *132*(1), 64-66.

[68] Yin, X. L., Calatayud, M., Qiu, H., Wang, Y., Birkner, A., Minot, C., & Wöll, C. Diffusion versus desorption: complex behavior of H Atoms on an oxide surface. *Chem. Phys. Chem.*, **2008**, *9*(2), 253-256.

[69] Baciocchi, E., Del Giacco, T., Ferrero, M. I., Rol, C., & Sebastiani, G. V. Oxidation of aromatic sulfides photosensitized by TiO2 in CH3CN in the presence of Ag2SO4. The role of TiO2 in the chemistry of sulfide radical cations. *The Journal of Organic Chemistry*, **1997**, *62*(12), 4015-4017.

[70] Guo, J.; Watanabe, S.; Janik, M.; Ma, X.; Song, C. Density functional theory study on adsorption of thiophene on TiO2 anatase (0 0 1) surfaces. *Catal. Today* **2010**, *149*, 218-223.

[71] Arrouvel, C., Toulhoat, H., Breysse, M., & Raybaud, P. (2004). Effects of P_{H2O}, P_{H2S}, P_{H2} on the surface properties of anatase–TiO_2 and Al_2O_3: a DFT study. *Journal of Catalysis*, *226*(2), 260-272.

[72] Nanayakkara, C. E., Pettibone, J., & Grassian, V. H. Sulfur dioxide adsorption and photooxidation on isotopically-labeled titanium dioxide nanoparticle surfaces: Roles of surface hydroxyl groups and adsorbed water in the formation and stability of adsorbed sulfite and sulfate. *Physical Chemistry Chemical Physics* **2012**, *14*(19), 6957-6966.

[73] Vuk, A. Š., Ješe, R., Orel, B., & Dražč, G. The effect of surface hydroxyl groups on the adsorption properties of nanocrystalline TiO 2 films. International Journal of Photoenergy **2005**, 7(4), 163-168.

[74] Matsumoto, Y., Nagai, H., & Sato, E. Photocatalytic oxidation of sulfur on titanium dioxide. *The Journal of Physical Chemistry* **1982**, *86*(24), 4664-4668.

[75] Hebenstreit, E. L. D., Hebenstreit, W., & Diebold, U. Structures of sulfur on $TiO_{2\ (110)}$ determined by scanning tunneling microscopy, X-ray photoelectron spectroscopy and low-energy electron diffraction. *Surface science*, **2001**, *470*(3), 347-360.

[76] Li, S. C., & Diebold, U. Reactivity of TiO2 rutile and anatase surfaces toward nitroaromatics. *Journal of the American Chemical Society* **2009**, *132*(1), 64-66.

[77] Yin, X. L., Calatayud, M., Qiu, H., Wang, Y., Birkner, A., Minot, C., & Wöll, C. Diffusion versus desorption: complex behavior of H Atoms on an oxide surface. *Chem. Phys. Chem.* **2008**, *9*(2), 253-256.

[78] Baciocchi, E., Del Giacco, T., Ferrero, M. I., Rol, C., & Sebastiani, G. V. Oxidation of aromatic sulfides photosensitized by TiO2 in CH3CN in the presence of Ag2SO4. The role of TiO2 in the chemistry of sulfide radical cations. *The Journal of Organic Chemistry* **1997**, *62*(12), 4015-4017.

[79] Guo, J.; Watanabe, S.; Janik, M.; Ma, X.; Song, C. Density functional theory study on adsorption of thiophene on TiO2 anatase (0 0 1) surfaces. *Catal. Today* **2010**, *149*, 218-223.

[80] Arrouvel, C., Toulhoat, H., Breysse, M., & Raybaud, P. Effects of P_{H2O}, P_{H2S}, P_{H2} on the surface properties of anatase–TiO_2 and Al_2O_3: a DFT study. *Journal of Catalysis* **2004,** *226*(2), 260-272.

[81] George, G. N., & Gorbaty, M. L. Sulfur K-edge X-ray absorption spectroscopy of petroleum asphaltenes and model compounds. *Journal of the American Chemical Society* **1989**, *111*(9), 3182-3186.

[82] Gorbaty, M. L., George, G. N., & Kelemen, S. R. Direct determination and quantification of sulphur forms in heavy petroleum and coals: 2. The sulphur K edge X-ray absorption spectroscopy approach. *Fuel* **1990**, *69*(8), 945-949.

[83] Kasrai, M., Bancroft, G. M., Brunner, R. W., Jonasson, R. G., Brown, J. R., Tan, K. H., & Feng, X. Sulphur speciation in bitumens and asphaltenes by X-ray absorption fine structure spectroscopy. *Geochimica et cosmochimica acta* **1994**, *58*(13), 2865-2872.

[84] Waldo, G. S., Carlson, R. M., Moldowan, J. M., Peters, K. E., & Penner-Hahn, J. E. Sulfur speciation in heavy petroleums: Information from X-ray absorption near-edge structure. *Geochimica et Cosmochimica Acta* **1991**, *55*(3), 801-814.

[85] Pickering, I. J., Prince, R. C., Divers, T., & George, G. N. Sulfur K-edge X-ray absorption spectroscopy for determining the chemical speciation of sulfur in biological systems. *FEBS letters* **1998**, *441*(1), 11-14.

[86] Wong, J., Lytle, F. W., Messmer, R. P., & Maylotte, D. H. K-edge absorption spectra of selected vanadium compounds. *Physical Review B* **1984**, *30*(10), 5596.

[87] Sayers, D.E., Stern, E.A., and Lytle, F.W. New Technique for Investigating Noncrystalline Structures: Fourier Analysis of the Extended X-Ray—Absorption Fine Structure. *Phys. Rev. Lett.* **1971**, Vol. 27, pp. 1204-1207.

[88] Bunker, G. Introduction to XAFS: A Practical Guide to X-ray Absorption Fine Structure Spectroscopy. Cambridge : Cambridge University Press, 2010.

[89] Koeningsberger, D.C., Prins, R. X-ray Absorption: principles, applications and techniques of EXAFS, SEXAFS and XANES Wiley, 1988.

[90] Mansour, A. N., Sayers, D. E., Cook Jr, J. W., Short, D. R., Shannon, R. D., & Katzer, J. R. X-ray absorption studies of some platinum oxides. *J. Phys. Chem.* **1984**, Vol. 88, 1778-1781.

[91] Jaklevic, J., Kirby, J.A., Klein, M.P., Robertson, A.S., Brown, G.S., Eisenberger, P. FLUORESCENCE DETECTION OF EXAFS: SENSITIVITY ENHANCEMENT FORDILUTE SPECIES AND THIN FILMS. *Solid State Communications* **1977**, Vol. 23, pp. 679-682.

[92] Conradson, Steven. *XAFS - A technique to probe local structure.* 2000, Los Alamos Science, Vol. 26, pp. 422-435.

[93] Sayers, D.E.; Heald, S.M.; Pick, M.A.; Budnick, J.I.; Stern, E.A.; Wong, J. X-ray Beam Line at the NSLS for X-ray Absorption Studies in Material Science. *Nucl. Instrum. Methods Phys. Res.* **1983**, *208*, 631.

[94] Mansour, A.N. Discussions with Research Scientist. 2010-2013.

[95] Elam, W.T., Kirkland, J. P., Neiser, R. A., Wolf, P. D. Depth dependence for extended x-ray-absorption fine-structure spectroscopy detected via electron yield in He and in vacuum. *Physical Review B* **1988**, Vol. 38, pp. 26-30.

[96] Kordesch, M. E., & Hoffman, R. W. Electron-yield extended x-ray absorption fine structure with the use of a gas-flow electron detector. *Physical Review B* ***1984***, *29*(1), 491.

[97] Newville, Matthew. *Fundamentals of EXAFS.* Chicago : University of Chicago, 2004.

[98] M. Newville, IFEFFIT: interactive EXAFS analysis and FEFF fitting. *J. Synchrotron Rad.* **2001**, 8, 322—324.

[99] Ravel, B., Newville, M. ATHENA, ARTEMIS, HEPHAESTUS: data analysis for X-ray absorption spectroscopy using IFEFFIT. *J. Synchrotron Rad*. **2005**, 12, 537--541.

[100] Newville, M., Līviņš, P., Yacoby, S. Y., Rehr, J. J., & Stern, E. A.Near-edge x-ray-absorption fine structure of Pb: A comparison of theory and experiment. *Physical Review B* **1993,** Vol. 47, 14126-14131.

[101] Bauchspieβ, K. R. EXAFS background substraction using splines. *Physica B: Condensed Matter* **1995**, Vol. 208, 183-184.

[102] Koningsberger, D.C., Mojet, B.L., van Dorssen, G.E., Ramaker, D.E. XAFS spectroscopy; fundamental principles and data analysis. *Topics in Catalysis* **2000**, Vol. 10, pp. 143–155.

[103] Ravel, Bruce. [Ifeffit] S02 parameter . [Online] cars.aps.anl.gov, May 4, 2010. [Cited: March 14, 2013.] http://www.mail-archive.com/ifeffit@millenia.cars.aps.anl.gov/msg02237.html.

[104] Wilkinson, A. D. McNaught and A. IUPAC. Compendium of Chemical Terminology, 2nd ed. (the "Gold Book"). [Online] Blackwell Scientific Publications, 1997. [Cited: March 14, 2013.]

[105] Ravel, Bruce. [Ifeffit] Amplitude and the EXAFS equation . [Online] cars.aps.anl.gov, October 29, 2002. [Cited: March 14, 2013.] http://millenia.cars.aps.anl.gov/pipermail/ifeffit/2002-October/000151.html.

[106] Nair, S., Tatarchuk, B. J. Characteristics of sulfur removal by silver-titania adsorbents at ambient conditions. Adsorption **2011**, 17(4), 663-673.

[107] Behyan, S., Hu, Y., & Urquhart, S. G. Sulfur 1s near edge x-ray absorption fine structure spectroscopy of thiophenic and aromatic thioether compounds. *J Chem. Phys.* **2013**, 138, 214302-1-10.

[108] Sayers, D.E.; Heald, S.M.; Pick, M.A.; Budnick, J.I.; Stern, E.A.; Wong, J. X-ray Beam Line at the NSLS for X-ray Absorption Studies in Material Science. *Nucl. Instrum. Methods Phys. Res.* **1983**, *208*, 631.

[109] Stern, E.A.; Kim, K. Thickness Effect on the Extended X-ray Absorption Fine Structure Amplitude. *Phys. Rev. B* **1981**, *23*, 3781.

[110] Lu, K.Q.; Stern, E.A. Size effect of Powdered Sample on EXAFS Amplitudes. *Nucl. Instrum. Methods* **1983**, *212*, 475.

[111] Fulton, J.L.; Kathmann, S.M.; Schenter, G.K.; Balasubramainian, M. Hydrated structure of Ag(I) from symmetry-dependent, K- and L-edge XAFS multiple scattering and molecular dynamics simulations. *J. Phys. Chem. A*, **2009,** *113*, 13976-13984.

[112] Ankudinov, L.; Ravel, B.; Rehr, J.J.; Conradson, S.D. Real-space multiple-scattering calculation and interpretation of x-ray-absorption near-edge structure. *Phys. Rev. B.* **1998**, *58*, 7565-7576.

[113] Ankudinov, A.L.; Boulden, C.E.; Rehr, J.J.; Sims, J.; Hung, H. Parallellization and Lanczos: Parallel calculation of electron multiple scattering using Lanczos algorithms. *Phys. Rev. B* **2002**, *65*, 104107.

[114] Villars, P., Calvert L.D. Pearson's Handbook for Crystallographic Phases; American Society for Metals: Metals Park, 1985; Vol. 1.

[115] Wyckoff, R.W.G. Crystal Structures; R.E. Krieger Pub. Co.: Malabar, FL, 1982; Vol. 2, pp 362.

[116] Stern, E.A. Number of relevant independent points in x-ray-absorption fine-structure spectra. *Phys. Rev. B* **1993**, *48*, 9825-9827.

[117] Yang, C.Y., Penner-Hahn, J. E., & Stefan, P. M. NSLS X-19A Beamline Performance for X-Ray Absorption Measurements. *Nucl. Instrum. Phys. Res.* **1990**, A291, 157-161.

[118] Jaklevic, J., Kirby, J. A., Klein, M. P., Robertson, A. S., Brown, G. S., & Eisenberger, P. Fuorescence Detection of EXAFS: Sensitivity Enhancement for Dilute Species and Thin Films. *Solid State Commun.* **1977**, 23, 679-682

[119] Briggs, D.; Beamson, G. XPS studies of the oxygen 1s and 2s levels in a wide range of functional polymers. *Anal. Chem*. **1993**, *65*, 1517-1523.

[120] De Groot, F. M. F., Grioni, M., Fuggle, J. C., Ghijsen, J., Sawatzky, G. A., & Petersen, H. Oxygen 1s x-ray-absorption edges of transition-metal oxides. *Phys. Rev. B* **1989**, 40(8), 5715.

[121] Molder, J.F.; Stickle, W.F.; Sobol, P.E.; Bomben, K.D. *Handbook of X-ray Photoelectron Spectroscopy*; Chastain, J., King, R.C., Jr., Eds. ULVAC-PHI, Inc.: Chigasaki, Japan, 1995.

[122] Atuchin, V.V.; Kesler, V.G.; Pervukhina, N.V.; Zhang, Z. Ti 2p and O 1s core levels and chemical bonding in titanium-bearing oxides. *J. Electron spectroscopy Related Phenomena* **2006**, *152*, 18-24.

[123] Silva, A.G.; Bundaleski, N.; Moutinho, A.M.C.; Teodoro, O.M.N.D. Dynamics of water adsorption on TiO2 monitored by work function spectroscopy. *Appl. Surf. Sci* **2012**, *258*, 2006-2009.

[124] Jensen, H.; Soloviev, A.; Li, Z.; Søgaard, E.G. XPS and FTIR investigation of the surface properties of different titania nano-powders. *Appl. Surf. Sci.* **2005**, *246*, 239-249.

[125] Marsh, J.; Minel, L.; Barthés-Labrousse, M.G.; Gorse, D. The nature of the surface acidity of anodized titanium: an XPS study using 1,2-diaminoethane. *Appl. Surf. Sci.* **1996**, *99*, 335-343.

[126] McInyre, N.S.; Cook, M.G. X-ray photoelectron studies on some oxides and hydroxides of Cobalt, Nickel, and Copper. *Anal. Chem.* **1975**, *47*, 2208-2213.

[127] Schon, G. ESCA studies of Ag, Ag_2O and AgO. *Acta Chem. Scand.* **1973**, *27*, 2623-2333.

[128] Hammond, J.S.; Gaarenstroom, S.W., and Winograd, N. X-ray photoelectron spectroscopic studies of cadmium-and silver-oxygen surfaces. *Anal. Chem.* **1975**, 2193-2199.

[129] Weaver, J.F.; Hoflund, G.B. Surface characterization study of the thermal decomposition of AgO. *J. Phys. Chem.*, **1994**, *98 (34)*, 8519–8524.

[130] Wyckoff, R.W.G. *Crystal Structures;* R.E. Krieger Pub. Co.: Malabar, FL, 1982; Vol. 1, pp 331.

[131] Meyer, P.P.; Rimsky, A.; Chevalier, R. Strucuture du nitrate d'argent a pression et temperature ordinaries. Example de cristal parfait. *Acta Cryst.* **1978**, *B34*, 1457-1462.

[132] Scatturin, V.; Bellon, P.L.; Salkind, A.J. The structure of silver oxide determined by means of neutron diffraction. *J. Electrochem. Soc.* **1961**, *108*, 819-822.

[133] Huang, Y. H., Yan, C. H., Luo, F., Song, W., Wang, Z. M., & Liao, C. S. Large enhancement in room-temperature magnetoresistance and dramatic decrease in resistivity in La 0.7 Ca 0.3 MnO 3–Ag composites. *Applied physics letters* **2002**, 81(1), 76-78.

[134] Tseung, A. C. C., & Wong, L. L. The preparation and characterization of high performance Ag/C oxygen electrocatalysts. *Journal of Applied Electrochemistry* **1972**, 2(3), 211-215.

[135] Villars, P., Calvert L.D. Pearson's Handbook for Crystallographic Phases; American Society for Metals: Metals Park, 1985; Vol. 1.

[136] Weaver, J. F., & Hoflund, G. B. Surface characterization study of the thermal decomposition of Ag2O. *Chemistry of materials* **1994**, 6(10), 1693-1699.

[137] Czyyk, M. T., de Groot, R. A., Dalba, G., Fornasini, P., *Kisiel, A., Rocca, F., & Burattini, E. Ag2O band structure and x-ray-absorption near-edge spectra. Physical review. B, Condensed matter* **1989**, 39(14), 9831.

[138] Behrens, P. Bonding in silver-oxygen compounds from Ag L3 XANES spectroscopy. *Solid state communications* **1992**, 81(3), 235-239.

[139]Shimizu, K. I., Kamiya, Y., Osaki, K., Yoshida, H., & Satsuma, A. The average Pd oxidation state in Pd/SiO2 quantified by L3-edge XANES analysis and its effects on catalytic activity for CO oxidation. *Catalysis Science & Technology* **2012**, 2(4), 767-772.

[140] Manceau, A., & Nagy, K. L. Quantitative analysis of sulfur functional groups in natural organic matter by XANES spectroscopy. *Geochimica et Cosmochimica Acta* **2012**, 99, 206-223.

[141] Chen, Y., Xie, C, Li, Y., Song, C. & Bolin, T. B. Sulfur Poisoning of Steam Reforming Catalysts: an X-ray Absorption Near Edge Structure (XANES) Spectroscopic Study. *Phys. Chem. Chem. Phys.* **2010**, 12, 5707-5711.

[142] McKeown, D. A., Muller, I. S., Gan, H., Pegg, I. L., & Stolte, W. C. Determination of sulfur environments in borosilicate waste glasses using X-ray absorption near-edge spectroscopy. *Journal of non-crystalline solids* **2004**, 333(1), 74-84.

[143] Mijovilovich, A., Pettersson, L. G., Groot, F. M. D., & Weckhuysen, B. M. Functional Groups and Sulfur K-Edge XANES Spectra: Divalent Sulfur and Disulfides. *J. Phys. Chem. A* **2010***,* 114(35), 9523-9528.

[144] Sarret, G., Connan, J., Kasrai, M., Eybert-Berard, L., & Bancroft, G. M. Characterization of sulfur in asphaltenes by sulfur K-and L-edge XANES spectroscopy. *Journal of Synchrotron Radiation* **1999**, 6(3), 670-672.

[145] Wu, Z. Y., Lemoigno, F., Gressier, P., Ouvrard, G., Moreau, P., Rouxel, J., & Natoli, C. R. Experimental and theoretical studies of the electronic structure of TiS2. *Phys. Rev. B* **1996**, 54(16), R11009.

[146] Armand, P., Ibanez, A., & Philippot, E. Structural Characterization of Ge-S and GeS2-Ag2S Glassy Range by Sulfur K-Edge X-Ray Absorption Spectroscopy. *J. Solid State Chem.* **1993**, 104(2), 308-318.

[147] Kasrai, M., Bancroft, G. M., Brunner, R. W., Jonasson, R. G., Brown, J. R., Tan, K. H., & Feng, X. (1994). Sulphur speciation in bitumens and asphaltenes by X-ray absorption fine structure spectroscopy. *Geochimica et cosmochimica acta* **1994**, 58(13), 2865-2872.

[148] Elam, W. T., Kirkland, J. P., Neiser, R. A., & Wolf, P. D. Depth dependence for extended x-ray-absorption fine-structure spectroscopy detected via electron yield in He and in vacuum. *Physical Review B* **1998**, 38(1), 26.

[149] Brydson, R., Sauer, H., Engel, W., Thomass, J. M., Zeitler, E., Kosugi, N., & Kuroda, H. Electron energy loss and X-ray absorption spectroscopy of rutile and anatase: a test of structural sensitivity. *Journal of Physics: Condensed Matter* **1989**, 1(4), 797.

[150] Hebenstreit, E.L.D.; Hebenstreit, W.; Diebold, U. Adsorption of sulfur on $TiO_{2(110)}$ studied with STM, LEED and XPS: temperature-dependent change of adsorption site combined with O–S exchange. *Surf. Sci.* **2000**, *461*, 87-97.

[151] Lai, X.; Clair, T.P.S.; Goodman, D.W. Oxygen-induced morphological changes of Ag nanoclusters supported on TiO2 (110). *Faraday Discuss. Chem. Soc.* **1999**, *114*, 279-284.

[152] Luo, K.; St. Clair, T.P.; Lai, X.; Goodman, D.W. Silver Growth on $TiO_{2(110)}$ (1 × 1) and (1 × 2). *J. Phys. Chem.* **2000**, *104*, 3050-3057.

[153] Martin, D.; Jupille, J.; Borensztein, Y. Silver particle sizes and shapes as determined during a deposit by in situ surface differential reflectance. *Surf. Sci.* **1998**, *404*, 433-436.

[154] Martin, D.; Creuzet, F.; Jupille, J.; Borensztein, Y.; Gadenne, P. 2D and 3D silver adlayers on $TiO_{2(110)}$ surfaces. *Surf. Sci.* **1997**, *379*, 958-962.

[155] Chen, D.A.; Bartelt, M.C.; McCarty, K.F. Small, uniform, and thermally stable silver particles on $TiO_{2(110)-(1\times 1)}$. *Surf. Sci.* **2000,** *464*, L708-L714.

[156] Diebold, U. The surface science of titanium dioxide. *Surf. Sci. Reports* **2003**, *48*, 53-229.

[157] Mansour, A.N. Evidence for an Ag4O3 Phase of Silver Oxide. *J. Phys. Chem.* **1990**, *94*, 1006-1010.

[158] Yamaguchi, T., Lindqvist, O., Boyce, J. B., & Claeson, T. Determination of the hydration structure of silver ions in aqueous silver perchlorate and nitrate solutions from EXAFS using synchrotron radiation. Acta Chem. Scand., **1984**, (6), 423-428.

[159] Seward, T. M., Henderson, C. M. B., Charnock, J. M., & Dobson, B. R. An X-ray absorption (EXAFS) spectroscopic study of aquated Ag+ in hydrothermal solutions to 350° C. Geochimica et cosmochimica acta,**1996**, 60(13), 2273-2282.

[160] Vairavamurthy, A. Using X-ray absorption to probe sulfur oxidation states in complex molecules. *Spectrochimica Acta Part A: Molecular and Biomolecular Spectroscopy* **1998**, 54(12), 2009-2017.

[161] Zhao, D. S., Li, F. T., Zhou, E. P., & Sun, Z. M. Kinetics and Mechanism of the Photo-oxidation of Thiophene by O2 Adsorbed on Molecular Sieves. *Chemical Research in Chinese Universities*, **2008**, 24(1), 96-100.

[162] Hebenstreit, E. L. D., Hebenstreit, W., & Diebold, U. Adsorption of sulfur on TiO2 (110) studied with STM, LEED and XPS: temperature-dependent change of adsorption site combined with O–S exchange. *Surface science* **2000**, *461*(1), 87-97.

[163] Alonso Mori, R., Paris, E., Giuli, G., Eeckhout, S. G., Kavcic, M., Zitnik, M., ... & Glatzel, P. Electronic structure of sulfur studied by X-ray absorption and emission spectroscopy. *Analytical Chemistry* **2009**, 81(15), 6516-6525.

[164] Fleet M. E. XANES spectroscopy of sulfur Earth materials. *Can. Mineral.* **2005**, 43, 1811–1838.

[165] Fleet M. E., Liu X., Harmer S. L. and King P. L. Sulfur K-edge XANES spectroscopy: chemical state and content of sulfur in silicate glasses. *Can. Mineral.* **2005**, 43, 1605–1618.

[166] Fleet, M. E., Harmer, S. L., Liu, X., & Nesbitt, H. W. Polarized X-ray absorption spectroscopy and XPS of TiS3: S K-and Ti L-edge XANES and S and Ti 2p XPS. *Surface Science* 2005, 584(2), 133-145.

[167] Ohno, Y., Hirama, K., Nakai, S., Sugiura, C., & Okada, S. X-ray absorption spectroscopy of layer transition-metal disulfides. *Phys. Rev. B* **1983**, 27(6), 3811.

[168] Wu, Z. Y., Ouvrard, G., Moreau, P., & Natoli, C. R. Interpretation of preedge features in the Ti and S K-edge x-ray-absorption near-edge spectrain the layered disulfides TiS2 and TaS2. *Phys. Rev. B* **1997**, 55(15), 9508.

[169] Métrich, N., Berry, A. J., O'Neill, H. S. C., & Susini, J. The oxidation state of sulfur in synthetic and natural glasses determined by X-ray absorption spectroscopy. *Geochimica et Cosmochimica Acta* **2009**, 73(8), 2382-2399.

[170] Klimm, K., Kohn, S. C., O'Dell, L. A., Botcharnikov, R. E., & Smith, M. E. The dissolution mechanism of sulphur in hydrous silicate melts. I: Assessment of analytical techniques in

determining the sulphur speciation in iron-free to iron-poor glasses. *Chemical Geology* **2012**, 322, 237-249.

[171] Klimm, K., Kohn, S. C., & Botcharnikov, R. E. The dissolution mechanism of sulphur in hydrous silicate melts. II: Solubility and speciation of sulphur in hydrous silicate melts as a function of fO2. *Chemical Geology* **2012**, 322, 250-267.

[172] Klimm, K., Botcharnikov, R.E., The determination of sulfate and sulfide species in hydrous silicate glasses using Raman spectroscopy. *American Mineralogist* **2010**, 95, 1574–1579.

[173] Stelling, J., Behrens, H., Wilke, M., Göttlicher, J., & Chalmin-Aljanabi, E. Interaction between sulphide and H2O in silicate melts. *Geochimica et Cosmochimica Acta* **2011**, 75(12), 3542-3557.

[174] Kohn, S.C. The dissolution mechanisms of water in silicate melts; a synthesis of recent data. *Mineralogical Magazine* 2000, 64 (3), 389–408.

[175] Vuk, A. Š., Ješe, R., Orel, B., & Dražč, G. The effect of surface hydroxyl groups on the adsorption properties of nanocrystalline TiO 2 films. *International Journal of Photoenergy 2005,* 7(4), 163-168.

[176] Henderson, M. A. The interaction of water with solid surfaces: fundamental aspects revisited. *Surface Science Reports* **2002**, 46(1), 1-308.

[177] Mock, W. L. Stable thiophene sulfoxides. *Journal of the American Chemical Society* **1970**, 92(26), 7610-7612.

[178] MgSO4 and ZNSO4 Reference, R. W. G Wyckoff, Crystal Structures, Vol. 3, 2nd edition, page 41; John Wiley &Sons, New York, 1965.

[179] Almkvist, G., Boye, K., & Persson, I. K-edge XANES analysis of sulfur compounds: an investigation of the relative intensities using internal calibration. Journal of synchrotron radiation **2010**, 17(5), 683-688.

[180] Luca, V., Djajanti, S., & Howe, R. F. (1998). Structural and electronic properties of sol-gel titanium oxides studied by X-ray absorption spectroscopy. *J. Phys. Chem. B* **1998**, 102(52), 10650-10657.

[181] Wu, Z. Y., Ouvrard, G., Gressier, P., & Natoli, C. R. Ti and OK edges for titanium oxides by multiple scattering calculations: Comparison to XAS and EELS spectra. *Physical Review B* **1997**, 55(16), 10382.

[182] Parlebas, J. C., Khan, M. A., Uozumi, T., Okada, K., & Kotani, A. Theory of many-body effects in valence, core-level and isochromat spectroscopies along the 3d transition metal series of oxides. *Journal of electron spectroscopy and related phenomena* **1995**, 71(2), 117-139.

[183] Kubo, T., & Nakahira, A. (2008). Local structure of TiO2-derived nanotubes prepared by the hydrothermal process. *J. Phys. Chem.* C **2008**, 112(5), 1658-1662.

[184] Stelling, J., Behrens, H., Wilke, M., Göttlicher, J., & Chalmin-Aljanabi, E. Interaction between sulphide and H2O in silicate melts. *Geochimica et Cosmochimica Acta* **2011**, 75(12), 3542-3557.

[185] Yin, X. L., Calatayud, M., Qiu, H., Wang, Y., Birkner, A., Minot, C., & Wöll, C. Diffusion versus desorption: complex behavior of H Atoms on an oxide surface. *Chem. Phys. Chem.* **2008**, 9(2), 253-256.

[186] Jiang, N., Su, D., & Spence, J. C. H. Determination of Ti coordination from pre-edge peaks in Ti K-edge XANES. *Physical Review B* **2007**, 76(21), 214117.

[187] Bair, R. A., & Goddard III, W. A. Ab initio studies of the x-ray absorption edge in copper complexes. I. Atomic Cu2+ and Cu(ii)Cl2. *Physical Review B* ***1980***, 22(6), 2767.

[188] Farges, F., Brown, G. E., & Rehr, J. J. Ti K-edge XANES studies of Ti coordination and disorder in oxide compounds: Comparison between theory and experiment. *Physical Review B* **1997**, 56(4), 1809.

[189] Bocharov, S., Dräger, G., Heumann, D., Šimůnek, A., & Šipr, O. Polarized x-ray-absorption spectra of TiS2, TiSe2, and TiTe2. *Physical Review B* **1998**, 58(12), 7668.

[190] Gutiérrez-Alejandre, A., Larrubia, M. A., & Ramirez, J. FT-IR evidence of the interaction of benzothiophene with the hydroxyl groups of H-MFI and H-MOR zeolites. *Vibrational Spectroscopy* **2006**, 41(1), 42-47.

[191] Anbar, M., Meyerstein, D., & Neta, P. The reactivity of aromatic compounds toward hydroxyl radicals. J. Phys. Chem. **1966**, 70(8), 2660-2662.

[192] Chapman, I. D., & Hair, M. L. The role of the surface hydroxyl groups in catalytic cracking. *Journal of Catalysis* **1963**, 2(2), 145-148.

[193] Saunders, B. B., Kaufman, P. C., & Matheson, M. S. Reactions of thiophene with radiolytically produced radicals. 1. The hydroxyl radical. J. Phys. Chem. **1978**, 82(2), 142-150.

[194] Saunders, B. B. Reactions of thiophene with radiolytically produced radicals. 2. The solvated electron and the hydrogen atom. J. Phys. Chem. **1978**, 82(2), 151-154.

[195] Marye Anne Fox, James K. Whitesell. Organic Chemistry**.** Boston : Jones & Bartlett Learning, 1997.

[196] Henderson, M. A. The interaction of water with solid surfaces: fundamental aspects revisited. *Surface Science Reports* **2002**, 46, 1-308.

[197] mymcat. Aromaticity Introduction. [Online] February 13, 2009. [Cited: March 14, 2013.] http://www.mymcat.com/wiki/Aromaticity_Introduction.

[198] Sweeney, Z.K., Polse, J.L., Bergman, R.G., Andersen, R.A. Dihydrogen Activation by Titanium Sulfide Complexes. *Organometallics* **1999**, 18, 5502–5510.

[199] Naicker, P., Cummings, P., Zhang, H., Banfield, J. Characterization of Titanium Dioxide Nanoparticles Using Molecular Dynamics Simulations *J. Phys. Chem. B* **2005**, 109, 15243-15249.

[200] Tibbetts, G. G., & Burkstrand, J. M. Auger and photoelectron study of codeposited sulfur and oxygen layers on silver (111*). Journal of Vacuum Science and Technology* **1978**, 15, 497-501.

[201] Bowmaker GA, Skelton BW, White AH. Structural and infrared spectroscopic studies of some novel mechanochemically accessed adducts of silver(I) oxoanion salts with thiourea*. Inorg Chem*. **2009**, 48, 3185-97.

[202] Nair, Sachin. Desulfurization of Hydrocarbon Fuels at Ambient Conditions Using Supported Silver Oxide-Titania Sorbents. Auburn : Auburn University, 2010.

[203] M. Anbar, D. Meyerstein , P. Neta The reactivity of aromatic compounds toward hydroxyl radicals. *J. Phys. Chem.* **1966**, 70, 2660-2662.

[204] Cusumano, J.A., Low, M. J. D. *Interactions between surface hydroxyl groups and adsorbed molecules. I. The thermodynamics of benzene adsorption.* J. Phys. Chem. 1970, 74, 792–797.

[205] Electronegativities of the elements (data page). [Online] Wikipedia, March 7, 2013. [Cited: March 14, 2013.] http://en.wikipedia.org/wiki/Electronegativities_of_the_elements_(data_page).

[206] Takeda, S., Fukawa, M., Hayashi, Y., Matsumoto, K**.** Surface OH group governing adsorption properties of metal oxide films. *Thin Solid Films* **1999**, 1-2, 220-224.

[207] Han, X., Kuang, Q., Jin, M., Xie, Z., Zheng, L. Synthesis of titania nanosheets with a high percentage of exposed (001) facets and related photocatalytic properties. *J. Am. Chem. Soc*. **2009**, 131, 3152.

[208] Devriendt, K., Poelman, H., Fiermans, L. The V2O5/TiO2 (anatase) model catalyst structure: XPD study and single scattering cluster simulations. *Surf. Interface Anal*. 2000, 29, 139-144.

[209] Zhao, Z., Li, Z., Zou, Z.Surface properties and electronic structure of low-index stoichiometric anatase TiO2 surfaces. *J. Phys.: Condens. Matter* 2010, 22, 1-18.

[210] Wang, S.G., Wen, X., Cao, D., Li, Y., Wang , J., Jiao, H. Formation of oxygen vacancies on the TiO2(110) surfaces. *Surface Science* **2005,** 577, 69-76.

[211] Massoth, F. E., Kibby, C. L. Studies of molybdena-alumina catalysts: V. Relation between catalyst sulfided state and activity for thiophene hydrodesulfurization. *Journal of Catalysis* **1977**, 47, 300-315.

[212] Nanayakkara CE, Pettibone J, Grassian VH. Sulfur dioxide adsorption and photooxidation on isotopically-labeled titanium dioxide nanoparticle surfaces: roles of surface hydroxyl groups and adsorbed water in the formation and stability of adsorbed sulfite and sulfate. *Phys Chem Chem Phys*. **2012**, 14, 6957-6966.

[213] Margitan, J. J. Mechanism of the atmospheric oxidation of sulfur dioxide. Catalysis by hydroxyl radicals. J. Phys. Chem. 1984, 88, 15, 3314–3318.

[214] Igor F. Perepichka, Dmitrii F. Perepichka. Handbook of Thiophene-Based Materials: Applications in Organic Electronics and Photonics. E-book : John Wiley & Sons, 2009.

[215] Juzo Nakayama, Yoshiaki Sugihara. Chemistry of Thiophene 1,1-Dioxides**.** Berlin : Springer Berlin Heidelberg, 1999.